Present and Future Wind Energy Resources in Western Canada

by

Jeffrey Thomas Daines
B.A., Oberlin College, 1970
LL.B., University of Toronto, 1974
M.Sc., University of Calgary, 1994

A Thesis Submitted in Partial Fulfillment of the
Requirements for the Degree of

MASTER OF SCIENCE

in the School of Earth and Ocean Sciences

Present and Future Wind Energy Resources in Western Canada

by

Jeffrey Thomas Daines
B.A., Oberlin College, 1970
LL.B., University of Toronto, 1974
M.Sc., University of Calgary, 1994

Supervisory Committee

Dr. Adam H. Monahan, Co-Supervisor
(School of Earth and Ocean Sciences)

Dr. Charles L. Curry, Co-Supervisor
(School of Earth and Ocean Sciences)

Dr. David E. Atkinson, Outside Member
(Department of Geography)

Supervisory Committee

Dr. Adam H. Monahan, Co-Supervisor
(School of Earth and Ocean Sciences)

Dr. Charles L. Curry, Co-Supervisor
(School of Earth and Ocean Sciences)

Dr. David E. Atkinson, Outside Member
(Department of Geography)

ABSTRACT

Wind power presently plays a minor role in Western Canada as compared to hydroelectric power in British Columbia and coal and natural gas thermal power generation in Alberta. However, ongoing reductions in the cost of wind power generation facilities and the increasing costs of conventional power generation, particularly if the cost to the environment is included, suggest that assessment of the present and future wind field in Western Canada is of some importance.

To assess present wind power, raw hourly wind speeds and homogenized monthly mean wind speeds from 30 stations in Western Canada were analyzed over the period 1971-2000 (past). The hourly data were adjusted using the homogenized monthly means to attempt to compensate for differences in anemometer height from the standard height of 10m and changes in observing equipment at stations.

A regional reanalysis product, the North American Regional Reanalysis (NARR), and simulations conducted with the Canadian Regional Climate Model (CRCM) driven with global reanalysis boundary forcing, were compared to the adjusted station wind-speed time-series and probability distributions. The NARR had a better temporal correlation with the observations ($R^2 \approx 0.35$), than the CRCM ($R^2 \approx 0.22$). We posit this is due to the NARR assimilating regional observations, whereas the CRCM did not. The NARR was generally worse than the CRCM in reproducing

the observed speed distribution, possibly due to the crude representation of the regional topography in NARR. While the CRCM was run at both standard (45 km) and fine (15 km) resolution, the fine grid spacing does not always provide better results: the character of the surrounding topography appears to be an important factor for determining the level of agreement.

Multiple simulations of the CRCM at the 45 km resolution were also driven by two global climate models (GCMs) over the periods 1971-2000 (using only historic emissions) and 2031-2060 (using the A2 emissions scenario). In light of the CRCM biases relative to the observations, these simulations were calibrated using quantile-quantile matching to the adjusted station observations to obtain ensembles of 9 and 25 projected wind speed distributions for the 2031-2060 period (future) at the station locations. Both bias correction and change factor techniques were used for calibration. At most station locations modest increases in mean wind speed were found for most of the projected distributions, but with a large variance.

Estimates of wind power density for the projected speed distributions were made using a relationship between wind speed and power from a CRCM simulation for both time periods using the 15km grid. As would be expected from the wind speed results and the proportionality of wind power to the cube of wind speed, wind power at the station locations is more likely than not to increase in the 2031-2060 period from the 1971-2000 period.

Relative changes in mean wind speeds at station locations were found to be insensitive to the station observations and choice of calibration technique, suggesting that we estimate relative change at all 45km grid points using all pairs of past/future mean wind speeds from the CRCM simulations. Overall, our results suggest that wind energy resources in Western Canada are reasonably likely to increase at least modestly in the future.

Contents

List of Tables

List of Figures

ACKNOWLEDGEMENTS

I would like to thank:

My wife, Janet, for her support and encouragement over a project that took rather longer than expected.

The Pacific Institute for Climate Solutions for the award of a Pacific Institutes for Climate Solutions Graduate Fellowship.

The Faculty of Graduate Studies for the award of a University of Victoria Fellowship.

My co-supervisors, Adam Monahan and Charles Curry, for their guidance and support and, in particular, for their careful and detailed review of my thesis.

For conducting the CRCM simulations, the Ouranos Consortium and the University of Victoria as part of the NSERC-funded Collaborative Research and Development project, Dynamical Downscaling of Western and Eastern Canadian Hydroclimate (A. Weaver and D. Caya, PIs), with infrastructure funding from Canadian Foundation for Innovation and the British Columbia Knowledge Development Fund.

Michel Gigure (Ouranos Consortium) for running the simulations, and Mourad Labassi (Ouranos Consortium), Ed Wiebe (University of Victoria), and Jean des Rosiers for technical support.

Chapter 1

Introduction

In the Canadian provinces of Alberta and British Columbia electrical power is generated primarily from fossil fuels (in Alberta) and hydropower (in British Columbia) (Alberta Energy, 2015; B.C. Ministry of Energy and Mines, 2015). Fossil fuel use in Alberta may eventually be phased out in response to climate change concerns, so other sources of energy will be required. The latest hydroelectric dam approved by the government of British Columbia may be the last, so further generating capacity will eventually be needed in that province as well (Eagland, 2015). In addition, the electrical power transmission systems of the two provinces are linked with interties, which are used to buy and sell power on a daily basis, so that in reality British Columbia imports power generated by Alberta's coal fired thermal plants at night when it is cheaper (because the thermal power plants cannot respond quickly to demand changes) and exports hydroelectric power to Alberta during the day when Alberta's power requirements peak (Kiani et al., 2013). Considering the future generation of electrical power in the future in the two provinces together makes sense, particularly if they were to cooperate to reduce overall use of fossil fuels.

Wind energy use for generating electrical power is expanding rapidly worldwide and has already been developed to some extent in Alberta (installed wind energy capacity of 1,471 MW) and to a lesser extent in British Columbia (installed wind energy capacity of 488.7 MW)(Canadian Wind Energy Association, 2015). The expansion of existing wind farms or construction of new ones should take into account the possibility that climate change caused by increasing greenhouse gas emissions could alter the wind resource and its variability. Studies in other regions may not be applicable here due to the complex topography of the region. The overall goal of this study is therefore to estimate future changes in wind power resources in this region resulting

from climate change.

For this study observational data and simulated winds from climate models were obtained as wind speeds at a nominal height of 10 m. According to Betz's law (Manwell et al., 2012), the maximum energy that a wind turbine can be capture from the wind is 59.3% of the wind power density, which is given by:

$$E = \frac{1}{2}\rho V^3$$

where E is the wind power density in W/m^2; ρ is the air density, which unless otherwise stated is taken as 1.225 kg/m^3 (approximately the density at sea level and 15 degrees Celsius); and V is the instantaneous wind speed in m/s. Where possible, wind power density is calculated in this study using highest time resolution wind speeds available. Observations are sampled hourly, while climate model simulation results are available as 3 or 6-hourly means. For varying wind speeds the wind power density may be underestimated, depending upon the time scale of the variability.

One way to project future wind climate is to look for trends in historical observations (Wan et al., 2010) or in regional reanalysis products in which historical regional observations are assimilated into a model that is driven by global climate data (Pryor et al., 2012). Neither of these is pursued here as past trends may not accurately reflect future changes. In addition to the forced response to such increases, both models and observations feature natural climate variability, which limits the utility of extrapolation-based approaches.

Global climate models (GCMs) can be used to obtain wind speeds near the surface, but have a spatial resolution that fails to represent many features of this region that influence wind speed, such as mountain ranges and narrow valleys. Desirable wind turbine sites such as ridges are completely missed by the topography used in GCMs. To estimate regional wind climate there are two main methods (and some hybrids) used to "downscale" winds from GCMs to a regional scale. Statistical downscaling uses statistical relationships between local observations and large-scale GCM variables(Breslow and Sailor, 2002; Mansbach and Cayan, 2010; Sailor et al., 2008), while in dynamical downscaling relatively high resolution regional climate model (RCM) is driven by a GCM. In this study dynamical downscaling results from multiple RCM simulations from each of two GCMs are used to estimate future changes in wind climate in British Columbia and Alberta. Dynamical downscaling has been used for projecting temperature and precipitation in this region (Curry et al., 2015) and in

the U.S. Pacific Northwest (Salathe et al., 2008), but dynamical downscaling of the wind climate is not examined in those studies. Dynamical downscaling of the wind climate has, however, been used to project future changes in wind speed in wind farm regions in California (Rasmussen et al., 2011).

While projecting the future wind climate from historical trends is not pursued here, past observations are needed in order to calibrate simulations produced by climate models to remove systematic errors (Ho et al., 2012). Different calibration pathways exist that are not equivalent, and all calibration approaches are based upon assumptions which may not be valid. One way to calibrate the future simulations is to use observations from weather stations. The weather stations in Alberta and British Columbia for which there is long-term hourly data are few and the data are of variable quality (Wan et al., 2010). In this study, these data will be considered in detail and a discussion of data quality presented. Alternatively, previous studies have used wind speeds from regional reanalysis products as pseudo-observations. For that reason, a regional reanalysis (the North American Regional Reanalysis, NARR) is compared with station wind speed data to determine whether it could be used for calibration. As will demonstrated, a critical assessment indicates that the near-surface winds obtained from NARR are problematic in the domain under consideration.

In this study, the accuracy of a regional climate model or RCM (specifically, the Canadian Regional Climate Model, CRCM) used for downscaling is tested by comparing its output with historical observations when the RCM is driven by a global reanalysis product. Also, since RCM simulations are available at two different resolutions, an investigation of how differing resolution affects the modelled wind field is carried out. Since we have multiple RCM simulations for each GCM we can generate an ensemble of calibrated future simulations that can be used to evaluate the range of possible future wind statistics.

Finally, there are many uncertainties in the simulated future winds discussed in this study. In particular, there is uncertainty in station data, the choice of GCM, the choice of calibration method, the accuracy and resolution of the RCM, and variability in the ensemble of calibrated simulations for each GCM. A primary goal of this study is to assess the relative magnitudes of these uncertainties.

This study is organized as follows. Chapter 2 provides a description of the region, the observational data used, and the models. In Chapter 3, the historical station data are compared to the results obtained from the NARR reanalysis product and the CRCM driven by global reanalysis. In Chapter 4 the output of the CRCM driven

by two GCMs is calibrated using the observations to project future wind climate at stations in the region. Chapter 5 examines the uncertainties and sensitivities encountered in the projection of future wind climate and their relative importance to the results. As part of this analysis, an attempt is made to estimate relative change in the wind climate over the entire region, not just at the station locations. The main conclusions of the thesis are summarized in Chapter 6.

Chapter 2

Data and Models

This Chapter introduces the observational data and models used in this study to estimate wind power resources in the present and future.

2.1 Station Data

To be useful for estimating the wind power available at a location, continuous frequent observations (at least hourly) for long time periods, rather than monthly or daily means or daytime only observations, are needed. Sites for wind power generating facilities are generally chosen by observing wind speed using temporary test towers at prospective sites, but the data collected from such towers is necessarily of short duration compared to the service life of wind turbines that may be installed there. Hence, sites for test towers are preferably selected using long-term observations as close as possible to a prospective site. Such long-term observations are generally from meteorological stations mounted at altitudes well below turbine hub height (e.g., 10 m as opposed to 100 m).

This study uses observed wind speed distributions for 1971-2000 to assess the performance of regional climate models and to calibrate simulations of wind speed distributions for 2031-2060 that were obtained from regional climate models. As such it is necessary to obtain accurate observed hourly wind speeds for as many stations as possible in the region under study.

2.1.1 Station Locations and Distribution

The Environment Canada (EC) public website `http://climate.weather.gc.ca/advanceSearch/searchHistoricData_e.html` is the source of the observed near-surface (nominally 10 metre height) wind speed data used in this study. The particular stations for which data were obtained are those thirty stations in the provinces of Alberta (AB) and British Columbia (BC) for which EC provides monthly mean wind speeds (in most cases from 1953 to 2011) adjusted (homogenized) for equipment, location, and environmental changes in addition to raw hourly wind speeds from 1953 to the present. A topographic map of British Columbia and AB with the stations identified by number is shown in Figure 2.1. Table 2.1 lists the station names and their latitudes, longitudes, and elevations as provided by EC. With one exception (McInnes Island), all of these stations are located at airports.

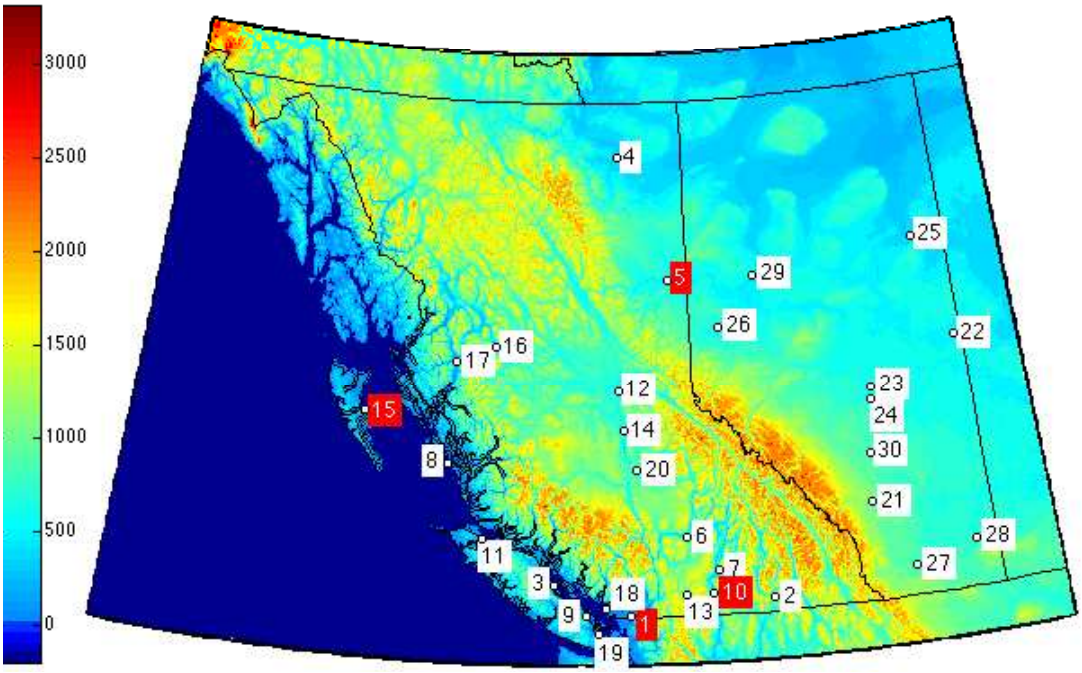

Figure 2.1: Topographic map of British Columbia and Alberta using one arc-minute resolution elevations from ETOPO1 (Amante and Eakins, 2009) and EC station locations enumerated as in Table 2.1. Map borders are latitudes 48 and 61 degrees North and longitudes 140 and 108 degrees West. The stations with red markers are the "representative stations" referred to in the text. Elevations are in metres.

The Alberta - British Columbia region can be divided into four sub-regions. The division into sub-regions was subjective and based on inspection of the data. For

No.	Station Name	Prov	Lat (deg N)	Lon (deg W)	Elev (m)
1	Abbotsford Airport	BC	49.03	122.36	59.1
2	Castlegar Airport	BC	49.30	117.63	495.0
3	Comox Airport	BC	49.72	124.90	26.0
4	Fort Nelson Airport	BC	58.84	122.60	382.0
5	Fort St John Airport	BC	56.24	120.74	695.0
6	Kamloops Airport	BC	50.70	120.44	345.0
7	Kelowna Airport	BC	49.96	119.38	429.5
8	McInnes Island	BC	52.26	128.72	26.0
9	Nanaimo Airport	BC	49.05	123.87	28.0
10	Penticton Airport	BC	49.46	119.60	344.0
11	Port Hardy Airport	BC	50.68	127.37	22.0
12	Prince George Airport	BC	53.89	122.68	691.0
13	Princeton Airport	BC	49.47	120.51	700.0
14	Quesnel Airport	BC	53.03	122.51	545.0
15	Sandspit Airport	BC	53.25	131.81	6.0
16	Smithers Airport	BC	54.82	127.18	522.0
17	Terrace Airport	BC	54.47	128.58	217.0
18	Vancouver International Airport	BC	49.20	123.18	4.0
19	Victoria International Airport	BC	48.65	123.43	19.0
20	Williams Lake Airport	BC	52.18	122.05	940.0
21	Calgary International Airport	AB	51.11	114.02	1084.0
22	Cold Lake Airport	AB	54.42	110.28	541.0
23	Edmonton City Centre Airport	AB	53.57	113.52	671.0
24	Edmonton International Airport	AB	53.32	113.58	723.0
25	Fort McMurray Airport	AB	56.65	111.22	369.0
26	Grande Prairie Airport	AB	55.18	118.89	669.0
27	Lethbridge Airport	AB	49.63	112.80	929.0
28	Medicine Hat Airport	AB	50.02	110.72	717.0
29	Peace River Airport	AB	56.23	117.45	571.0
30	Red Deer Airport	AB	52.18	113.89	905.0

Table 2.1: Station numbers for Figure 2.1, names, locations (latitude degrees N and longitude degrees W) and elevations (metres) of all stations in British Columbia and Alberta with hourly raw wind speeds and monthly homogenized wind speed data available from EC.

each sub-region a representative station with wind speed observations for the period 1971-2000 was chosen for the following discussion. Fort St. John (#5) is typical of the stations east of the Rocky Mountains. Penticton (#10) is typical of the interior of British Columbia in that it lies in a valley between mountain ranges, Abbotsford (#1) is typical of a near coastal station that is not exposed to the open ocean, and Sandspit (#15) is a station exposed to the open ocean. These four representative stations (indicated with red markers in Figure 2.1) will be used throughout this study to illustrate differing wind properties across the larger region.

2.1.2 Hourly Raw Data

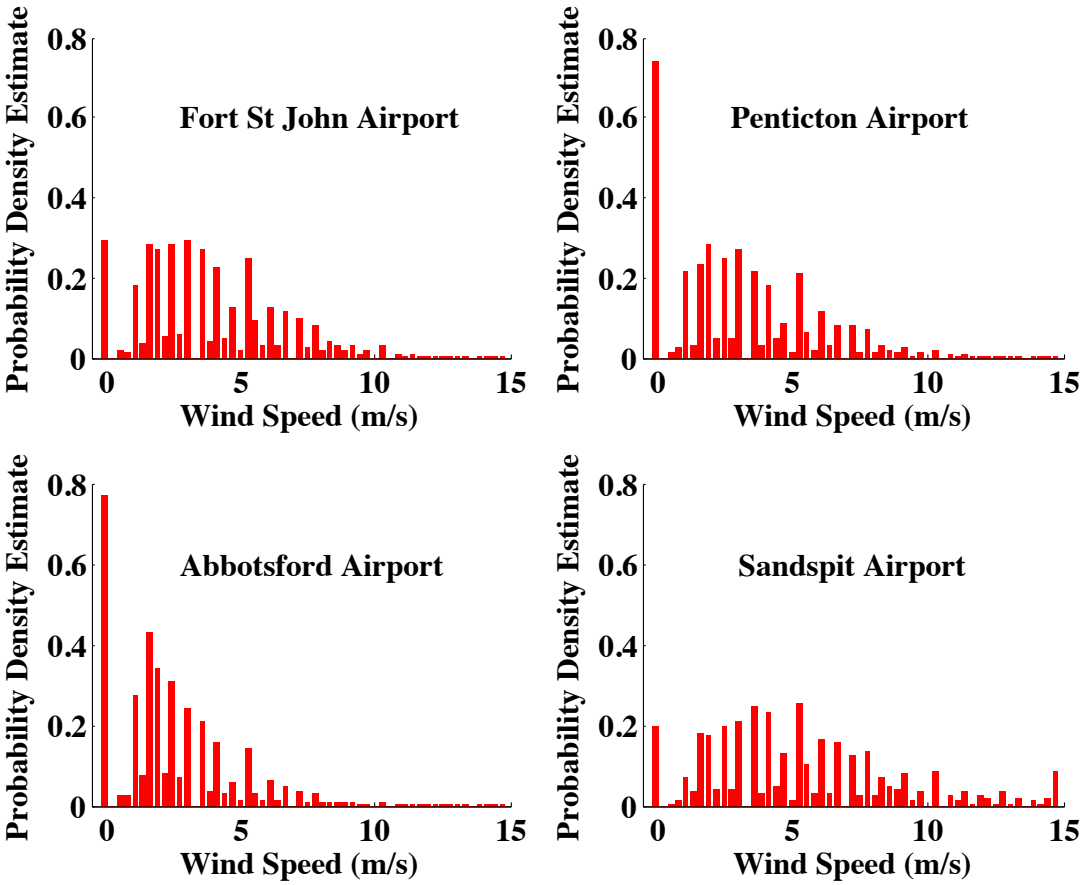

Figure 2.2: Histograms of the raw hourly wind speeds obtained from EC for the period 1971-2000 with the bin size set at one km/hr to show effect of recording in statute miles per hour or knots and then archiving in km/hr.

The hourly wind speeds recorded at the stations were one-minute mean wind

speeds ending at the time of the observation for years prior to 1996 and two-minute mean wind speeds since 1996, with speeds recorded to the nearest knot since 1996 and the nearest statute mile per hour prior to 1996 (Wan et al., 2010). A statute mile per hour is exactly 0.44704 m/s and a knot is approximately 0.514444 m/s. However, the downloadable wind speeds are provided in integer kilometres per hour. As a result, the range of speeds is not spanned continuously by the data. Further, the time series of hourly wind speeds also contain a large number of zero and missing wind speeds for some of the stations. Figure 2.2 shows examples of the distributions of raw hourly wind speeds obtained from EC with the bin size set at 1 km/hr for the period 1971-2000 for the four stations representative of sub-regions of western Canada. The absence or low occurrence frequency of wind speeds in some bins is a result of the original recording of wind speeds rounded to integer knots in some years and statute miles per hour in other years. The histograms of Figure 2.2 are typical of the data downloaded from EC for many of the stations. Zero wind speeds are included; Table 2.2 shows their relative fraction.

Table 2.2 contains the percentages of missing and zero wind speeds in the raw hourly data from EC for the period 1971-2000. Six stations have missing hours in excess of 1%. Observational records for Nanaimo (#9) and McInnes Island (#8) are problematic for climate studies due to either a very long period of only a few recorded wind speeds per day (McInnes Island) or, in the case of Nanaimo, eight hours of observations missing from every day for almost the entire 1971-2000 period. For Kelowna (#7), Quesnel (#14), Princeton (#13), and Castlegar (#2) there are years for which the percentage of missing observations is less than 1%, but in each case there are many years for which the percentage of missing observations for every month is from 20% to 50%. The percentage of missing data for a particular station usually stays constant for many months, indicating that the observations were not being recorded for part of each day in some years.

In some studies zero wind speeds have been treated as missing data (Curry et al., 2012). However, it appears more likely that the zero wind speeds in the observational data used in this study are "calms", corresponding to wind speeds less than some minimum value, not bad data that should be removed. Confirmation of this can be found in Appendix A. Table 2.2 also includes percentages of zero wind speeds for December through February (DJF) and July through August (JJA). There is no general preponderance of zero wind speed measurements in DJF or JJA across the study domain.

No.	Station Name	% Zeros All	% Zeros DJF	% Zeros JJA	% Missing
1	Abbotsford	21.4	16.6	25.1	0.2
2	Castlegar	25.7	25.2	24.0	12.7
3	Comox	12.8	15.0	8.6	0.1
4	Fort Nelson	32.7	46.8	24.2	0.1
5	Fort St John	8.1	10.3	8.2	0.2
6	Kamloops	25.5	27.5	25.1	0.1
7	Kelowna	36.1	39.3	32.4	4.8
8	McInnes Island	2.3	1.4	3.3	48.9
9	Nanaimo	26.0	34.5	19.2	33.5
10	Penticton	20.6	17.1	21.1	0.0
11	Port Hardy	17.7	13.4	21.9	0.1
12	Prince George	21.4	23.0	22.0	0.1
13	Princeton	36.5	50.2	25.4	22.7
14	Quesnel	42.0	44.3	42.8	8.1
15	Sandspit	5.4	5.3	6.3	0.6
16	Smithers	35.7	34.6	36.3	0.2
17	Terrace	18.4	19.1	15.6	0.2
18	Vancouver	9.1	10.0	7.3	0.0
19	Victoria	12.9	10.8	15.5	0.1
20	Williams Lake	23.2	23.3	26.2	0.2
21	Calgary	8.9	10.1	8.6	0.0
22	Cold Lake	13.2	17.7	12.8	0.1
23	Edmonton City	7.8	8.9	7.2	0.2
24	Edmonton	8.1	9.2	9.3	0.0
25	Fort McMurray	16.8	21.9	16.4	0.1
26	Grande Prairie	18.8	27.9	13.0	0.1
27	Lethbridge	6.1	7.3	6.1	0.1
28	Medicine Hat	11.2	12.8	11.1	0.2
29	Peace River	9.5	11.5	9.3	0.4
30	Red Deer	9.2	10.6	9.8	0.2

Table 2.2: Percentages of the missing and zero speeds in raw hourly wind speeds 1971-2000.

In this study, zeros were retained in the hourly wind speed time series and were averaged over three- and six-hour periods to form time series for comparison with model wind speeds, which are means over three- and six-hour periods. For the purposes of projecting wind energy into the future, the stations with higher fractions of zero wind speeds should be used with care in de-biasing models. As the primary goal is to characterize the wind energy resource in the future, it is unlikely that areas near these stations are useful sites for wind power generation due to their past observed low mean wind speeds. However, projection of wind speeds into the future at those stations with lower mean wind speeds may be useful for other purposes, such as characterizing dispersal of air pollutants. For that reason, projections for all of the 30 stations are included in this study.

2.1.3 Homogenizing and Correcting Hourly Raw Data

Homogenization is a process that adjusts observed time series for discontinuities and spurious trends, which may be caused by changes in station location (including elevation), recording equipment, and surrounding environment (buildings and vegetation) (Wan et al., 2010). Homogenized monthly mean wind speeds were obtained from EC. EC does not provide homogenized hourly wind speeds, but using the homogenized monthly mean wind speeds, corrected raw hourly wind speeds were found by multiplying each raw hourly wind speed by the ratio of the homogenized to raw monthly means for the relevant month. The resulting wind speeds are hereafter referred to as "corrected". The typical monthly correction factor for stations remains constant for long periods as illustrated in Figure 2.3 for the Grande Prairie Airport station. The correction process is problematic because (1) it does not generally agree with station metadata (changes in the observing system were made that are not reflected in changes in the difference between the homogenized monthly means and the raw monthly means) and (2) the EC homogenization program nominally lasted through 2011, yet the difference between the homogenized monthly means and the raw monthly means ended for all stations at or before the end of 2010, in some cases several years before. For example, the height of the anemometer at the Kelowna Airport station was changed from 19.8m to 13m in 1978 and then to 10m in 1982, yet the difference between the homogenized and raw monthly means was essentially constant from 1971 to 2000, yet in 2000 the difference abruptly changes to zero. In the balance of this study, results using both corrected and raw observations will be discussed. For most

purposes, these data give essentially the same results. However, it may be advisable to consider the results for stations for which little or no correction was applied as being more reliable.

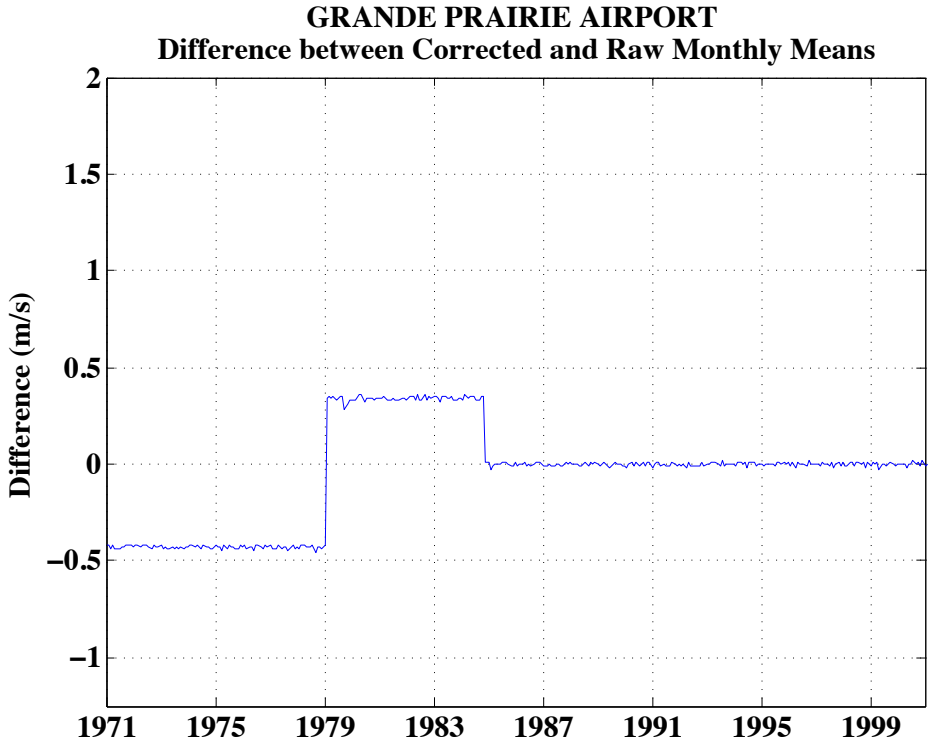

Figure 2.3: Difference between the corrected monthly mean and the raw monthly mean wind speed at the Grande Prairie station for the 1971-2000 period (m/s).

The correction process does not produce homogenized hourly wind speeds, but it produces corrected wind speeds whose monthly means match the homogenized means. In this process, the standard deviation of the raw wind speeds is also affected. This modification of the distribution of observed wind speeds needs to be kept in mind when the corrected wind speeds are used to calibrate future simulated wind speeds.

In some cases the correction had a significant effect on the mean wind speed. Table 2.3 lists the mean raw and homogenized mean wind speeds for the period 1971-2000 sorted in order of decreasing corrected mean wind speed. By construction, the monthly means of the corrected wind speeds are exactly equal to the homogenized monthly means obtained from EC.

No.	Station Name	Corrected (m/s)	Raw (m/s)	% Change
8	McInnes Island	6.3	5.8	7%
15	Sandspit	5.3	5.4	-1%
27	Lethbridge	5.1	5.1	0%
28	Medicine Hat	4.9	3.9	24%
17	Terrace	4.8	3.7	29%
5	Fort St John	4.4	3.8	16%
21	Calgary International	4.1	4.1	0%
3	Comox	3.7	3.5	7%
18	Vancouver International	3.7	3.3	12%
22	Cold Lake	3.6	3.0	18%
23	Edmonton City Centre	3.6	3.4	6%
6	Kamloops	3.4	3.0	14%
24	Edmonton International	3.4	3.4	0%
30	Red Deer	3.4	3.6	-4%
11	Port Hardy	3.2	3.2	0%
29	Peace River	3.2	3.5 -	9%
1	Abbotsford	3.1	2.4	25%
10	Penticton	3.1	3.1	0%
19	Victoria International	3.1	2.5	27%
26	Grande Prairie	3.1	3.1	-2%
20	Williams Lake	2.8	2.8	1%
25	Fort McMurray	2.8	2.6	4%
12	Prince George	2.7	2.6	3%
16	Smithers	2.5	1.8	36%
9	Nanaimo	2.3	1.8	29%
4	Fort Nelson	2.1	1.8	16%
2	Castlegar	2.0	2.3	-10%
14	Quesnel	1.8	1.8	0%
7	Kelowna	1.7	1.5	14%
13	Princeton	1.3	1.3	0%

Table 2.3: Mean raw and corrected wind speeds for the period 1971-2000.

The minimum annual mean wind speed for utility-scale development of wind farms is generally taken to be 5.1 to 5.6 m/s at 10m above the surface (National Renewable Energy Laboratory, 2014). Only Lethbridge (#27), McInnes Island (#8), and Sandspit (#15) have corrected mean wind speeds equal to or exceeding 5.1 m/s. Calgary International (#21), Medicine Hat (#28), and Fort St. John (#5) are close to existing commercial wind farms so that there is a possibility that wind speeds in the area are sufficiently high for commercial wind power. McInnes Island (#8) and Sandspit (#15) are coastal and exposed to the Pacific Ocean. Lethbridge (#27) is near the largest concentration of existing wind farms in the region. Port Hardy (#11), while relatively close to a wind farm near Cape Scott, has a modest mean wind speed as it is not directly exposed to the Pacific Ocean (Penner, 2014).

2.1.4 Weibull Distributions Representing Corrected Speeds

The two-parameter Weibull distribution is the most common parametric distribution presently used for empirical modelling of wind speed (Monahan, 2014). For example, (Curry et al., 2012) use the Weibull distribution as an approximation to the observed histogram of wind speeds. If the observed wind speeds are found to be characterized well by the Weibull distribution, this distribution can be used in the process of calibrating future wind speeds (Tye et al., 2014).

In Figure 2.4, histogram estimates of the probability density function of the corrected hourly wind speeds for the four representative stations are plotted and overlaid with Weibull distributions fitted using the method of moments (Monahan, 2014). The probability density function of a Weibull distribution is given by:

$$p\left(x\right) = \frac{k}{A}\left(\frac{x}{A}\right)^{k-1} e^{-\left(\frac{x}{A}\right)^{k}}$$

where x is the wind speed and the Weibull parameters A and k, known respectively as the scale and shape parameters, are shown on the plots in Figure 2.4.

The agreement between the histogram estimates and the distributions is not very good, particularly because of the large number of calms. From visual inspection of Figure 2.4 it appears that if one were to shift most of the reported zero (calm) wind speeds to the 1 m/s bin, as appears to have happened in the most recent observations, then the resulting histograms would look reasonably close to the Weibull distributions. Instead of considering hourly wind speeds, we can also consider the 3-

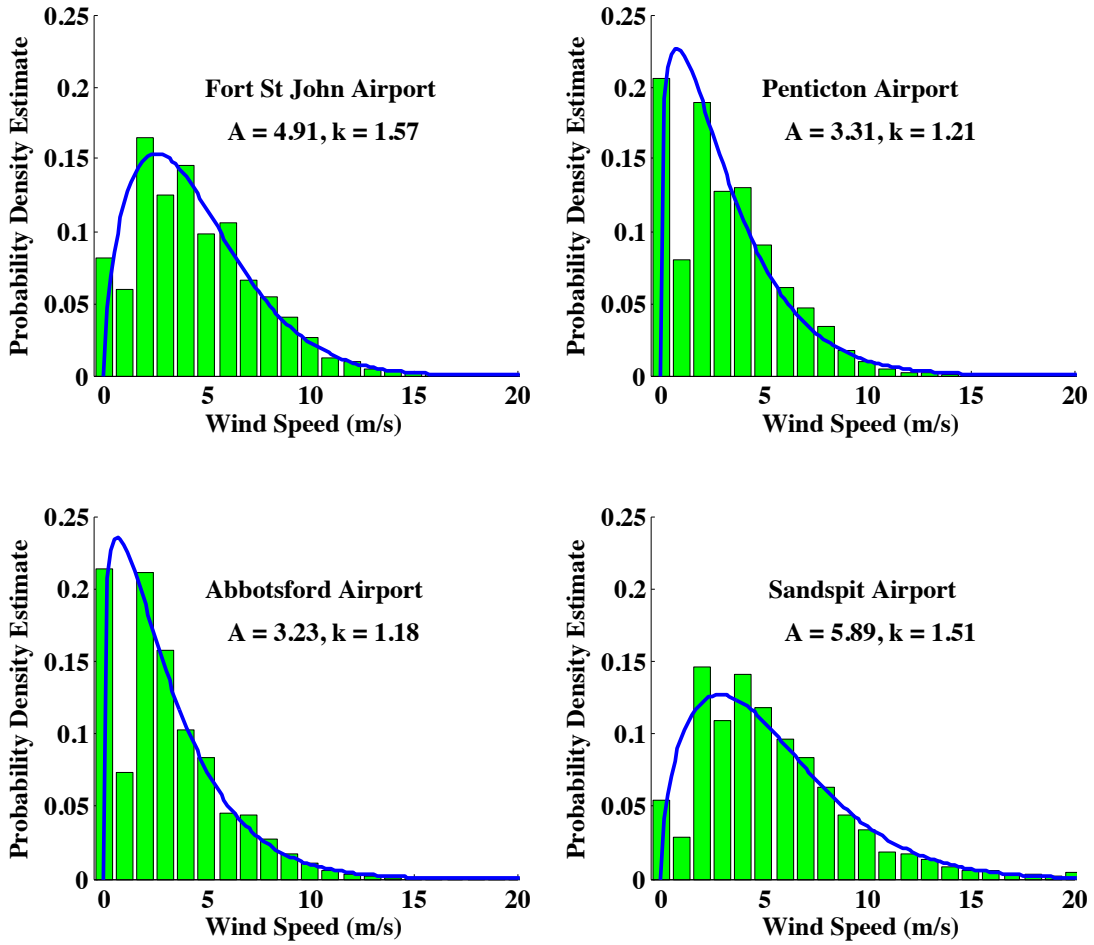

Figure 2.4: Histogram estimates of the probability density function of the corrected hourly wind speeds and the best-fit Weibull distributions for the representative stations for the period 1971-2000.

hour and 6-hour means of the observations that will be used to calibrate future wind speeds. For the time-averaged data, the Weibull fits improve as shown in Figures 2.5 and 2.6, particularly for the 3-hour means. The process of taking the means does, however, reduce the variance so that the peak probability density function estimates increase and the distributions narrow. While agreement improves, the differences from observed data are still sufficiently large that characterizing the observed distributions by their fitted Weibull parameters will be avoided in this study.

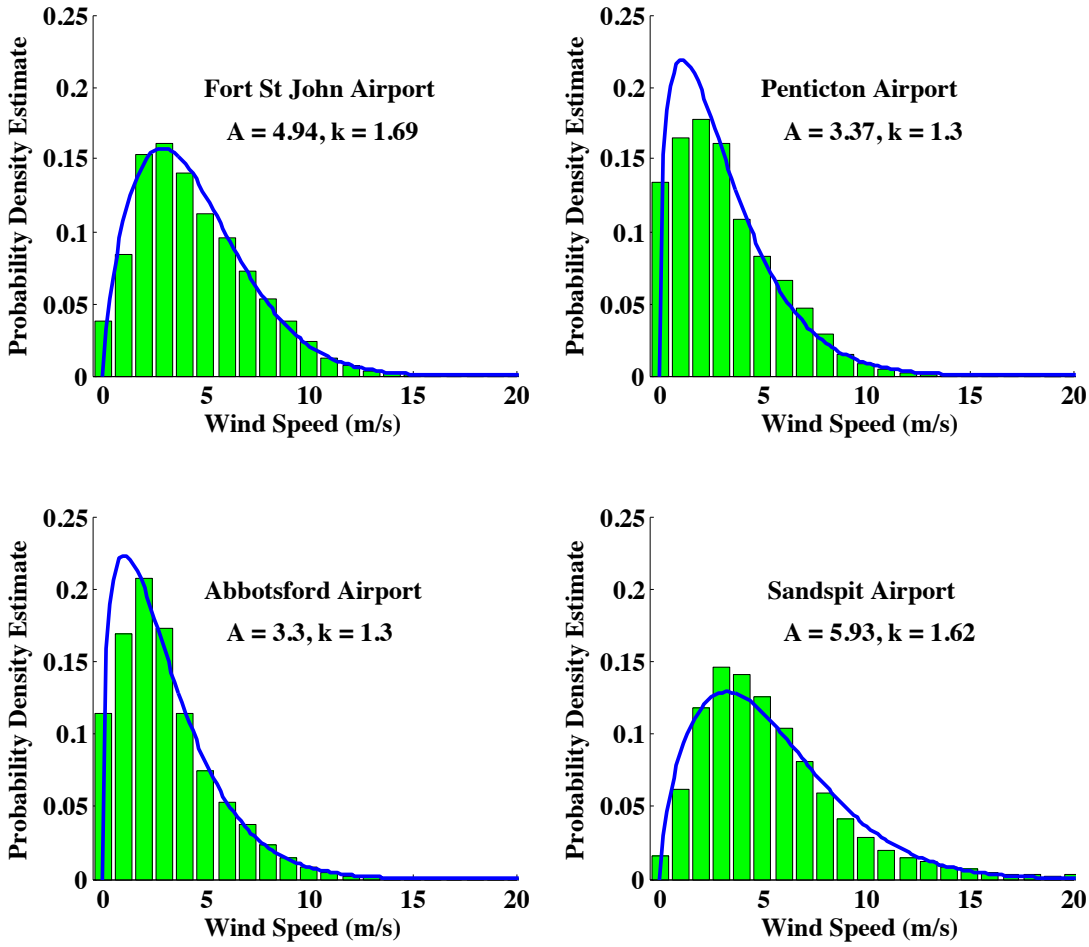

Figure 2.5: As in Figure 2.4 using 3-hour means.

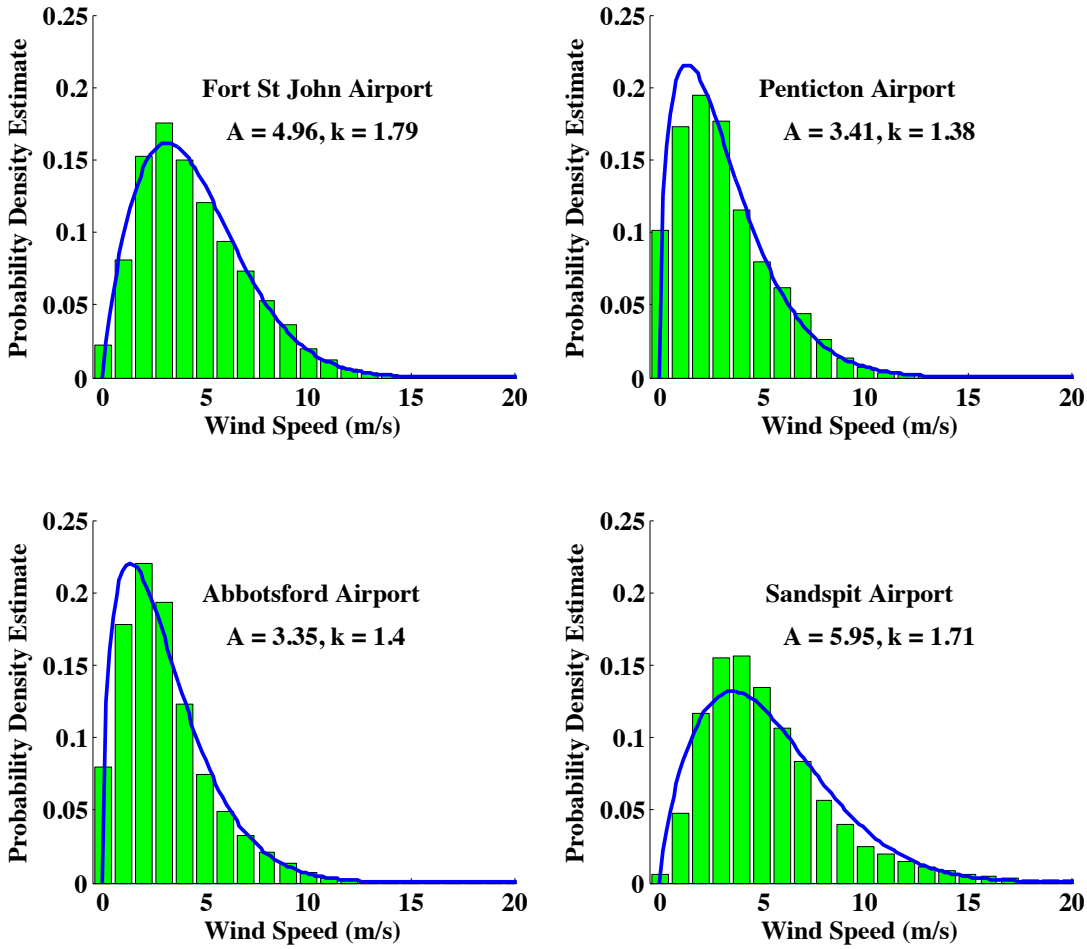

Figure 2.6: As in Figure 2.4 using 6-hour means.

The effects on the wind speed distributions of the corrections and of time averaging, which also needs to be applied to observed winds if they are to be used in the calibration of future simulated wind speeds, are shown in Figure 2.7 for the four representative stations and are generally typical of all stations.

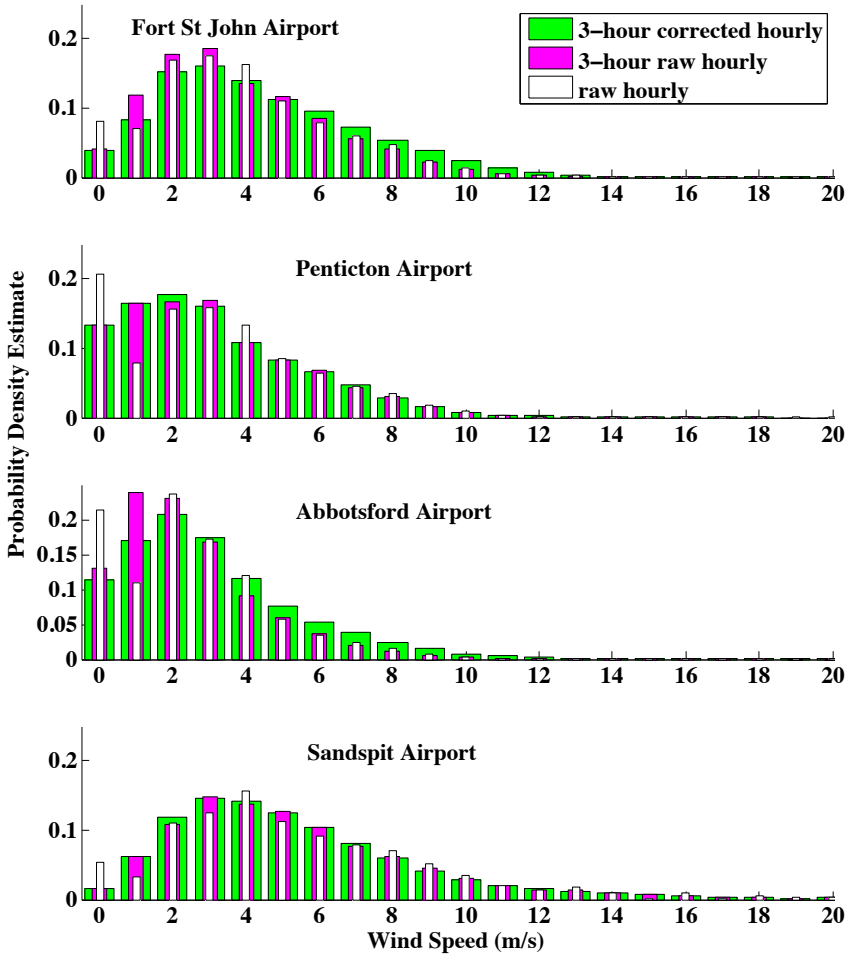

Figure 2.7: Histogram estimates of the probability density function of the 3-hour means of the corrected hourly wind speeds with the raw 3-hour means and the raw hourly wind speeds overlaid for the four representative stations for the period 1971-2000.

Averaging and correction modify the raw hourly wind speeds in two ways: First, the temporal averaging of the raw hourly wind speeds has reduced the large number of calm winds (zeros) in the raw data. Second, the correction process using the homogenized monthly means has in some cases changed the shape of the distribution, for example, by producing considerably more high wind speeds at Fort St. John.

2.2 North American Regional Reanalysis

Gridded reanalyses provide an alternative to station observations of wind speeds with much better coverage of the region, but are not direct observations of near-surface wind speeds. The North American Regional Reanalysis (NARR) is a regional reanalysis product that is driven by the NCEP/NCAR Global Reanalysis (Kalnay et al., 1996) as well as assimilating observations from within its regional boundaries (Mesinger et al., 2006). The NARR provides a number of climate variables at grid points spaced approximately 32 kilometres apart and at the surface and 45 pressure levels, including surface (10m) winds (Mesinger et al., 2006). Each NARR grid point is identified by the centre of a square grid box for the purposes of this study. The NARR fields are interpreted as averages across these grid boxes.

For this study, the wind speeds at 10 metres above the surface for the portion of the NARR grid shown in Figure 2.8 were used. The grid points do not align along lines of latitude and longitude as NARR uses a Lambert conformal conic grid.

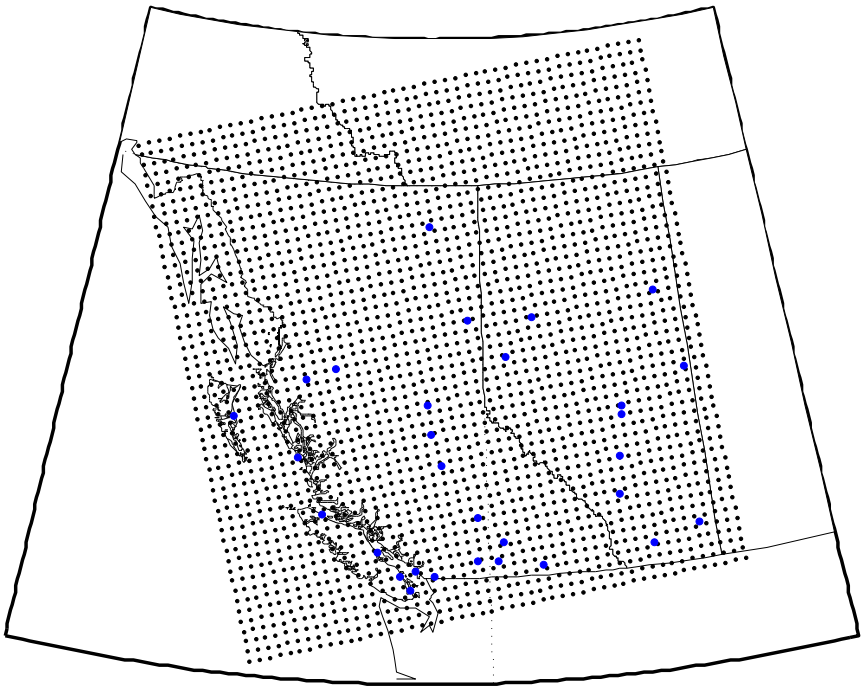

Figure 2.8: Map of the region of Figure 2.1 showing the boundaries of Alberta and British Columbia with the portion of the NARR grid that overlaps the region. The EC station locations are shown as blue dots for reference. Map borders are latitudes 46 and 64 degrees North and longitudes 140 and 105 degrees West.

Even though the NARR is a regional reanalysis product, the grid boxes are still

quite large (approximately 32 x 32 km, resulting in 2600 grid boxes in the portion of the NARR grid shown in Figure 2.8). An important feature of NARR for the purposes of this study is that the elevations of the grid boxes are quantized into a small number of discrete values (24 for the grid points ranging from zero to 3309 metres in this region). Figure 2.9 compares a topographic map prepared using the grid point heights used in the NARR topography (at the 32 km resolution of the NARR grid interpolated and smoothed) with the station altitudes provided by Environment Canada.

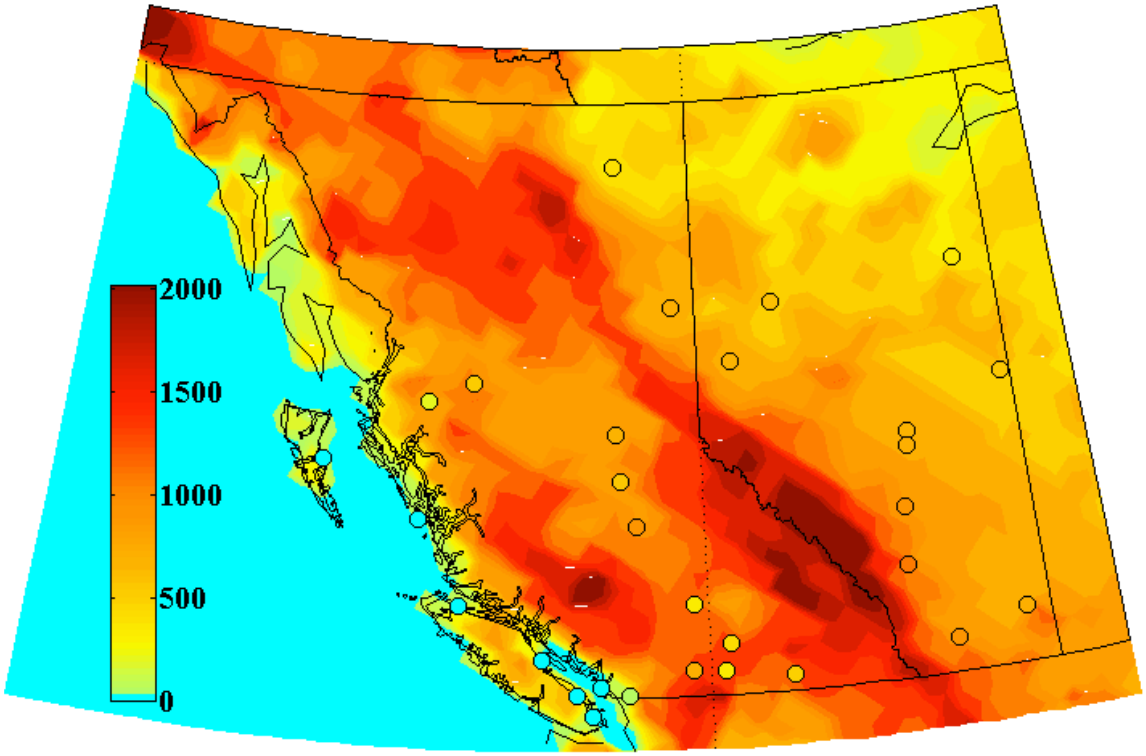

Figure 2.9: Topographical map at NARR grid resolution with the station elevations shown as circles filled according to their height (in metres) provided by EC.

From inspection of Figure 2.9, there is fairly close correspondence between the station elevations given by EC and the grid heights used by NARR for stations in Alberta and in northeastern British Columbia. However, NARR overestimates the elevation of the locations of many of the interior British Columbia stations. About half of the stations on or near the coast of British Columbia are overestimated by several hundred metres elevation, but at the scale of the map this is not evident.

For example, Figure 2.10 shows a topographic map at one arc-minute resolution around the Penticton Airport station, which is located in a narrow north-south valley

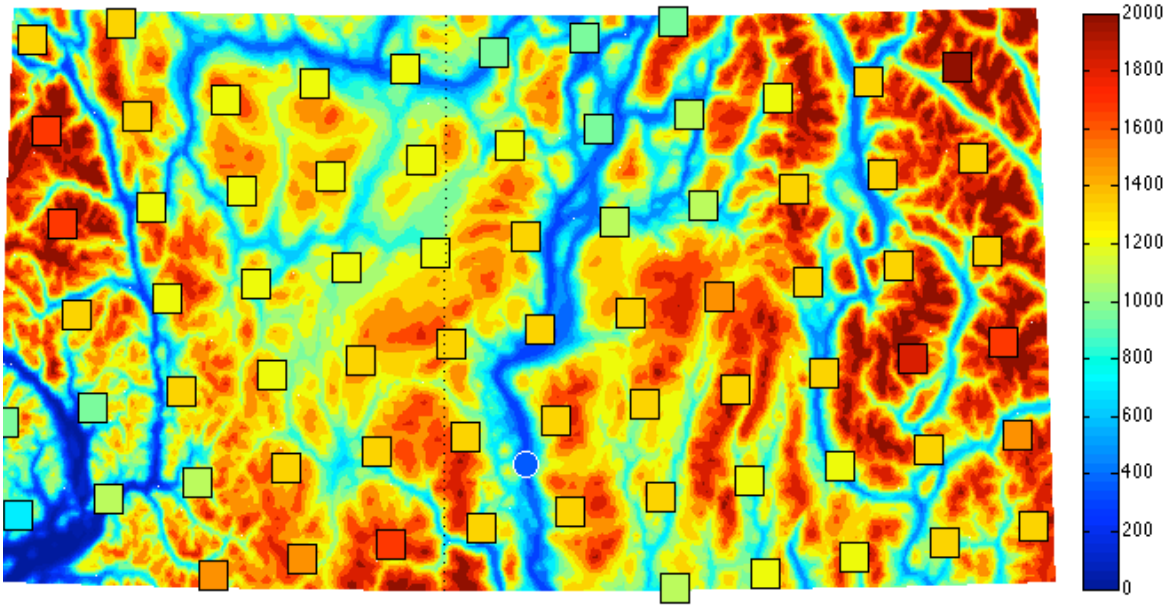

Figure 2.10: Topographical map at one arc-minute resolution around Penticton Airport station (scale in metres). The filled squares are centred on NARR grid points and the fill colour represents the height according to the NARR topography. The blue-filled white circle in the lower centre of the map is at the station location and its fill colour represents the elevation (344m) provided by EC.

surrounded by steep mountains. At 50 degrees north this resolution is about 1.85 km north-south and 1.19 km east-west. Moreover, the NARR elevations are insensitive to both the valley in which the station is located and the surrounding topography, giving the impression of a smooth plateau of middling height.

2.2.1 NARR Wind Speed Time series

NARR provides vector wind speeds (zonal and meridional components) every 3 hours from January 1, 1979 at each grid point. The vector winds through 2011 were downloaded and the wind speeds calculated at each grid point in the NARR grid as the amplitude of the 3-hour mean wind vector. For the purpose of comparison with the corrected hourly station data, wind speeds at the station locations were then calculated using a bilinear interpolation from the wind speeds at the four nearest NARR grid points. The interpolated NARR wind speeds are used throughout this study rather than the wind speed at the grid point nearest to the station location.

2.2.2 NARR Wind Speeds and Weibull Distributions

In Figure 2.11, the NARR wind speeds interpolated to representative station locations are presented together with best-fit Weibull distributions.

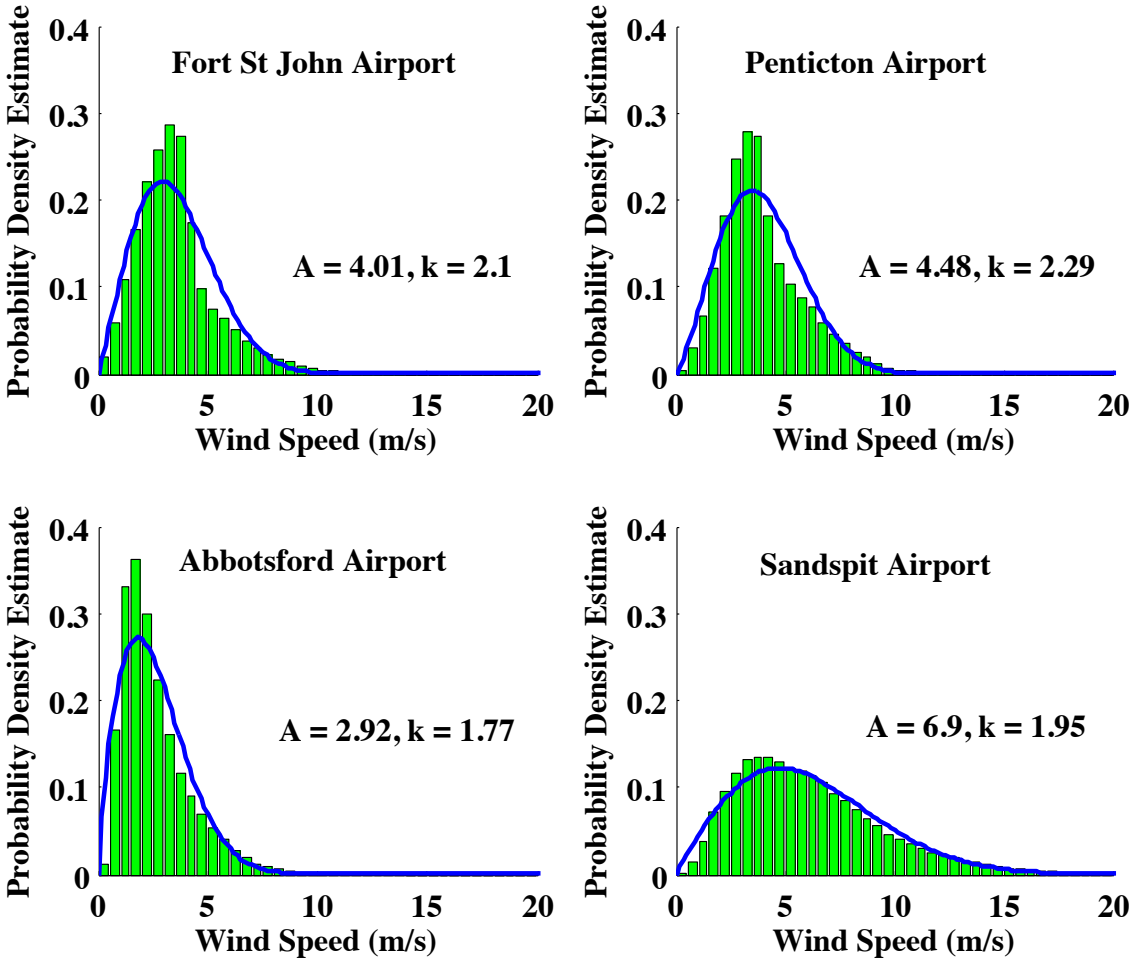

Figure 2.11: Histogram estimates of the probability density function of the NARR wind speeds for the period 1979-2000 interpolated to the locations of the representative stations overlaid with the best-fit Weibull distributions.

The Weibull distribution is less sharply peaked at intermediate wind speeds than the empirical distribution of the NARR wind speeds, particularly in the case of the Fort St. John and Penticton stations. At these and other locations, it appears that the distribution of NARR wind speeds reflects the presence of multiple underlying distributions. For example, in Figure 2.12, the histogram for the Penticton Airport station in Figure 2.11 is split into histograms for the middle of the night (9 UTC) local time and midday local time (21 UTC) for all days for the 1979-2000 period. The

nighttime NARR wind speed distribution is more skewed and less similar to a Weibull distribution than the daytime one. This is consistent with observations elsewhere (He et al., 2010; Monahan et al., 2015). This characteristic is not apparent in the station data shown in Figure 2.4 for the same stations.

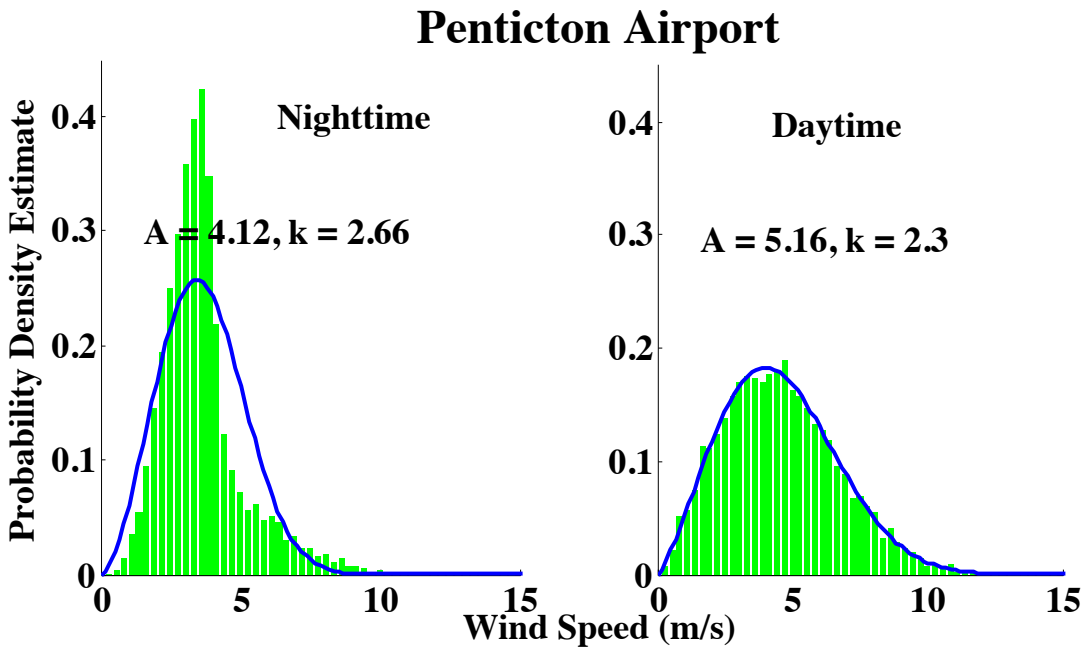

Figure 2.12: Histogram estimates of the probability density function of the NARR wind speeds for the Penticton Airport station location for the period 1979-2000 overlaid with best-fit Weibull distributions showing the diurnal distributions.

2.2.3 Spatial Resolution of NARR Wind Speeds

NARR has sometimes been used as a proxy for observations (Holt and Wang, 2012). In the course of debugging a procedure to interpolate NARR wind speeds to station locations, a potentially serious question regarding the usefulness of NARR wind speeds in this region arose. The problem can be illustrated with the map of the region showing mean wind speed for the 1979-2011 period based upon the mean NARR wind speeds at the grid points in Figure 2.13. The map shows the NARR grid boxes centred on the NARR grid points to emphasize the coarse spatial resolution of the NARR wind speed field. In places lines of squares having the same colour appear, indicating extended regions with similar mean wind speeds over the 33-year period. While this is not necessarily unphysical, the linear structure is surprising. In checking

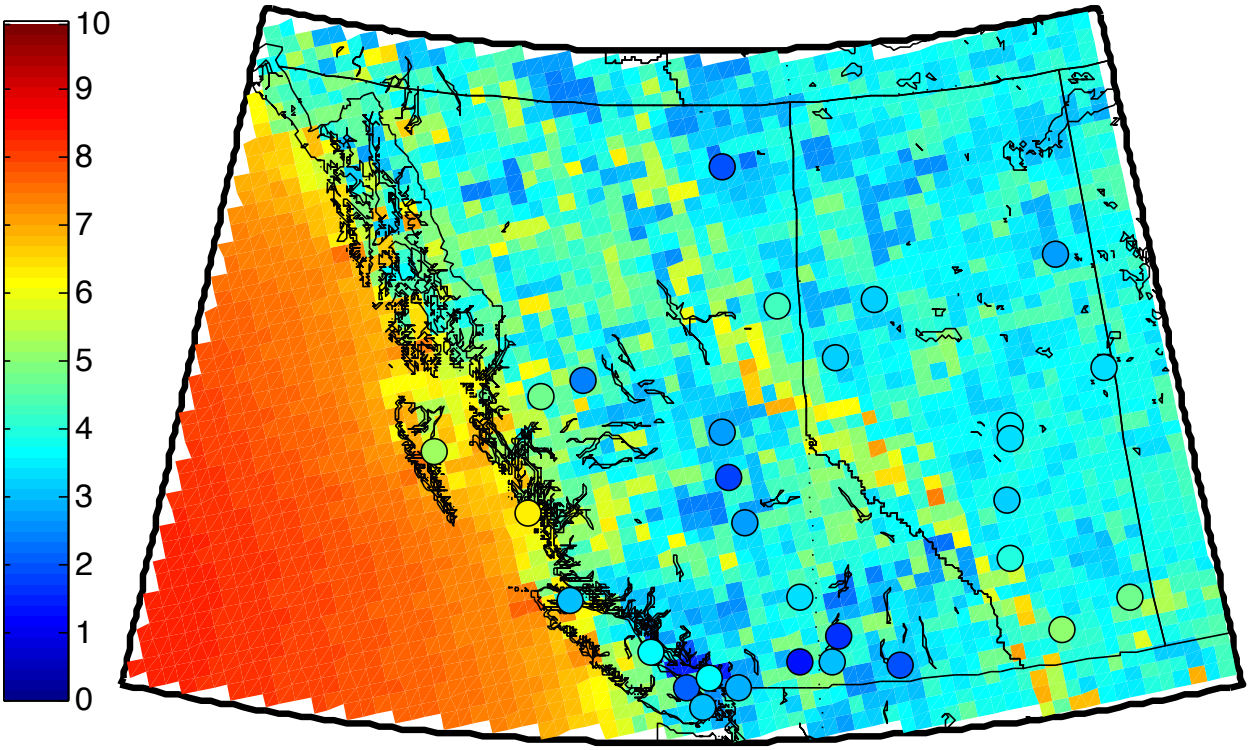

Figure 2.13: Means of the NARR 3-hourly wind speeds with the observed station means as filled circles for 1979-2011 (scale in m/s).

the interpolation process, it was found that NARR wind speed time series at many pairs of adjacent grid points in this region are essentially identical over the entire period. For example, over 33 years of the wind speed time series at two adjacent grid points the wind speeds every three hours (96424 speeds) never differed by more than

0.015 m/s. For this reason, while NARR wind speeds will be discussed in this study in detail in this Chapter and compared directly with observed wind speeds in Chapter 3, it is suggested that NARR does not provide near-surface wind speeds at the nominal spatial resolution. As well, this unphysically extreme similarity of neighbouring grid points raises questions about how NARR wind fields are produced.

2.3 Canadian Regional Climate Model

A complement to regional reanalysis is to model the climate of a region using a regional climate model (RCM) driven by a global-scale model at its boundaries, without the RCM itself assimilating observations from within the region as NARR does. The driving global model may be either (1) a global reanalysis or (2) a global climate model (GCM) forced by anthropogenic or natural forcing or both. This approach

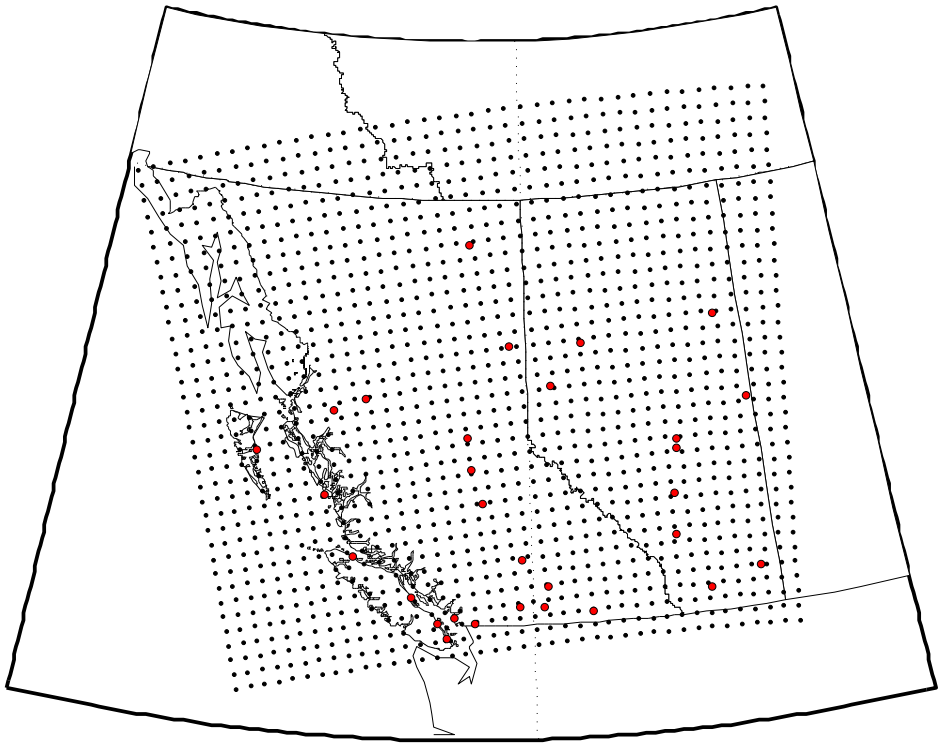

Figure 2.14: Map of the region of Figure 2.1 showing the boundaries of Alberta and British Columbia with the portion of the CRCM 45 km grid that overlaps the region. The EC station locations are shown as red dots for reference. The map borders are latitudes 46 and 64 degrees North and longitudes 140 and 105 degrees West.

is useful for our study since NARR cannot be used to simulate winds under future

greenhouse gas emissions scenarios and hence cannot be used for estimating future changes in wind power resources. The Canadian Regional Climate Model (CRCM) is used in this study (Caya and Laprise, 1999; Plummer et al., 2010). Different simulations are considered, in which the RCM is driven by (1) the European Centre for Medium range Weather Forecasting (ECMWF) ERA-40 global reanalysis or (2) by the ECHAM5 global coupled climate model (from the ECMWF) or (3) by Coupled Global Climate Model (CGCM3) model from the Canadian Centre for Climate Modelling and Analysis (CCCma). Simulations using the ECHAM5 and CGCM3 models are freely-evolving and driven by historical emissions of long-lived greenhouse gases until switching at the year 2000 to the A2 emissions scenario described in the Special Report on Emissions Scenarios of the Intergovernmental Panel on Climate Change (Nakicenovic et al., 2000).

Two spatial resolutions (45 km and 15 km) were used in the CRCM simulations used for this study. The two grids are coincident, with nine CRCM 15 km grid cells

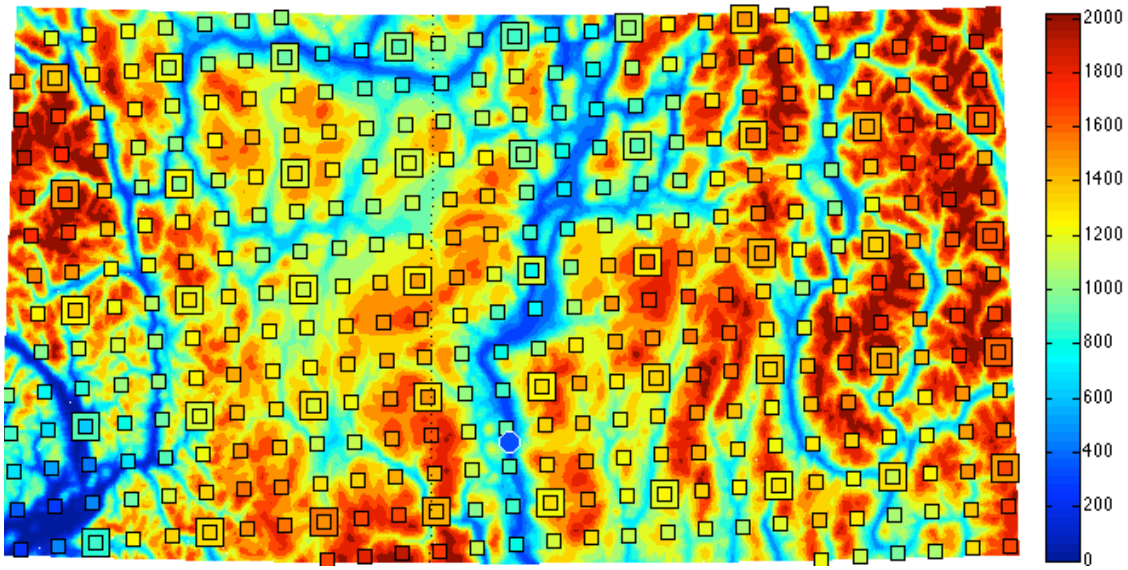

Figure 2.15: One arc-minute resolution topography around the Penticton Airport station (scale in metres). The small boxes represent the 15 km CRCM grid filled with colour for the 15 km CRCM grid heights superimposed over that large boxes, which represent the 45 km CRCM grid filled with colour for the 45 km CRCM grid heights. The blue-filled white circle in the lower centre of the map is at the station location and its fill colour represents the elevation (344m) provided by EC.

for every CRCM 45 km grid cell. The portion of the 45 km CRCM grid used in this study is 38x44 grid points roughly between latitudes 48 and 61 degrees North and

longitudes 140 and 108 degrees West (Figure 2.14). Each grid point is treated as the centre of a grid box approximately 45km square. As in the case of the NARR grid topography, the CRCM grid overestimates the elevation of the locations of many of the interior British Columbia stations. For example, Figure 2.15 shows a topographic map at one arc-minute resolution map of the region around the Penticton Airport station with both 45 and 15 km grid points shown. The 45 km grid points nearest to the station are significantly higher in elevation than the station. As in the case of the NARR topography, the valley in which the station is located does not appear in the 45 km topography. However, the 15 km topography does in fact resolve this valley, although it still overestimates the near-station elevation.

2.3.1 CRCM Driven by Reanalysis

The Canadian Regional Climate Model (CRCM) driven by the ERA-40 global reanalysis is referred to in this study as CRCM-R. From CRCM-R, two time series of mean wind speeds at 10 m above the surface were obtained, one from the model run with a 15 km grid spacing for 1973-1995 (CRCM15-R) and the other from the model run with a 45 km grid spacing for 1973-2001 (CRCM45-R). As these time series of wind speeds overlap for the period 1973-1995, it is possible to assess how use of a higher spatial resolution changes the distribution of wind speeds and how well the CRCM-R represents the station observations. These topics are dealt with in Chapter 3.

The CRCM-R simulations were completed as part of a larger project. In particular, (Curry et al., 2015) examined the capacity of the CRCM to represent observed extreme temperature and precipitation event and the impact of increased resolution.

2.3.2 CRCM Driven by Global Climate Models

The CRCM simulations driven by the ECHAM5 and CGCM3 global climate models, collectively referred to in this study as CRCM-GCM, provided the following:

(a) at 15 km resolution: a single simulation of 6-hour mean 10 m wind speeds and power density for the period 1958-2000 using historical emissions and for 2029-2060 using the SRES-A2 emissions scenario, driven by the ECHAM5 global climate model, referred to here as CRCM15-ECHAM5;

(b) at 45 km resolution: an ensemble of five simulations of 3-hour mean 10 m wind speeds for the period 1948-2060 using historical emissions and the SRES-A2 emissions scenario, driven by the CGCM3 global climate model, referred to here as CRCM45-CGCM3; and

(c) at 45 km resolution: an ensemble of three simulations of 6-hour mean 10 m wind speeds for the period 1958-2060 using historical emissions and the SRES-A2 emissions scenario, driven by the ECHAM5 global climate model, referred to here as CRCM45-ECHAM5.

In each case, the wind speeds were means of the model output at its 15-minute time steps for the three preceding hours for CRCM45-CGCM3 and the six preceding hours in the case of the CRCM45-ECHAM5. For the CRCM15-ECHAM5 wind speeds were means of the model output at its 5-minute times steps for the six preceding hours. The products of these simulations are used in Chapters 4 and 5 to estimate future wind energy resources. Wind power density will also be examined in this study.

As discussed in Subsection 2.1.4, how well past and future CRCM simulated wind speed distributions can be fit by Weibull distributions is important when considering the choice of calibration method. Figure 2.16 compares the ensembles of past (1971-2000) CRCM45-CGCM3 (five simulations) and the CRCM45-ECHAM5 (three simulations) represented by probability density histogram estimates with the best-fit Weibull distributions. Figure 2.17 compares the ensemble of future (2031-2060) CRCM45-CGCM3 and the CRCM45-ECHAM5 simulated wind speeds represented by probability density histogram estimates with the best-fit Weibull distributions. In both sets of plots the best-fit Weibull distributions are generally better than the comparable plots for the station data and the NARR in Figures 2.4 to 2.6 and 2.11.

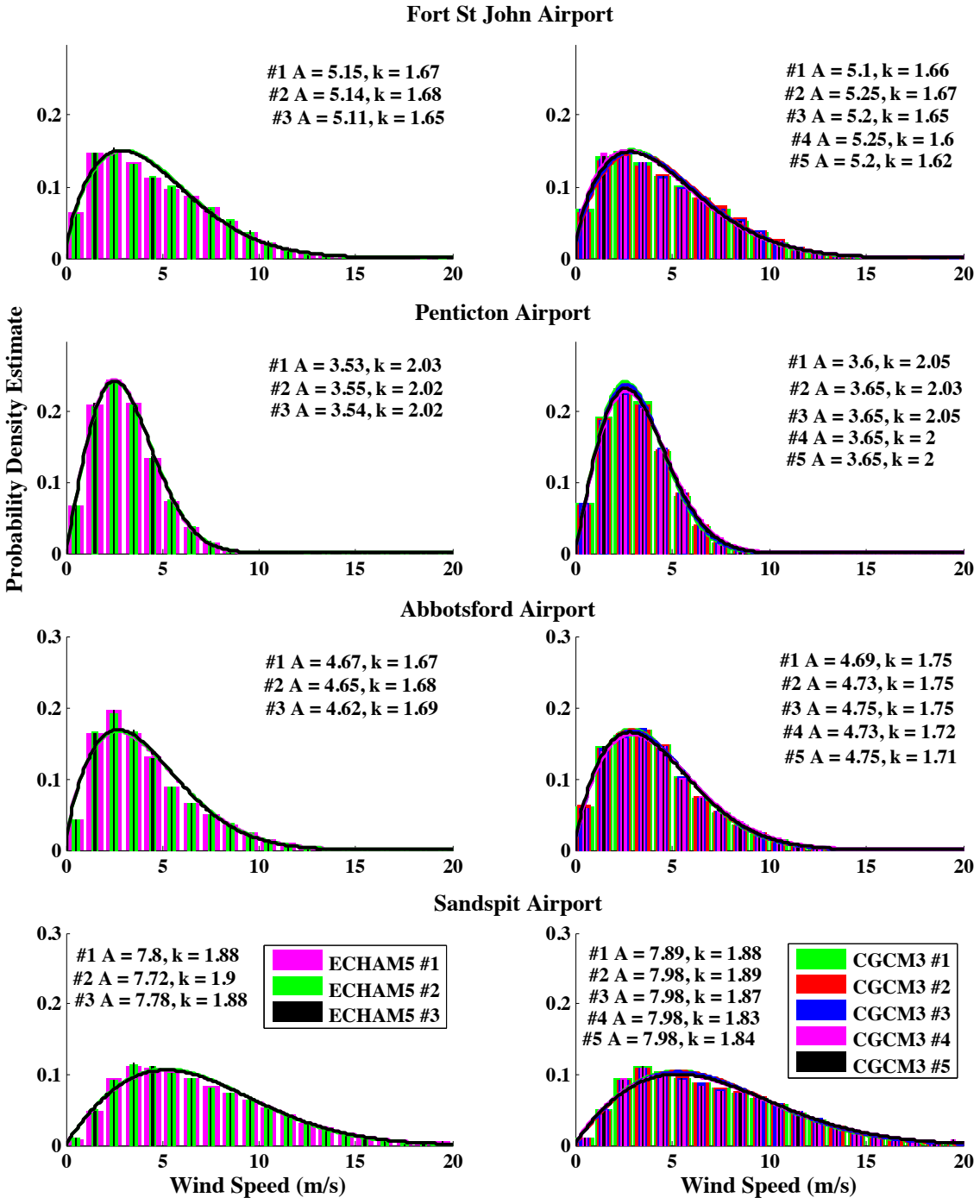

Figure 2.16: Histogram estimates of the probability density function for the CRCM45-CGCM3 and CRCM45-ECHAM5 distributions for 1971-2000 overlaid with best-fit Weibull distributions.

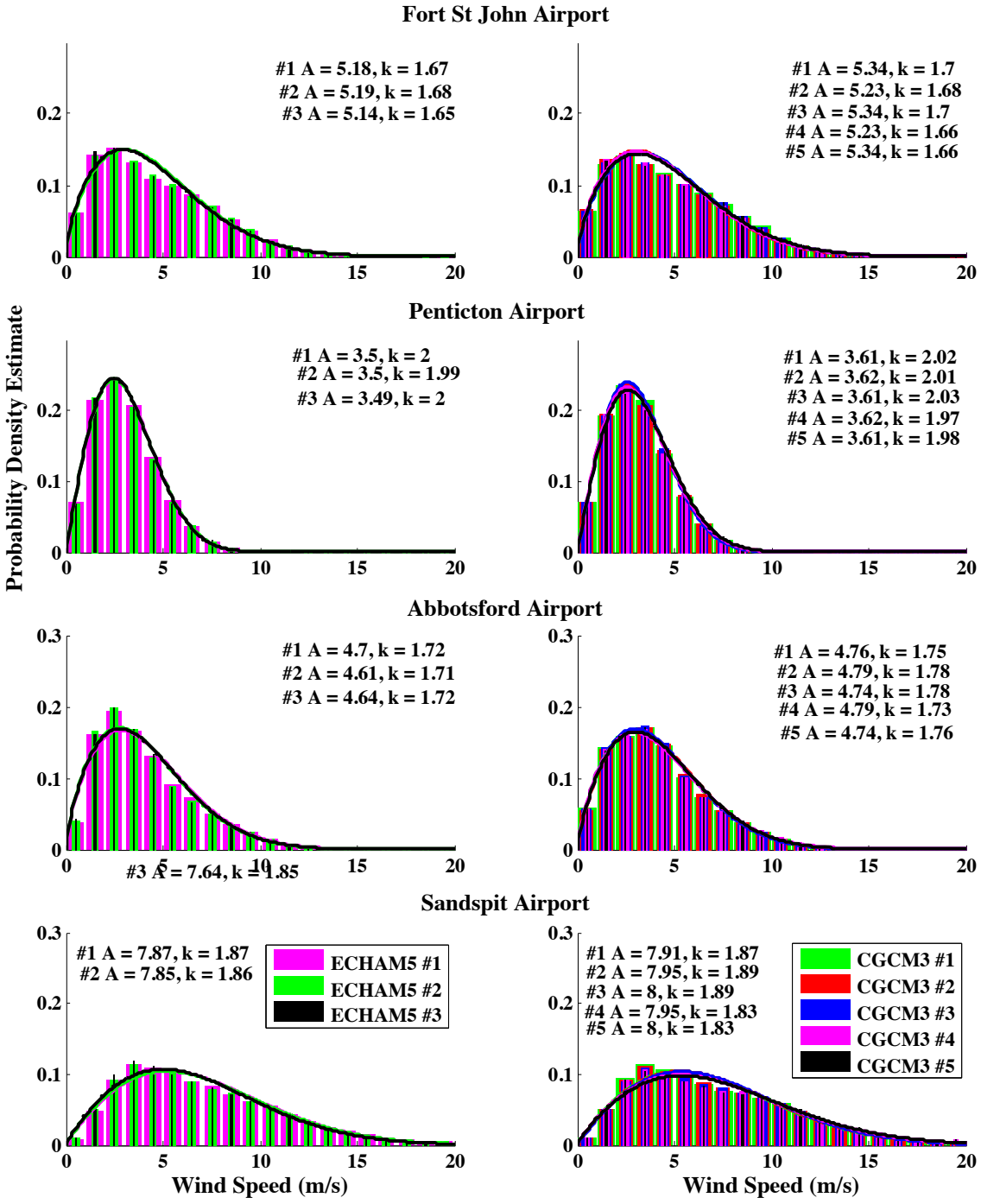

Figure 2.17: Histogram estimates of the probability density function for the CRCM45-CGCM3 and CRCM45-ECHAM5 distributions for 2031-2060 overlaid with best-fit Weibull distributions.

There are several important observations that can be made about Figures 2.16 and 2.17:

- There is very little variation among ensemble members for a given driving GCM.
- The Weibull parameters of the ensemble members vary widely from station to station.
- Despite this, the probability density functions at each station are very similar for the two driving GCMs.
- There is very little change from the past to the future in any of these simulations.

In this Chapter we have introduced the observational datasets and model simulations that we have to work with in projecting the past wind climate into the future. There are some concerns, which will need to be kept in mind. The station data may not accurately represent the wind climate at the stations due to instrumentation and data collection problems. NARR, which might provide wind speeds where observations are not available, may not have sufficient spatial resolution to represent the topography of the region. Spatial resolution may also be an issue for the 45 km grid CRCM model from which the simulations that will be used to project future wind speeds were obtained. In Chapter 4 these concerns are examined by comparing the station observations with NARR wind speeds and CRCM model simulations driven by global reanalysis. In the course of that comparison, the recent past wind climate is estimated using all three views of the regional wind climate (observations, NARR, and CRCM driven by reanalysis).

Chapter 3

Analysis of Historical Wind Speed and Wind Power Density

Using the data and models we have discussed above, the present wind climate at the stations can be compared between the station observations and the CRCM results at grid cells near the station locations. The wind climate away from the stations can also be estimated using the reanalysis or GCM-driven RCM wind speeds at the grid points of the models. In this Chapter, station observations are compared to wind speed time series obtained from the CRCM by (1) comparing the statistical moments and probability distributions of wind speeds from each and (2) examining the temporal correlation between reanalysis driven model simulations and observations over comparable past periods. The goal is to determine how similar the model wind speeds are to observations and thereby evaluate how the gridded wind speeds might be used to estimate present wind power resources.

3.1 Observed Wind Climate at Stations and Assessment of the Present-Day Wind Resource

The means of the corrected hourly wind speeds observed at the stations for the period 1979-2011 are shown in Figure 3.1. Figure 3.2 shows the standard deviation of those wind speeds at each location. Figures 3.3 and 3.4 show the corresponding values for the wind power density, which has been calculated using as 1.225 kg/m^3 (approximately the density at sea level and 15 degrees Celsius) as the density of air and the equation in Chapter 1. The time period (1979-2011) is the period of overlap

of availability of NARR wind speeds and the EC homogenized monthly mean wind speeds.

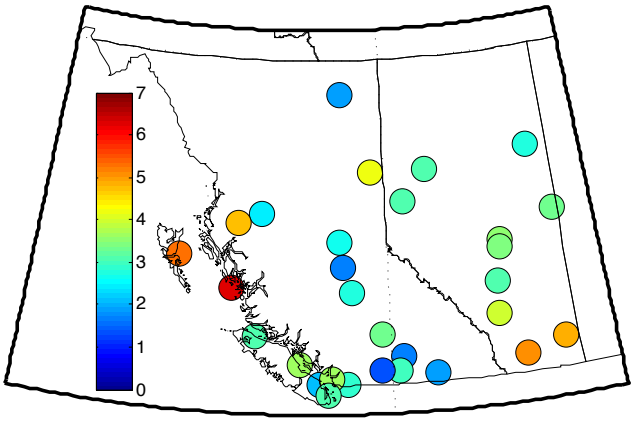

Figure 3.1: Means of the corrected hourly wind speeds at the stations for 1979-2011 (m/s).

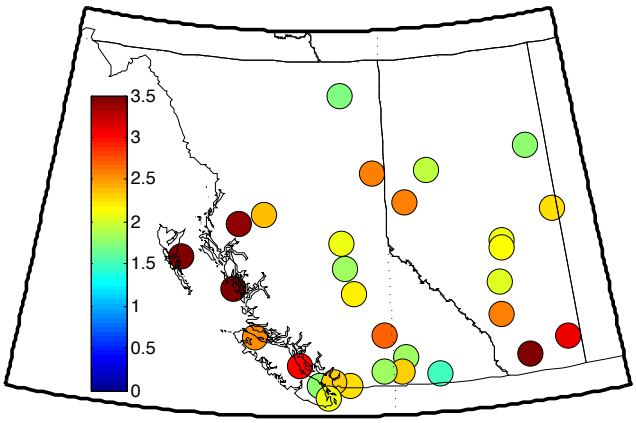

Figure 3.2: Standard deviations of the corrected hourly wind speeds at the stations for 1979-2011 (m/s).

Based upon Figures 3.1-3.4, the observed wind climate in the region can be organized geographically into several sub-regions. According to Figure 3.1, the stations in Alberta with the exception of Lethbridge and Medicine Hat in southern Alberta have generally similar mean wind speeds in the 3 to 4 m/s range over the 1979-2011 period that is somewhat low for commercial development of wind farms (see Subsection 2.1.3). The mean wind speeds at all stations in the interior and south coast of British Columbia and Vancouver Island vary with location but are all too low for wind farms.

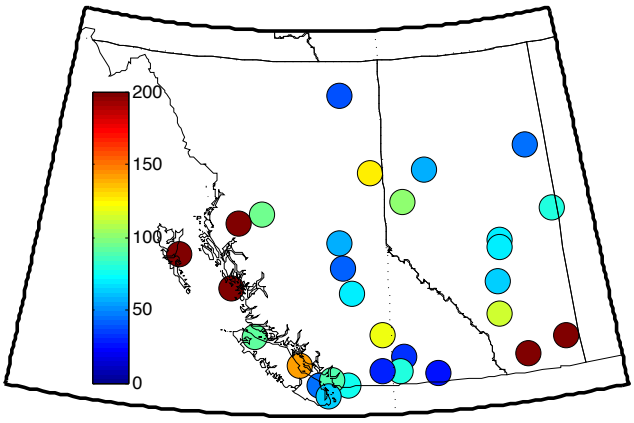

Figure 3.3: Means of the wind power density at the stations for 1979-2011 (W/m^2).

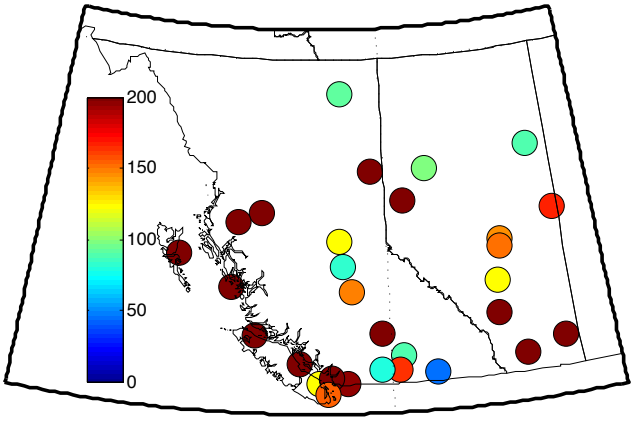

Figure 3.4: Standard deviations of the wind power density at the stations for 1979-2011 (W/m^2).

The north coast stations at Sandspit, McInnes Island, and Terrace have higher mean wind speeds that are in the range suitable for wind farms. According to Figure 3.2, the variability of the wind speed over the period is highest in southern Alberta, along the northern coast of British Columbia, and northern Vancouver Island, with some stations along the east slope of the Rocky Mountains in the north (Fort St. John and Grande Prairie) also having high standard deviations. Other stations in Alberta and the interior of British Columbia show generally low variability, with the exception of the Kamloops station. The interior British Columbia stations are somewhat less uniform in their standard deviations than those in Alberta away from the mountains. Similar patterns for wind power and its standard deviation are shown in Figures 3.3

and 3.4.

3.2 NARR Compared to Station Observations

Figures 3.5 and 3.7 show the percentage bias of the NARR mean wind speeds and mean of the cubed wind speeds relative to the corresponding station quantities. Figures 3.6 and 3.8 show the corresponding ratios of standard deviation of NARR quantities to station quantities.

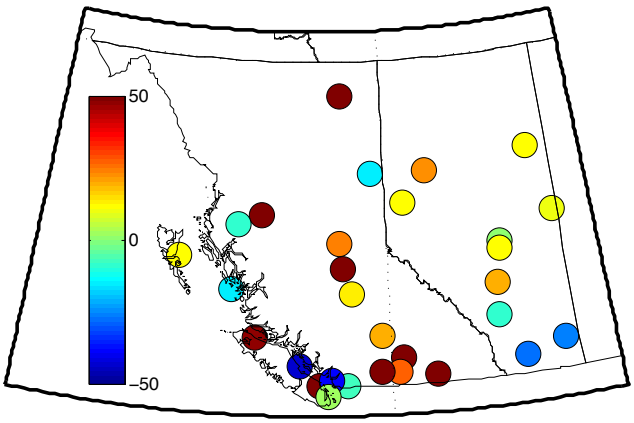

Figure 3.5: Percentage bias of the mean NARR 3-hourly wind speeds with respect to the mean station observations for 1979-2011.

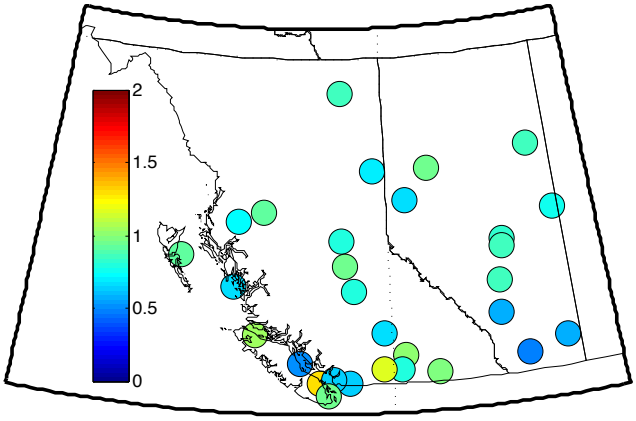

Figure 3.6: Ratio of standard deviation of the NARR 3-hourly wind speeds to the standard deviation of the station observations for 1979-2011.

There is no evident pattern to the biases between NARR and the station observations. In particular, even the portion of the region east of the Rocky Mountains, which is the most homogeneous topographically, does not show consistency among the station locations as to bias of mean or standard deviation of wind speed. Nearly all SD ratios are less than 1 for both wind speed and wind power density, so NARR underestimates sub-diurnal variability of both.

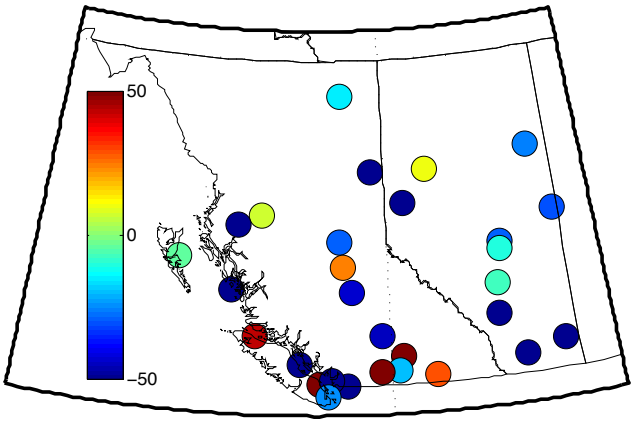

Figure 3.7: Percentage bias of the mean NARR 3-hourly wind speeds cubed with respect to the mean station observations cubed for 1979-2011.

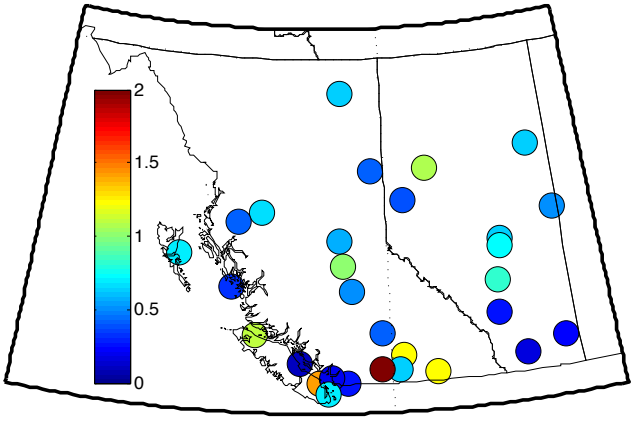

Figure 3.8: Ratio of the standard deviation of the NARR 3-hourly wind speeds cubed to the standard deviation of the station observations cubed for 1979-2011.

A more detailed look at the NARR wind speeds can be obtained by looking at histogram estimates of the probability density function for the representative stations. To allow for comparison with CRCM15-R and CRCM45-R, the NARR wind speeds

for the period 1979-1995 are used as during that period CRCM15-R and CRCM45-R are also available. In Figure 3.9, kernel density estimates for NARR wind speed distributions are plotted with histogram estimates of the probability density function of the observed hourly wind speeds for the representative stations for that period. The observed hourly wind speeds used are the corrected versions of those provided by EC for the same times as the NARR wind speeds (i.e., every third hour, not means) as the NARR wind speeds are snapshots. Each kernel density estimate is of the NARR wind speed distribution at the station location obtained by bilinear interpolation using the four nearest grid points to the station location.

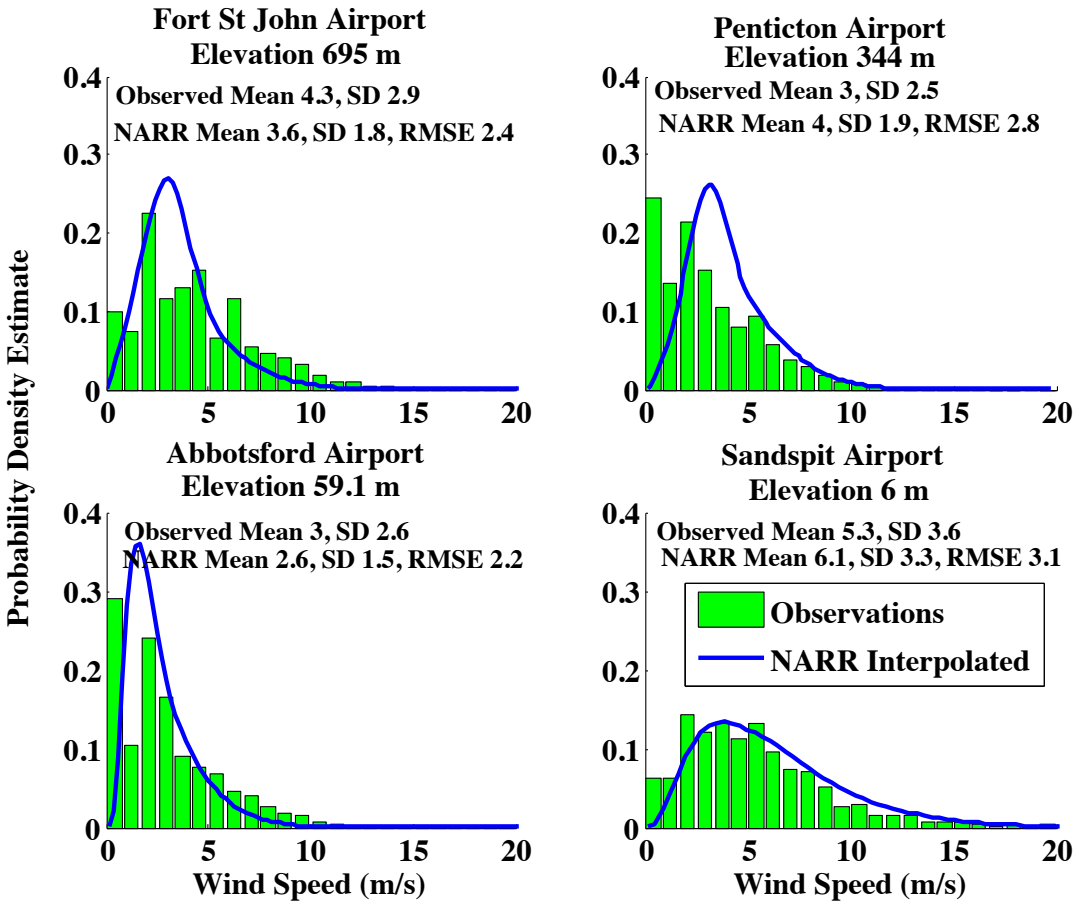

Figure 3.9: Histogram estimates of the probability density function for the corrected station wind speeds distributions every third hour plotted with kernel density estimates of NARR distributions for 1979-1995.

Figure 3.9 shows that although NARR represents the observed wind speed distribution at Sandspit fairly well, it compares poorly at the other three representative stations. NARR tends to underestimate the standard deviation in all cases (consis-

tent with Figure 3.6) and under-predicts the number of high wind speeds at Fort St. John and Abbotsford. The NARR means are also in poor agreement with the station observations at all four locations. A contributing factor to all of these differences is the spuriously large number of zero wind speed values in the observational record.

In the discussion of the large percentage of zeros in the station observations in Section 2.1.2, it was mentioned that in the last few years some stations appear to have different measuring equipment or recording practices that have in some cases greatly reduced the large percentage of wind speeds recorded as zero. If only the recent wind speed distributions are used, it appears that NARR may be a better representation of the wind speed at those stations. Figure 3.10 shows the kernel density estimates of

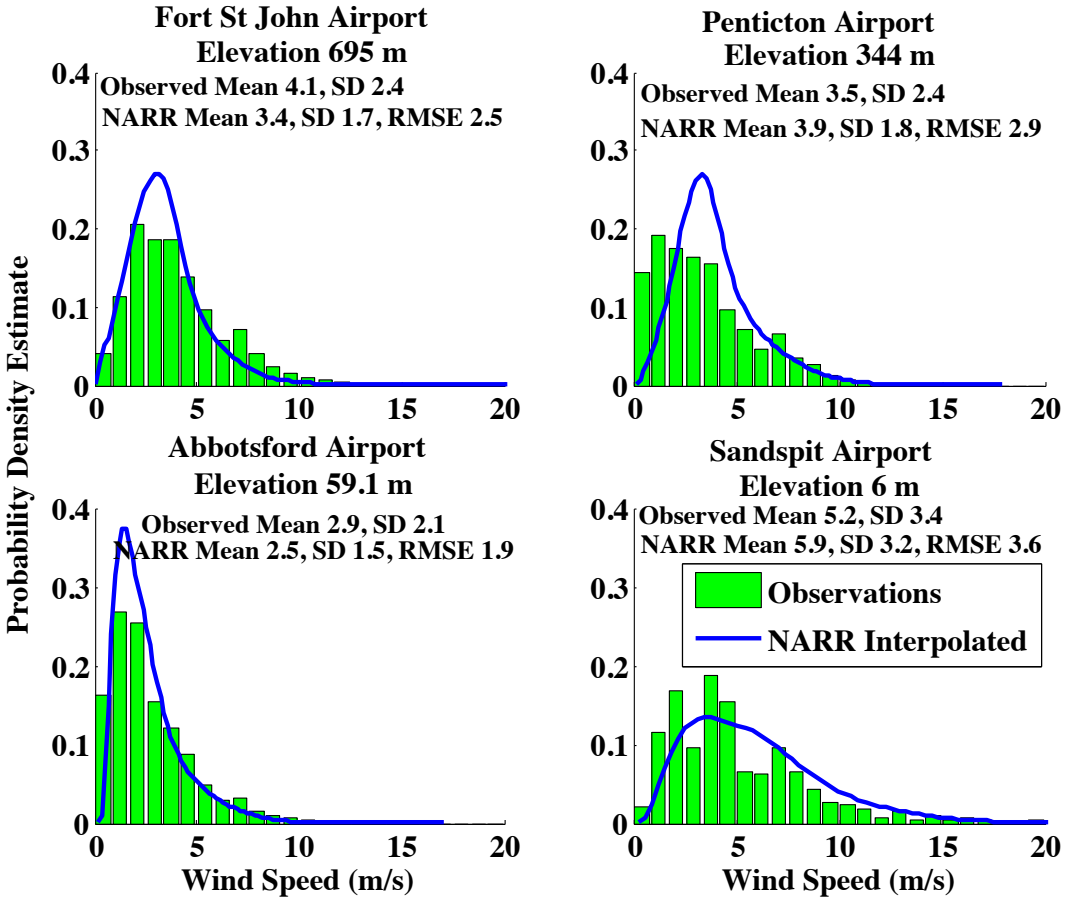

Figure 3.10: Histogram estimates of the probability density function for the corrected station wind speeds distributions every third hour plotted with kernel density estimates of the NARR distributions for 2013-2014.

the interpolated NARR wind speed probability density distribution at the representative stations plotted with a histogram estimate of probability density function of

the observed wind speed distribution. Especially in the case of Abbotsford and Fort St. John, there is an apparent improvement in the match between NARR and the observations over that shown in Figure 3.9. In particular, the shapes of the distributions are similar. Penticton may be a special case as NARR topography is such that the valley in which the station is located is not represented at all in NARR, resulting in a mean wind speed higher than that observed with less variability. The mean and standard deviation at Sandspit may also be affected by NARR not modelling the topography well.

Generally, when comparing station observations to NARR wind speeds, it is hard to determine if the disagreement is due to problems with the station data or biases in NARR resulting from not modelling the topography or assimilating enough near surface wind speed data. The improvement in agreement between them in recent years suggests that the poor quality of the station data is at least partially to blame.

3.3 CRCM15-R and CRCM45-R Compared to Station Observations

Figures 3.11 and 3.13 show the percentage biases of the CRCM15-R and CRCM45-R mean wind speeds and mean wind speed cubed relative to the station observations. Figures 3.12 and 3.14 show the corresponding ratios of standard deviation of CRCM15-R and CRCM45-R wind speeds and mean wind speed cubed.

Comparison of the CRCM15-R and CRCM45-R biases in Figures 3.11 - 3.14 shows the effect of increased resolution in the CRCM15-R. The CRCM15-R mean wind speed bias varies more between stations in Alberta, with a lower bias at most stations than that for the CRCM45-R. The coastal stations are biased high in both the CRCM15-R and CRCM45-R mean wind speeds, although near coastal stations at Terrace and Smithers are biased high in the CRCM45-R and low in the CRCM15-R. It appears that the CRCM15-R is resolving local topography at these stations and also at those stations in the interior of British Columbia where CRCM45-R does not. The ratios of the standard deviations in the wind speeds of the models to the observations are similar in both CRCM15-R and CRCM45-R, although the standard deviation ratios are somewhat lower in the interior for CRCM15-R than for CRCM45-R. Generally, both have ratios close to 1 along the coast and in Alberta. For wind speed cubed and the standard deviations of wind speed cubed there are more negative biases of higher

magnitude, and also the standard deviation ratio is more heterogeneous. There is also an indication of higher variability in the 15km than the 45km, i.e., more standard deviation ratios greater than 1.

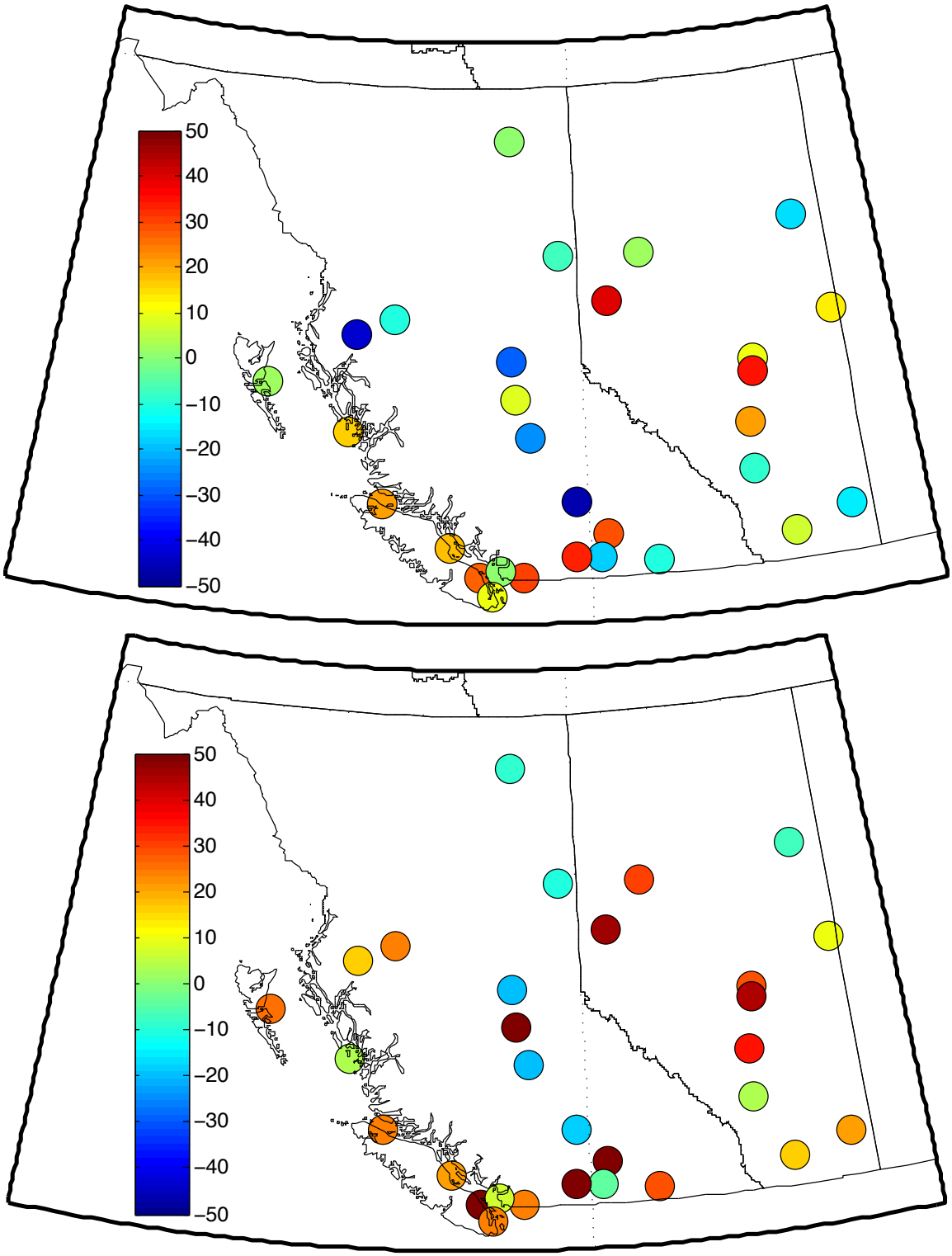

Figure 3.11: Percentage biases of the mean CRCM15-R wind speeds with respect to the mean station observations 1973-1995 (top panel) and of the mean CRCM45-R wind speeds with respect to the mean station observations for 1973-2001 (bottom panel).

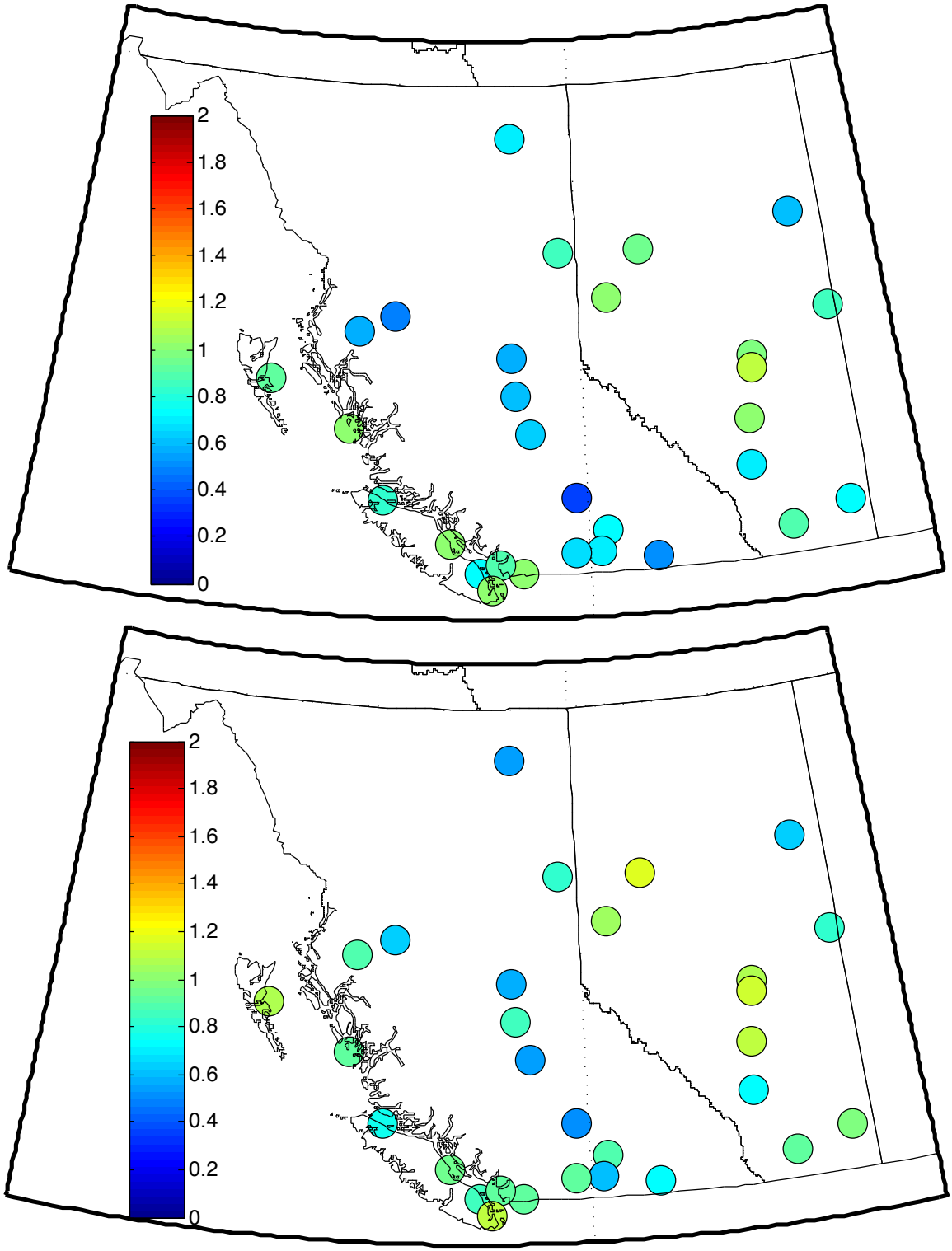

Figure 3.12: Ratios of the standard deviation of CRCM15-R wind speeds to the standard deviation of the station observations 1973-1995 (top panel) and of the standard deviation of CRCM45-R wind speeds to the standard deviation of the station observations 1973-2001 (bottom panel).

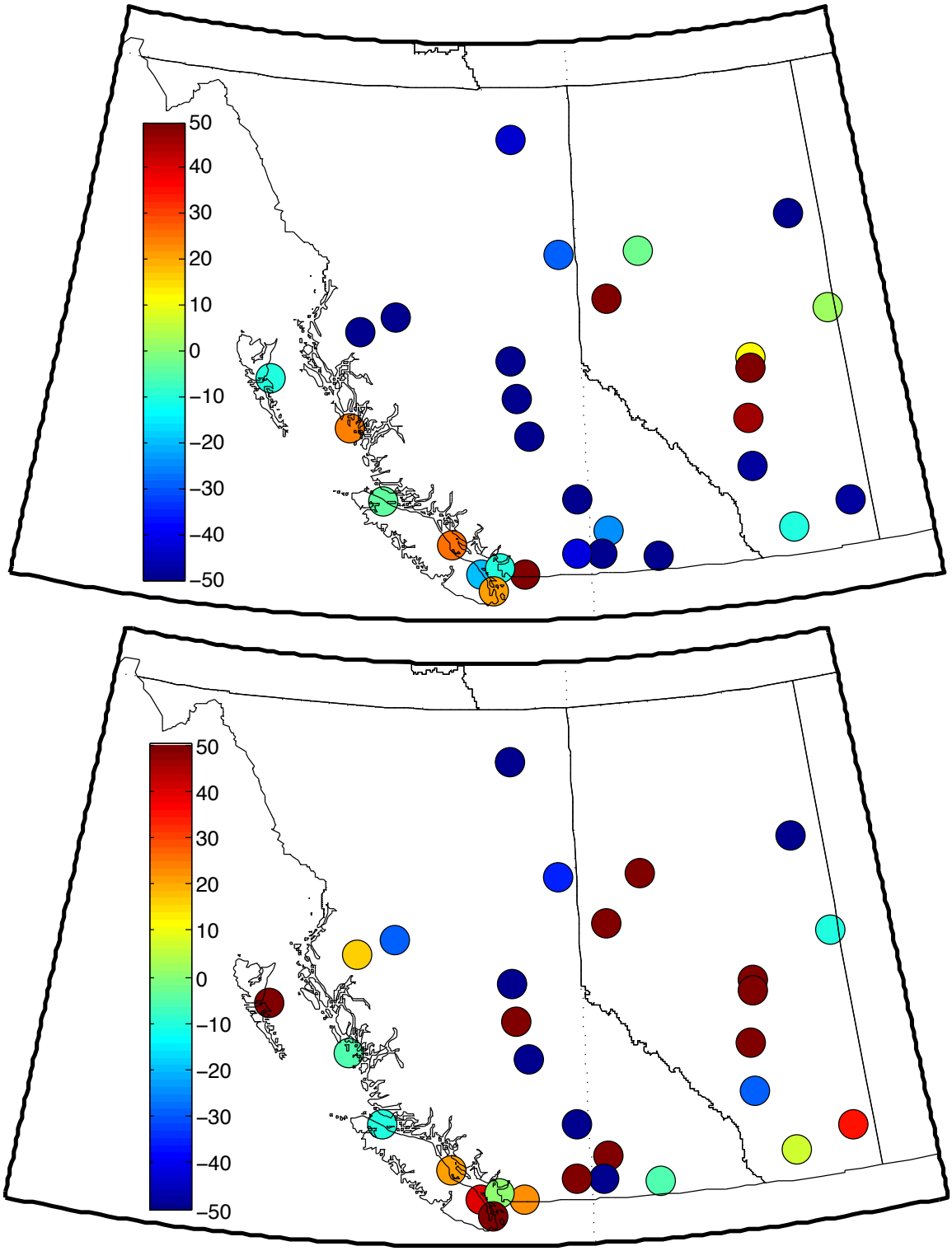

Figure 3.13: Percentage biases of the mean CRCM15-R wind speeds cubed with respect to the mean station observations cubed 1973-1995 (top panel) and of the mean CRCM45-R wind speeds cubed with respect to the mean station observations cubed 1973-2001 (bottom panel).

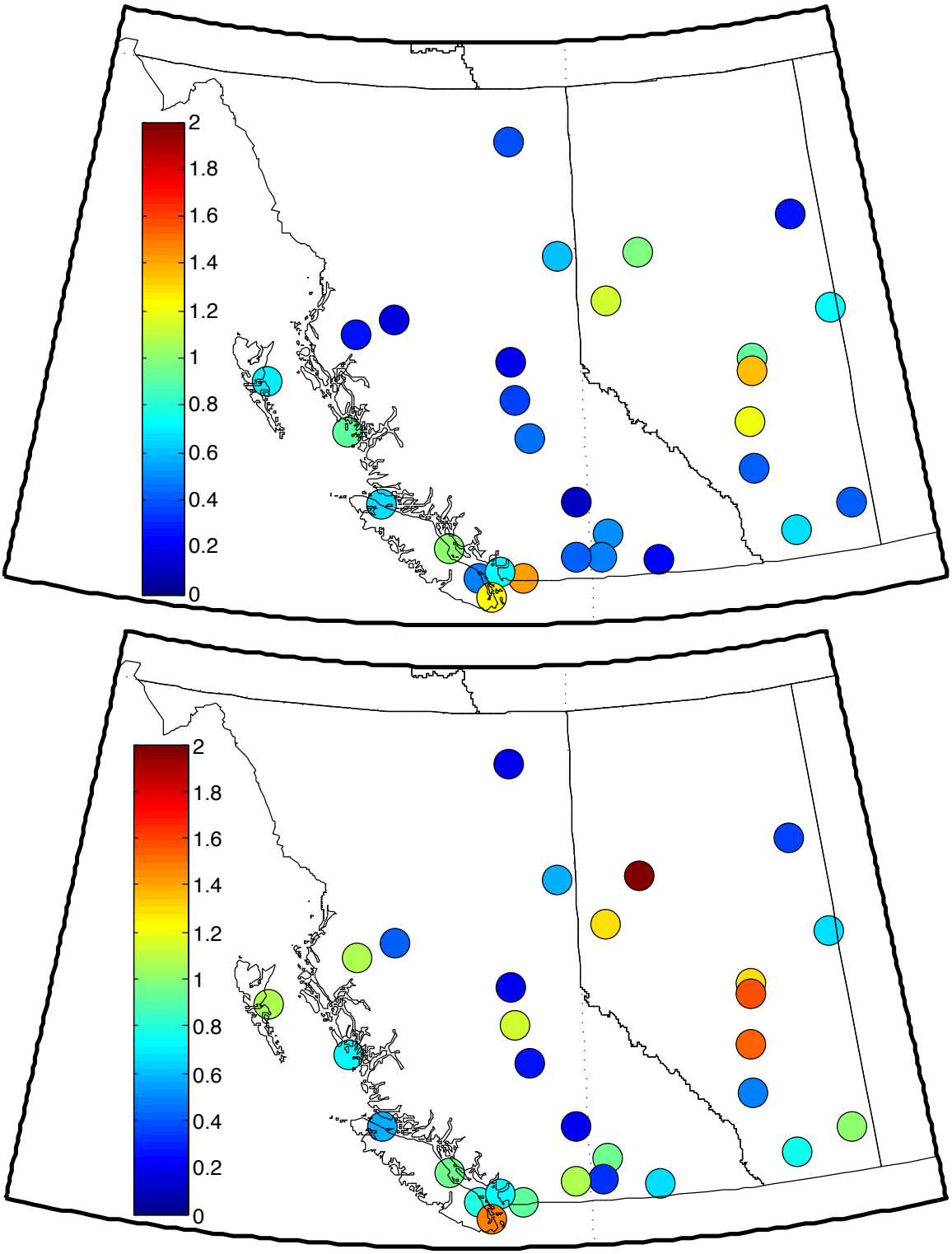

Figure 3.14: Ratios of the standard deviation of CRCM15-R wind speeds cubed to the standard deviation of the station observations cubed 1973-1995 (top panel) and of the CRCM45-R wind speeds cubed to the standard deviation of the station observations cubed 1973-2001 (bottom panel).

The effect of increased spatial resolution can also be assessed by looking at the histogram estimates of probability density functions. In Figure 3.15 station observations are plotted with kernel density estimates of the CRCM15-R and CRCM45-R distributions for the four representative stations. From Figure 3.15 there is no evident improvement in the simulation of the observations by the 15 km simulation compared to the 45 km time simulation.

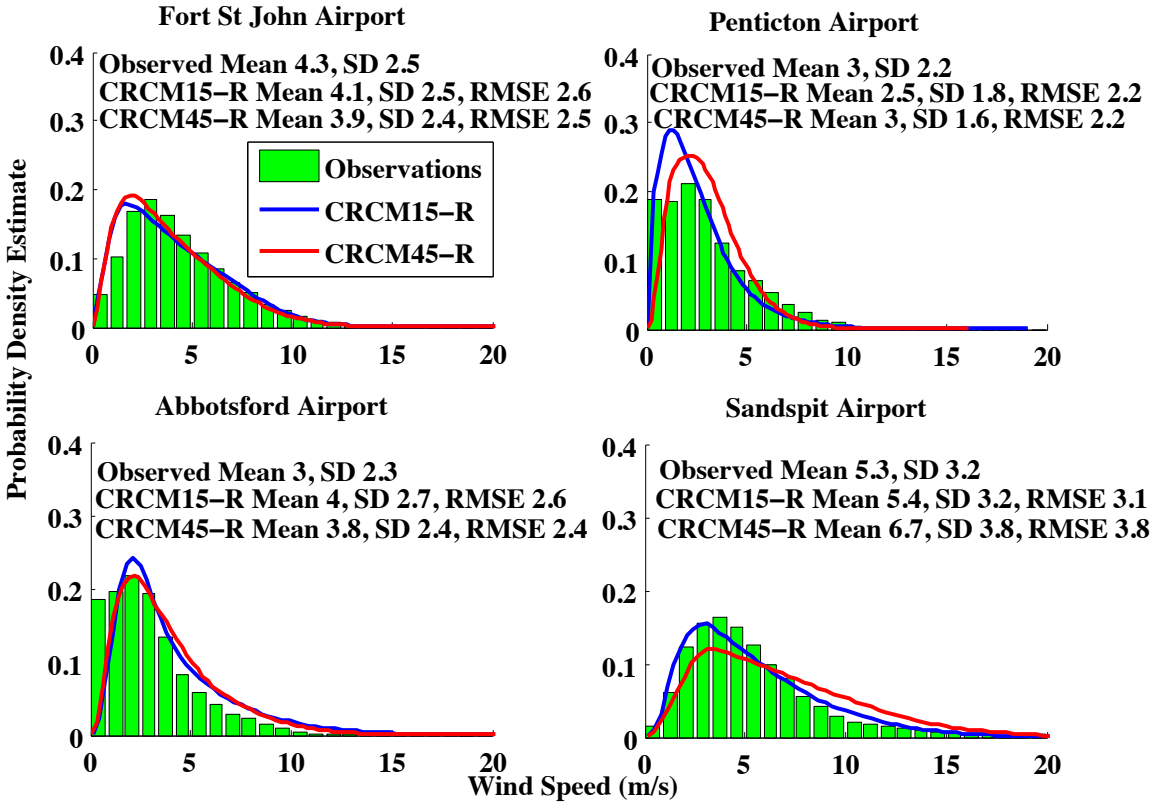

Figure 3.15: Histogram estimates of the probability density function for the corrected six-hourly mean station wind speed distributions plotted with kernel density estimates of the CRCM15-R and CRCM45-R distributions for 1979-1995. Mean and SD of each together with RMSE with respect to observations.

3.4 Root Mean Square Error of the Reanalysis Time Series with Respect to the Observations

One metric by which the capacity of NARR and the CRCM-R to reproduce the station observations may be assessed is the root mean square error (RMSE) of each with respect to the observation time series. The RMSE includes three pieces of information regarding two time series: the difference in mean, the difference in variance, and the correlation. The inclusion of correlation information makes it fundamentally different than the bias measures considered above.

According to (Mesinger et al., 2006), NARR assimilates surface wind speeds. Consequently, when wind speeds from the NARR grid points around a station location are interpolated to the station location, the interpolated wind speed should be relatively close to the observed wind speed. The situation for the CRCM-R is different as it does not assimilate regional observations. Hence it would not be expected to reproduce the observations as well as NARR. In particular, the RMSE should be lower for NARR with respect to the observations as it should exhibit a higher temporal correlation with the observations.

In Table 3.1, the RMSE of the NARR, CRCM15-R, and CRCM45-R time-series with respect to the observation time series are provided. NARR has a lower RMSE than both CRCM45-R and CRCM15-R at 22 of the 30 stations.Thus NARR performs better than the reanalysis-driven CRCM, presumably due to its assimilation of finer-scale observations. Comparing CRCM15-R and CRCM45-R, CRCM15-R has a lower RMSE at 20 of the 30 stations, showing that increased resolution reduces the RMSE somewhat for the stations even without assimilation of regional observations.

The above conclusions are supported by application of the binomial test. Adopting the null hypothesis that the CRCM15-R and CRCM45-R models produce results that have about equal RMSE, then using the binomial test, that hypothesis cannot be rejected at a confidence level of 95%. However, if the null hypothesis is that the NARR and either CRCM15-R and CRCM45-R model produce time series that have equally low RMSE, then that hypothesis can be rejected at a confidence level of 95%.

No.	Station Name	CRCM15-R (m/s)	NARR (m/s)	CRCM45-R (m/s)
1	Abbotsford	2.63	1.74	2.38
2	Castlegar	1.63	2.25	1.92
3	Comox	2.86	2.71	2.98
4	Fort Nelson	1.72	1.74	1.60
5	Fort St John	2.58	1.94	2.48
6	Kamloops	3.00	2.42	2.67
7	Kelowna	1.99	3.24	2.57
8	McInnes Island	3.84	2.67	3.53
9	Nanaimo	2.17	3.26	2.39
10	Penticton	2.19	2.52	2.20
11	Port Hardy	2.40	2.11	2.39
12	Prince George	1.95	1.64	1.73
13	Princeton	1.77	3.94	2.97
14	Quesnel	1.72	2.53	2.35
15	Sandspit	3.07	2.71	3.83
16	Smithers	1.91	2.87	2.13
17	Terrace	3.95	3.08	4.04
18	Vancouver International	2.52	2.46	2.68
19	Victoria International	2.32	1.78	2.60
20	Williams Lake	1.98	1.52	1.91
21	Calgary International	2.58	2.04	2.59
22	Cold Lake	2.54	1.57	2.41
23	Edmonton City Centre	2.31	1.37	2.67
24	Edmonton International	2.85	1.46	3.09
25	Fort McMurray	1.73	1.37	1.67
26	Grande Prairie	2.74	1.77	2.87
27	Lethbridge	3.15	2.81	3.25
28	Medicine Hat	2.91	2.45	3.43
29	Peace River	1.88	1.51	2.35
30	Red Deer	2.57	1.50	2.89

Table 3.1: RMSE for six hour mean speeds between the observations and NARR, CRCM15-R, and CRCM45-R for the period 1979-1995. Cyan cells indicate that the NARR RMSE is the lower than either the CRCM15-R or CRCM45-R RMSE. Mauve indicates lower of the CRCM15-R RMSE and the CRCM45-R RMSE.

3.5 Temporal Correlation of Reanalysis Time Series with Observations

The conclusion in Section 3.4 that the lower RMSE for NARR with respect to the observations is likely due to higher correlations due to the assimilation of surface observations can be assessed by investigating the temporal correlation of NARR and CRCM-R with observations. Figures 3.16 - 3.18 display the correlation coefficients for daily mean wind speeds for two distinct 22-year periods (1979-2000 for NARR in Figure 3.16 and 1974-1995 for CRCM15-R and CRCM45-R in Figures 3.17 and 3.18, respectively). In the case of NARR, which provides wind speeds every three hours, the correlation is between the means of eight consecutive NARR wind speeds and the means of 24 consecutive observed hourly wind speeds. In the case of the CRCM15-R and CRCM45-R, which are six-hour means, the correlation is between the means of four consecutive wind speeds and the mean of 24 consecutive observed hourly wind speeds. These R^2 values are each also presented in Table 3.2.

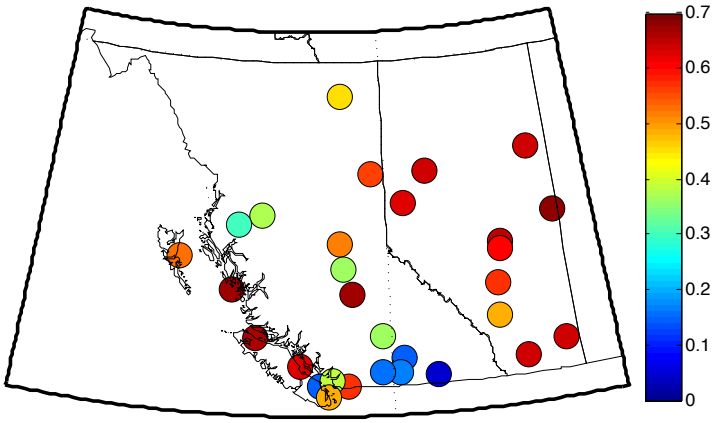

Figure 3.16: R^2 between the daily means of the NARR wind speeds and the observations 1979-2000.

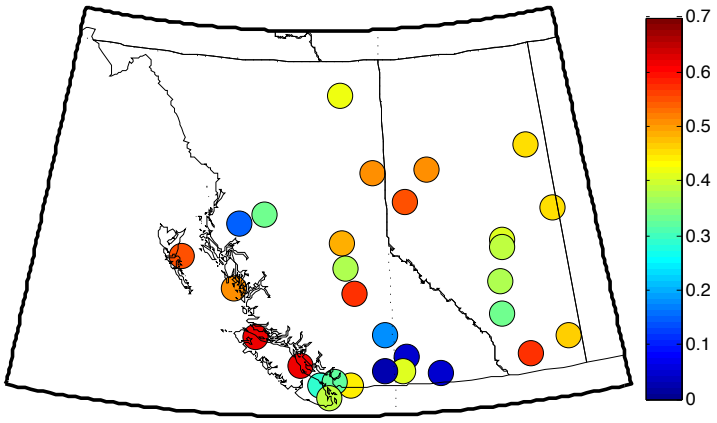

Figure 3.17: R^2 between the daily means of CRCM15-R wind speeds and the observations 1974-1995.

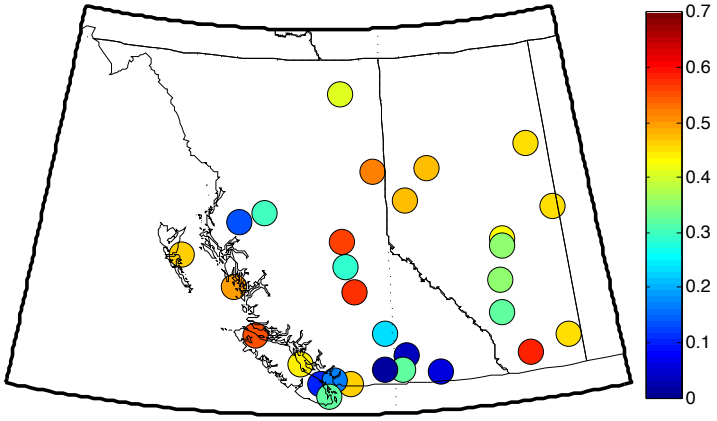

Figure 3.18: R^2 between the daily means of CRCM45-R wind speeds and the observations 1974-1995.

The NARR time series is better correlated with the observation time series than either of the CRCM15-R and CRCM45-R time series. This is to be expected as NARR assimilates at least some regional observations, whereas the CRCM15-R and CRCM45-R simulations are only driven at the boundaries by global reanalysis. The CRCM15-R time series is more highly correlated with the observation time series than CRCM45-R time series at the majority of station locations. According to the binomial test, this improvement in CRCM-15R compared to CRCM-45R is significant at the 95% confidence level.

No.	Station Name	CRCM15-R (m/s)	NARR (m/s)	CRCM45-R (m/s)
1	Abbotsford	0.439	0.577	0.461
2	Castlegar	0.054	0.047	0.062
3	Comox	0.623	0.631	0.441
4	Fort Nelson	0.416	0.449	0.413
5	Fort St John	0.505	0.561	0.515
6	Kamloops	0.182	0.361	0.239
7	Kelowna	0.045	0.148	0.034
8	McInnes Island	0.507	0.671	0.494
9	Nanaimo	0.292	0.151	0.107
10	Penticton	0.407	0.171	0.320
11	Port Hardy	0.614	0.663	0.553
12	Prince George	0.488	0.524	0.567
13	Princeton	0.032	0.158	0.011
14	Quesnel	0.382	0.364	0.288
15	Sandspit	0.550	0.525	0.462
16	Smithers	0.335	0.374	0.304
17	Terrace	0.144	0.299	0.134
18	Vancouver International	0.328	0.385	0.164
19	Victoria International	0.391	0.488	0.325
20	Williams Lake	0.579	0.671	0.578
21	Calgary International	0.331	0.482	0.324
22	Cold Lake	0.454	0.678	0.459
23	Edmonton City Centre	0.414	0.651	0.429
24	Edmonton International	0.383	0.607	0.350
25	Fort McMurray	0.455	0.639	0.456
26	Grande Prairie	0.550	0.631	0.479
27	Lethbridge	0.579	0.639	0.580
28	Medicine Hat	0.467	0.643	0.449
29	Peace River	0.509	0.641	0.476
30	Red Deer	0.372	0.574	0.351

Table 3.2: Temporal correlation coefficient R^2 for daily mean speeds between the observations and NARR for 1979-2000 and CRCM-R for 1974-1995. Cyan indicates NARR has larger R^2 than either CRCM15-R or CRCM45-R and mauve indicates that the CRCM15-R has larger R^2 than CRCM45-R

One noteworthy feature of Table 3.2 is that the temporal correlations are lowest for NARR at Castlegar and Kelowna and for both CRCM15-R and CRCM45-R at Princeton, Kelowna, and Castlegar. These stations are located in the valleys in the interior of British Columbia that the model topography does not adequately represent.

3.6 Spatial distribution of wind according to NARR and CRCM-R

The maps of mean wind speed for NARR, CRCM45-R and CRCM15-R are shown in Figure 3.19. The station mean wind speeds at the stations are shown in Figure 3.19 as smaller coloured patches so as not to obscure the grid boxes, but are otherwise identical to those in Figure 3.1. Should NARR, CRCM45-R and CRCM15-R be used as representative of the wind power resource in the region? With the exception of southern Alberta, the three sets of gridded means are roughly consistent with each other and with the station means. In southern Alberta NARR does not agree with either the CRCM45-R or the CRCM15-R wind speeds or the station mean wind speeds at Lethbridge and Medicine Hat. Since NARR's spatial resolution at 32 km is intermediate between the CRCM45-R and CRCM15-R one might expect an intermediate degree of granularity, but this does not occur. The discussion in subsection 2.2.3 may be relevant here.

Maps of mean wind power density for NARR, CRCM45-R and CRCM15-R are shown in Figure 3.20. Again, the station mean power densities at the stations are shown in Figure 3.20 as smaller coloured patches so as not to obscure the grid boxes, but are otherwise identical to those in Figure 3.3. According to the National Renewable Energy Laboratory (National Renewable Energy Laboratory, 2014) a wind power density of 150 to 200 W/m^2) or more is suitable for most utility-scale wind turbine applications. The CRCM45-R and CRCM15-R maps both suggest that southern Alberta meets this criterion. NARR does not at least close to Lethbridge, which itself has a wind power density at the station that more than meets the criterion. Other locations on the maps also appear to be suitable for utility-scale applications according to the CRCM-R. In particular, the extreme southwest corner of the Province of Saskatchewan (east of the Medicine Hat station), portions of northern British Columbia, as well as along the north coast of British Columbia and off-shore.

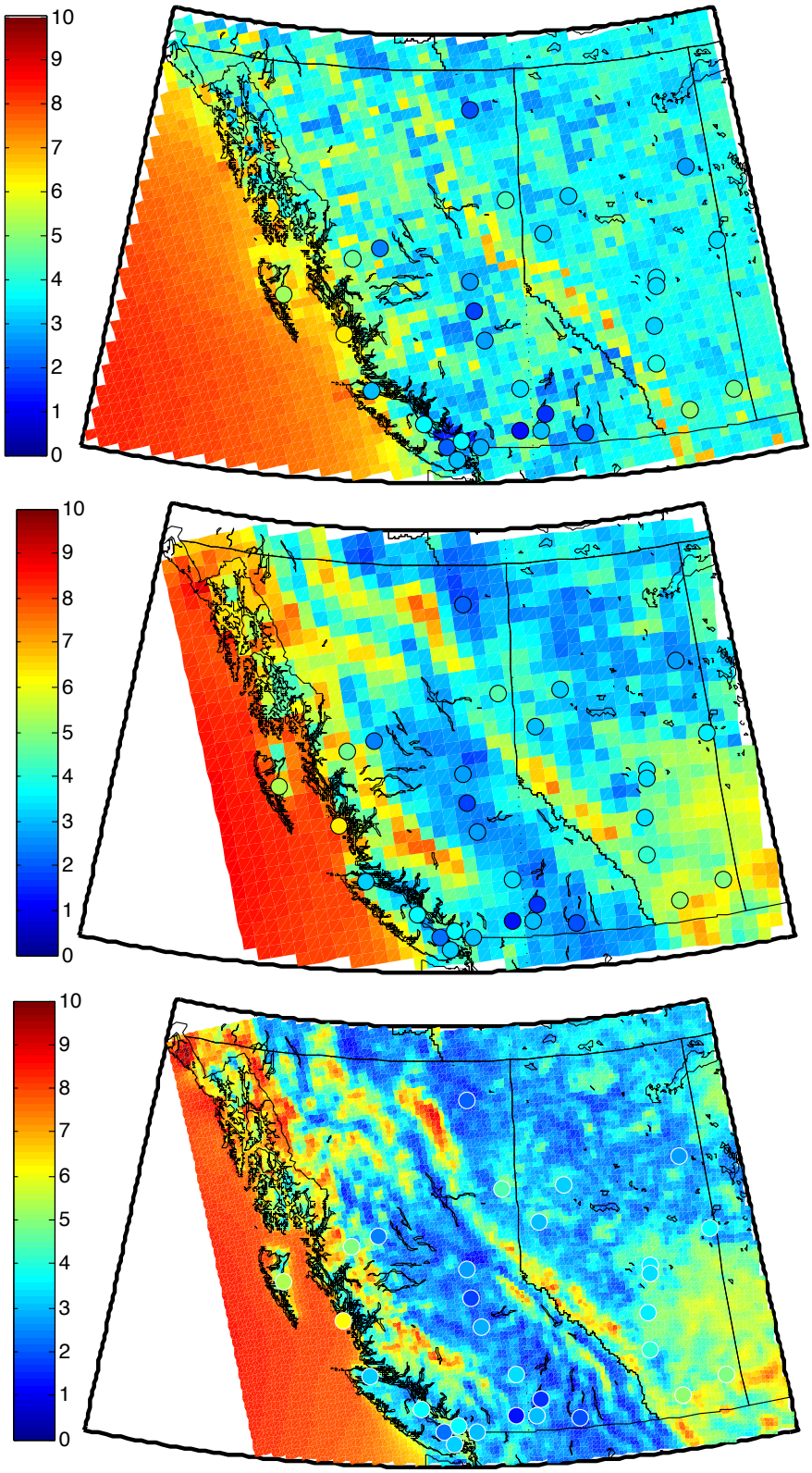

Figure 3.19: Means of the NARR 3-hourly wind speeds for 1979-2011 (top panel), CRCM45-R for 1973-2001 (middle panel), and CRCM15-R for 1973-1995 (lower panel) with the station means (scale in m/s).

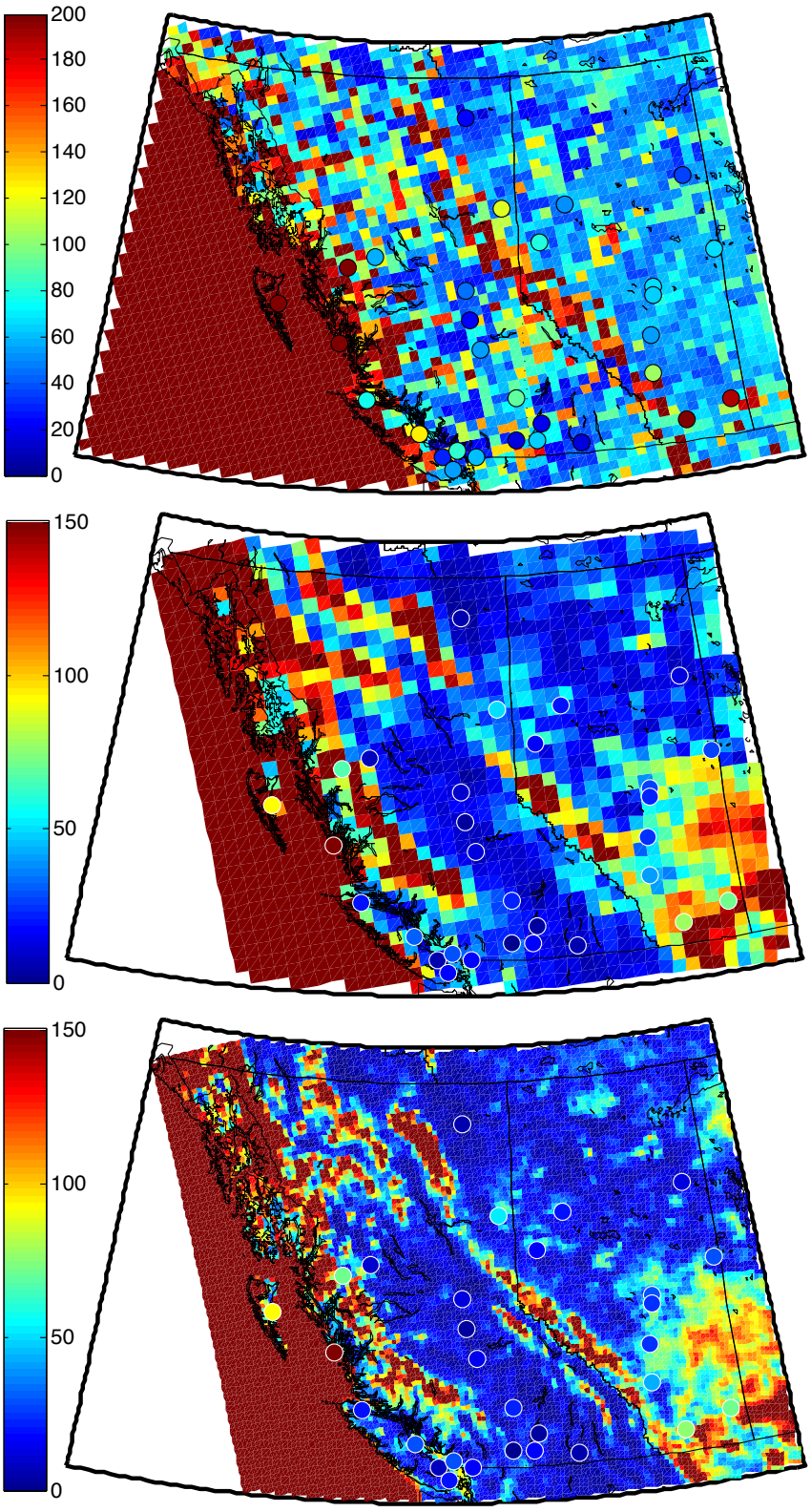

Figure 3.20: Means of the wind power for NARR for 1979-2011 (top panel), CRCM45-R for 1973-2001 (middle panel), and CRCM15-R for 1973-1995 (lower panel) with the station means (scale in W/m^2).

3.7 Calibration of Future-simulated Wind Speeds

In this Chapter a reanalysis product and simulations driven by reanalysis have been compared with observations. Before examining simulations of future wind speeds, it is worthwhile to consider how well RCM simulations of wind speeds over an historical period compare to observations. This analysis will demonstrate that calibration will be necessary for projected wind speeds. In Figure 3.21, histogram estimates

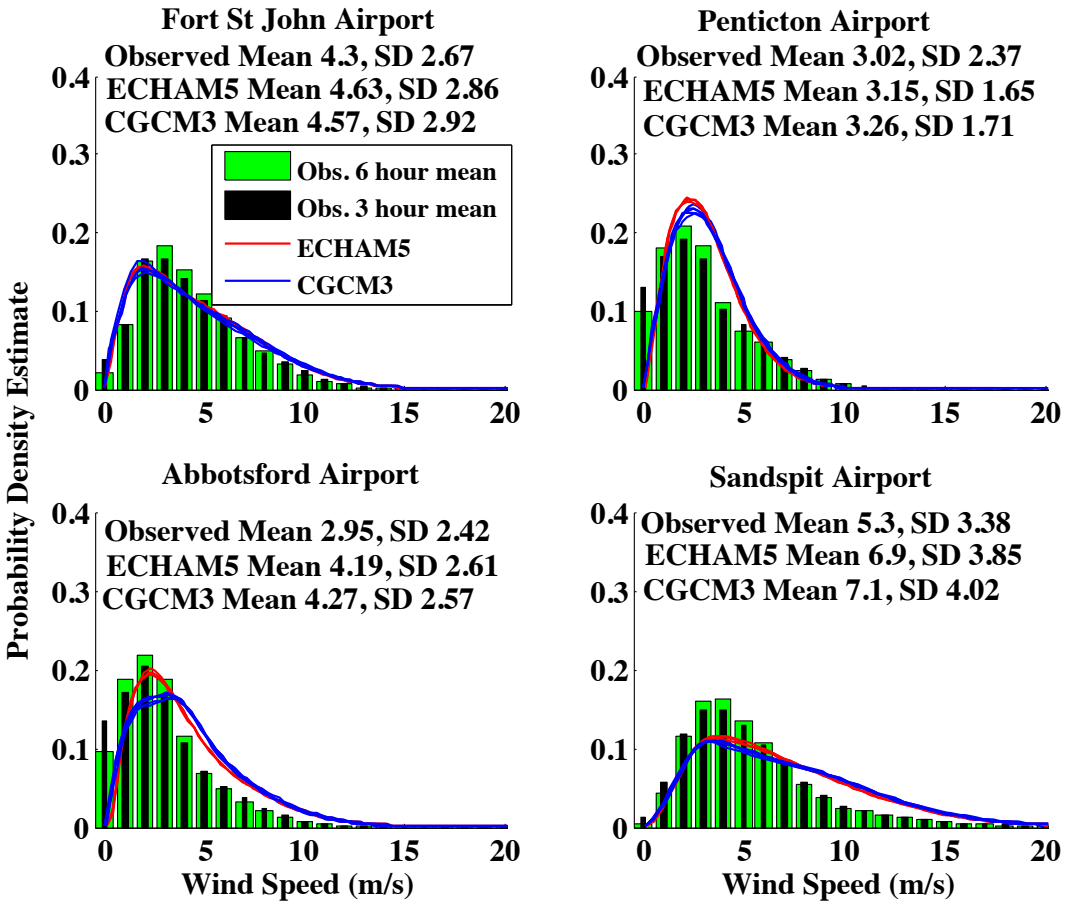

Figure 3.21: Histogram estimates of the probability density function for the corrected three- and six-hourly mean station wind speed distributions (black and green, respectively) plotted with kernel density estimates of CRCM45-CGCM3 (blue) and CRCM45-ECHAM5 (red) distributions for 1979-1995.

of probability density functions for the station observations are plotted along with kernel density estimates of the CRCM45-CGCM3 and CRCM45-ECHAM5 distributions. Each realization of both models is shown along with the means and standard deviations for each ensemble of realizations. Both the three and six hour means of

the station observations are shown as the CRCM45-CGCM3 wind speeds are means over three-hour periods and the CRCM45-ECHAM5 wind speeds are means over six-hour periods. Since these models are not driven by reanalysis it is not meaningful to consider the temporal correlation with respect to the observations.

From Figure 3.21, it appears that distributions of wind speeds from the CRCM45-CGCM3 and CRCM45-ECHAM5 simulations are biased with respect to the observations at least for the period 1979-1995 and that the bias is different for each of the representative station locations. As we shall see in Chapter 4, this is the case also for 1971-2000, which is the period chosen in this study for de-biasing future simulations. The existence of biases in the RCM simulations implies that future projections using these models must be calibrated in an effort to remove these biases. Calibration procedures assume that the bias in the future is related in some specified way to the bias in the past. Suppose we have a wind speed distribution for some location that we accept as "reality" in the past. We then find the relationship between it and the wind speed distribution that the model provides for that past period. That relationship is then applied without change to future wind speed distributions provided by that model to obtain a "calibrated" projected future wind speed distribution. The assumption that this is justified is the assumption of "stationarity". Calibration of model projections will be presented in Chapter 4.

Chapter 4

Future Wind Power Resources

In this Chapter the simulated wind speeds for the future period (2031-2060) obtained from the CRCM-GCM using the SRES-A2 emissions scenario are examined and calibrated using station observations to remove the biases discussed in Chapter 3.

4.1 Need for Calibration of Simulated Future Wind Speeds

The need for calibration of the simulated future wind speeds is illustrated in Figure 4.1, in which kernel density estimates of the CRCM distributions for 1971-2000 (in red) and 2031-2060 (in black) interpolated to the station locations are plotted along with the 1971-2000 histogram estimates (in green) of corrected mean station wind speed distributions for the four representative stations. A separate curve is plotted for each ensemble member. In most cases the plots for the two time periods are so similar that the 2031-2060 curves lie on top of the 1971-2000 curves. Two plots for each station are required as there are two driving GCMs. The CRCM driven by the ECHAM5 provides six-hour mean wind speeds, but when driven by the CGCM3 provides three-hour mean wind speeds. The observations used to estimate the histograms were averaged accordingly, and so the histograms differ slightly.

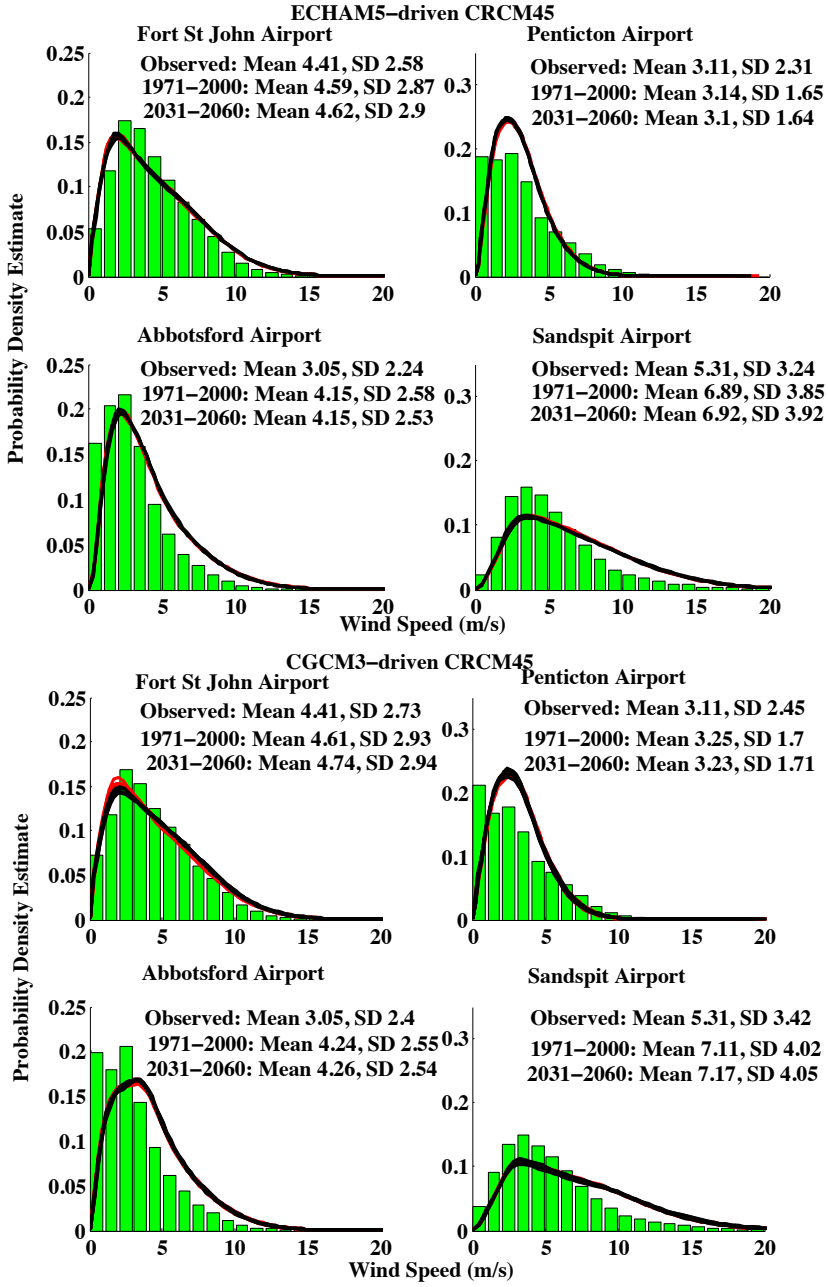

Figure 4.1: Histogram estimates of the 1971-2000 probability density function of corrected and time-averaged hourly station wind speed distributions plotted with kernel density estimates of GCM-driven CRCM simulated wind speed distributions for 1971-2000 (in red) and 2031-2060 (in black) interpolated to the station locations. The three ECHAM5-driven ensemble members are plotted in the left column and the five CGCM3-driven ensemble members are plotted in the right column for each period. "Means" are means of the ensemble means and "SDs" are means of the standard deviations of the ensemble distributions. All simulations use the 45 km grid. Observations are three-hour means for CGCM3-driven simulations and six-hour means for ECHAM5-driven simulations.

While the differences between the 1971-2000 and 2031-2060 simulated distributions in each plot are difficult to discern from curves in Figure 4.1, it is clear from the ensemble means and standard deviations appearing on the plots that there are small differences between the ensembles of simulations. For example, we note that at all four stations, the CGCM3-driven simulations have higher ensemble means than the ECHAM5-driven model simulations. More importantly, it is also apparent from Figure 4.1 that the 1971-2000 CRCM-simulated wind speeds are biased with respect to the observed wind speeds, consistent with the results presented in Chapter 3. In the balance of this Chapter an attempt is made to infer future variability of wind speeds through statistical calibration of the simulated future wind speed distribution.

4.2 Calibration Using Bias Correction and Change Factor Pathways

Calibration of climate forecasts uses statistical approaches to reduce model biases. This has most often been done in the context of surface temperature or precipitation (Ho et al., 2012; Piani et al., 2010; Haerter et al., 2011; Diaz-Nieto and Wilby, 2005). First, we can consider how past simulations are related statistically to past observations and then apply the same statistical relationship to the future simulations. This approach is known as the "bias correction (BC)" pathway for calibrating future simulations. Alternatively, we can consider how the past simulations are related to the future simulations and apply that statistical relationship to the past observations. This second approach is known as the "change factor (CF)" pathway for calibrating future simulations. There is no a priori reason to choose one pathway over the other, that is, both are equally valid. The functional form of the statistical relationships used for calibration is referred to as a transfer function.

The two calibration pathways, illustrated in Figure 4.2 from Ho et al. (2012), generally result in different calibrated projections. In the terminology of the present study X_0 denotes the observed station wind speeds, X_m is the distribution of one of the ensemble members of simulated past wind speeds, X'_m is the distribution of one of the ensemble members of simulated future wind speeds, and X'_0 is the distribution of one of the ensemble members of calibrated simulated future wind speeds. The goal is to estimate X'_0 from the other three quantities. The broken arrows in Figure 4.2 represent the transfer functions that transform the distribution of simulated past

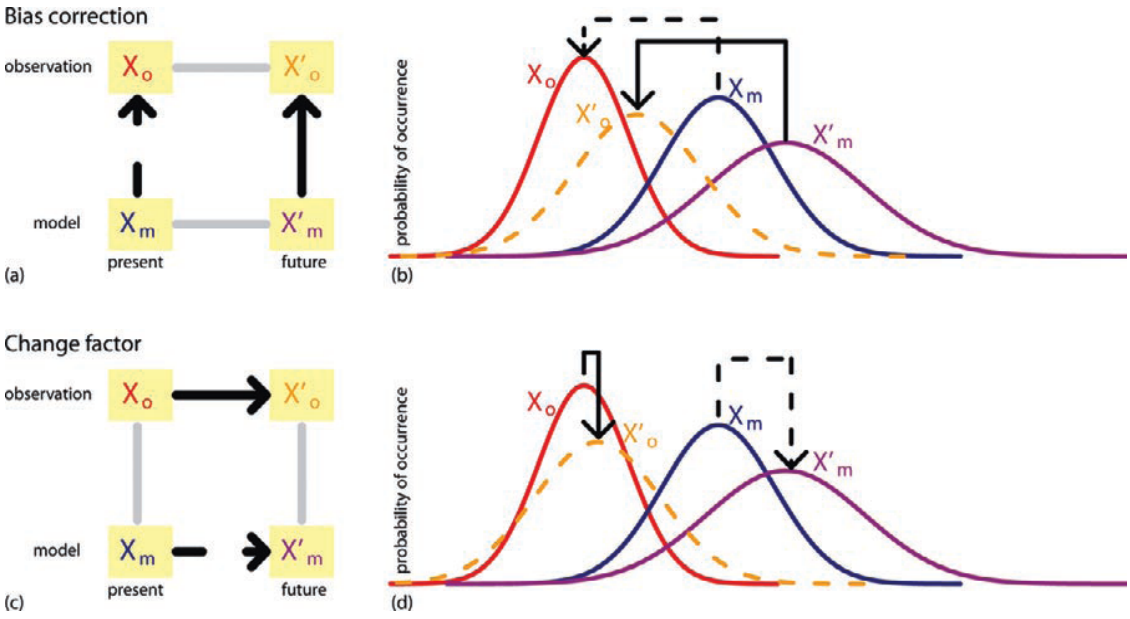

Figure 4.2: Illustration of the BC and CF calibration pathways from (Ho et al., 2012).

wind speeds X_m into either the distribution of observations X_0 (in the case of the BC pathway) or the distribution of simulated future wind speeds X'_m (in the case of the CF pathway). This transfer function is the statistical quantity to be estimated as the first step in the calibration process. The solid arrows represent the application of those transfer functions to the simulated future wind speeds X'_m or to the observations X'_0 to obtain the calibrated simulated future wind speeds X_0. As illustrated in Figure 4.2, these two calibration pathways result in different estimates of X'_0.

Because we have ensembles containing multiple realizations of past and future simulations multiple transfer functions are computed using each calibration pathway.

4.3 Transfer Functions: Q-Q Matching and Power Law Transforms

In this study, calibration will be done using both pathways and then the results compared. To apply either of the calibration methods, we need to find transfer functions that transform the wind speed distributions.

Wind speed distributions are transformed here using a procedure referred to as Quantile-Quantile (Q-Q) matching. The calibration of one distribution with respect to another using Q-Q matching proceeds as follows. We focus our discussion on the

calibration of a simulated distribution to an observed historical distribution for the same period (i.e. the BC pathway). First, a set of quantiles is selected. For a simple example, suppose that percentiles from 0 to 100 inclusive are used. The wind speed at each percentile of the simulated distribution and at each percentile of the observed distribution are then found. With those sets of wind speeds it is straightforward to match any speed from the simulated distribution to a corresponding speed in the observed distribution. For example, the median speed of the simulated distribution would be matched to the median speed of the observed distribution. Speed values between the selected percentiles in the simulated distribution are linearly interpolated between the corresponding percentiles in the observed distribution. The procedure is completely determined by the set of quantiles and the wind speeds at each quantile in each of the distributions and results in a unique transfer function between the observed and simulated distributions. The Q-Q matching procedure just described can also be used to create a transfer function for the CF pathway that relates the simulated historical and future distributions. To obtain calibrated future distributions, one then applies the appropriate transfer function to either the future distribution (BC pathway) or to the observed distribution (CF pathway).

One limitation of Q-Q matching is that if the range of values of the quantity to which the transfer function is applied extends beyond the range used to estimate the transfer function, there will be distortions in the resulting calibrated probability density function. The distortion can differ between the two pathways and depends upon the speeds in the observed and future simulation distributions that exceed the range of speeds in the historical simulation. When this happens, then those wind speeds are set to the 100th percentile of the calibrated future distribution. For example, if the future simulation distribution has no or very few speeds exceeding the historical simulation maximum speed, but the historical observations have many speeds exceeding that maximum speed, then mean speeds of the CF calibrated future distributions will be reduced relative to the mean speeds obtained by BC calibration.

As mentioned in (Ho et al., 2012), datasets with many data points of equal value can also be problematic for Q-Q matching if simple interpolation is used between percentiles. This is an issue for the observed wind speeds here due to the quantization of wind speeds resulting from rounding as mentioned in Chapter 2. To address this issue, a small random number between -0.01 and +0.01 m/s was added to all observed wind speeds. A power law transformation assuming Weibull distributions was also tried (Tye et al., 2014), but abandoned because the wind speed distributions were

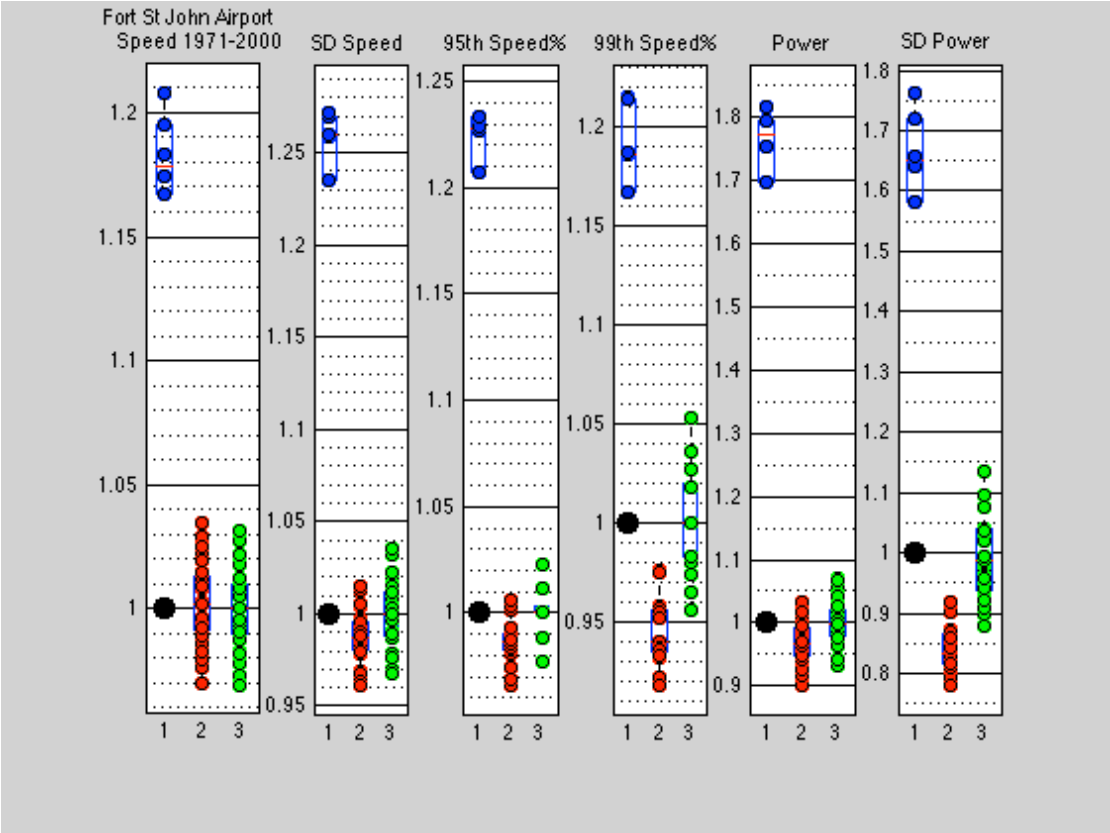

Figure 4.3: Comparison of transfer functions using Q-Q matching and power law transformations applied to 1971-2000 simulated wind speeds distributions, all normalized to observed 1971-2000 winds statistics (black dots). Blue dots represent 1971-2000 simulated wind speed means, red dots represent simulated wind means de-biased using power law transformations and green dots simulated wind means de-biased using Q-Q matching. Individual dots correspond to individual ensemble members.

sufficiently non-Weibull that the approach produced poor results, as illustrated in Figure 4.3. An ensemble of BC transfer functions were estimated over the 1971-2000 period using the power law transformation. These were applied to the past simulations and the statistics of these "calibrated" past simulations were compared to the past observations, again over the 1971-2000 period. The result (red dots in Figure 4.3) should have been an ensemble of de-biased distributions whose statistics closely matched the observations. This was the case for the mean speed, but not for the standard deviation of the mean speed, the 95th and 99th percentile speeds or the wind power density and its standard deviation. However, Q-Q matching produced ensembles (green dots in Figure 4.3) of de-biased distributions that were roughly symmetric

about the observed statistics and whose means were very close to the observed means for each statistic. The problem with using the power law transformations appears to be that only two free parameters are available to fit the distributions, and that these distributions differ substantially from a Weibull form. In contrast, the Q-Q matching transfer function can use an arbitrarily large number of parameters (by using many quantiles).

4.4 Distributions to be Matched

In the present study two ensembles of simulations are considered, one with three members (the ECHAM5-driven simulations), and the other with five members (the CGCM3-driven simulations), each providing both historical (1971-2000) and future (2031-2060) simulated wind speed distributions. It is expected that the ensembles of distributions will differ because ECHAM5 and CGCM3 are entirely different GCMs, and so have distinct climatologies and variability on all time scales. Hence, in the following, each will be dealt with separately. In addition, internal model variability results in differences between the realizations driven by the same GCM, although that fact is somewhat difficult to see in Figure 4.1 due to the averaging of results over a 30-year period.

From the three ECHAM5-driven historical simulations and the historical observations, there are three possible Q-Q transfer functions in the BC calibration pathway and nine in the CF pathway (resulting from combining each historical simulation with each future simulation). In interchanging past and future periods from different ensemble members, we assume that due to internal variability within a single model realization, the climate state at a given time is unrelated to that several decades in the future. As a result, each of the three BC transfer functions can be applied to any of the three future distributions, giving nine calibrated future states. These combinations broaden the spread of the ensemble of future projected simulations. Similarly, nine CF transfer functions are obtained because each of the three historical period simulations could result in any one of the three future period simulations. For the CGCM3-driven simulations, similar analysis reasoning gives 25 projected future wind speed distributions for each calibration pathway resulting from the various combinations of five historical and five future simulations.

4.5 Q-Q Matching Applied to GCM-driven CRCM Simulations

Figure 4.4 illustrates the result of applying Q-Q matching to the simulated wind speed time series interpolated to the representative station locations. There were 87,600 wind speeds in each CGCM3-driven simulations (3-hourly archiving) and 43,832 wind speeds in each ECHAM5-driven simulation (6-hourly archiving) for the two thirty-year periods. To provide a good basis for comparison between the calibration pathways and simulations 10,001 quantiles were used (0 to 100 by 0.01) in the final calculations. A sensitivity analysis indicated that the results are insensitive to using more quantiles. As discussed above, wind speeds exceeding the 100th percentile were set to the 100th percentile. Kernel density estimates of the resulting calibrated future distributions (nine for ECHAM5 and 25 for CGCM3) are plotted in Figure 4.4. The results of the BC and CF methods are shown in different colours, but are so similar that they are largely indistinguishable. The observed histograms are provided for comparison and show that the projected changes in the wind speed distribution are small for both the BC and CF pathways. The means and standard deviations of the CGCM3-driven simulations are higher than those of the ECHAM5-driven simulations, but only slightly.

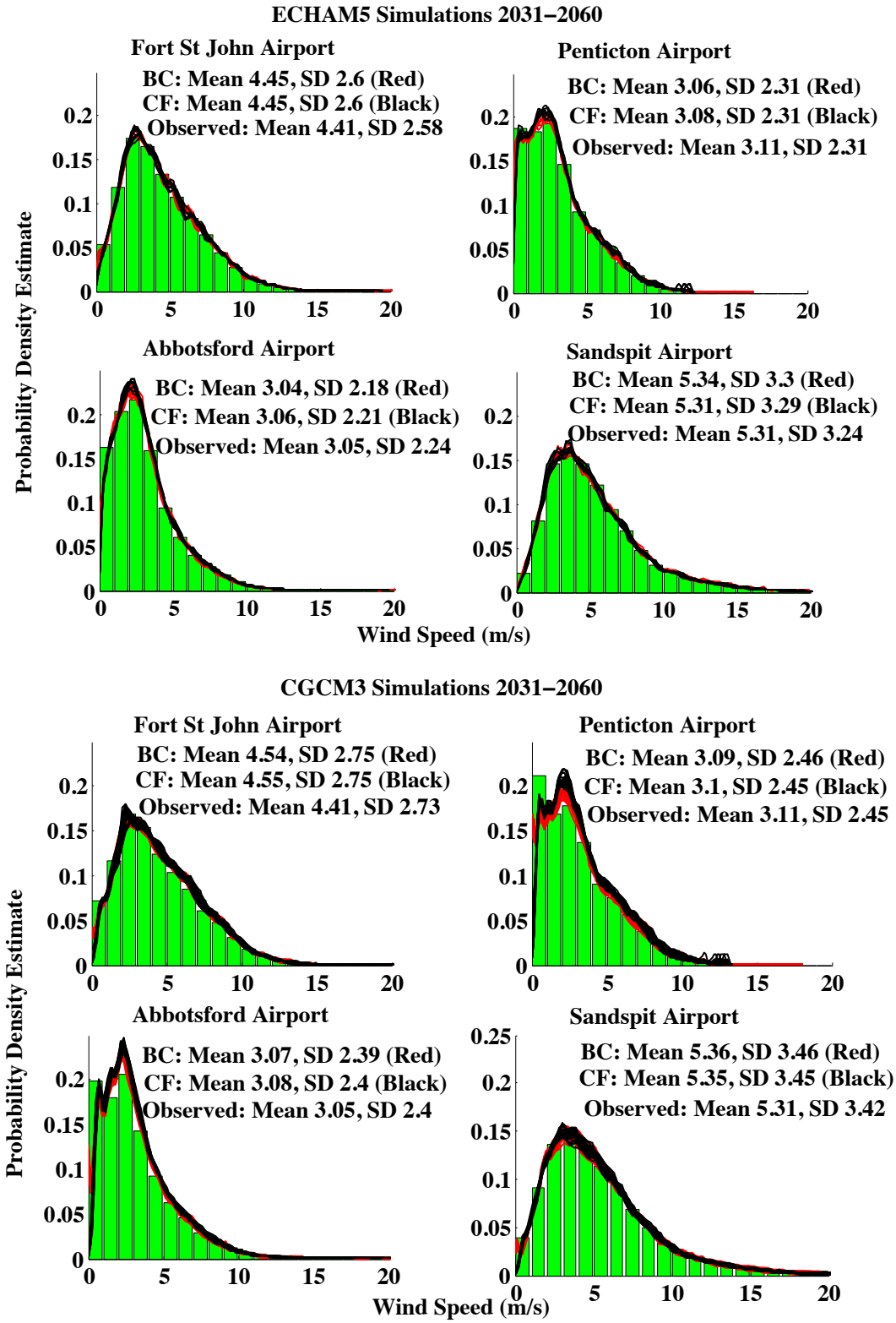

Figure 4.4: As in Figure 4.1 except that curves are calibrated GCM-driven CRCM wind speed distributions for 2031-2060 using BC (in red) and CF (in black) pathways.

4.6 Wind Power Density in Projected Future Distributions

As discussed in Chapter 1, the wind power density in W/m^2 depends upon air density and the cube of wind speed. Of these two factors, the cube of wind speed is much more variable than density. While the 45km resolution simulations do not provide wind power density, this quantity was explicitly calculated in the 15km resolution simulation (CRCM15-ECHAM5). In the following discussion, wind power density is estimated for each station location by multiplying the cube of the interpolated wind speed at the location at each time step with a factor determined for each station using wind speeds and power density from the CRCM15-ECHAM5 simulation.

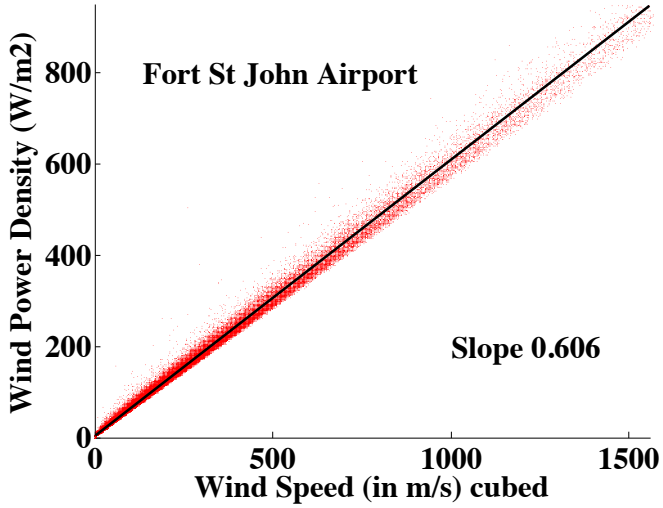

Figure 4.5: Wind power density as a function of wind speed cubed for the Fort St. John station using the CRCM15-ECHAM5 simulated wind speed and power density for 1971-2000 plotted with linear regression line (in black).

The multiplicative factor, which is 0.5 times the air density, was estimated for each station location as the slope of a linear regression between the wind speeds cubed and the wind power density from the CRCM15-ECHAM5 simulation at the interpolated station location and is approximately 0.6 and was used for plot of wind power density in Chapters 2 and 3.

For example, a scatter plot of the wind power density against wind speed cubed interpolated to the location of the Fort St. John station is shown for the period 1971-2000 along with the associated regression line in Figure 4.5. The factor used

in estimating the wind power density for this location is the slope of the regression line (intercepts from the regressions are not used). Because the air density varies somewhat, a more accurate approach would perform separate regressions for season of the year and time of day. A single regression was used here for simplicity.

4.7 Statistics of Calibrated Future Wind Speed and Power Density

The internal variability typical of the CRCM-projected wind speed distributions is shown for Fort St. John in more detail in Figure 4.6. In this Figure, several statistics of the ensemble members are displayed. Both calibration methods are shown separately for the CGCM3-driven simulations (upper set of plots) and the ECHAM5-driven simulations (lower set of plots). The black dots, representing the ensemble means, are a measure of the best guess change, while the ranges of green or yellow dots (the ensemble members) indicate the robustness of the projected change. In all cases, changes relative to the observed historical period rather than absolute quantities are shown.

For this station, almost all realizations project an increase in calibrated projected mean wind speeds relative to historical observed mean wind speed. Increases are also found in the 95th and 99th percentile wind speeds and the mean power. The difference between the ensemble means for BC and CF results is small, but the spread of values differs for the two pathways depending upon which statistic is considered. These results indicate that a small increase in the mean wind speed and power for the period 2031-2060 is projected for the Fort St. John station, but with a small possibility that the means could actually decrease (represented by one of the 25 CGCM3-driven simulations having a relative mean ratio less than 1). This is true for both CGCM3-driven and ECHAM5-driven simulations with both BC and CF pathways used for the calibration, although the range of the CGCM3 ensemble members is much larger than that of the ECHAM5 ensemble members. The question of the robustness of the projection of the projected small increase is considered further below, but in view of how few values fall below 1 in Figure 4.6, the projection is relatively robust. Figures similar to Figure 4.6 for all stations are provided in Appendices B and C.

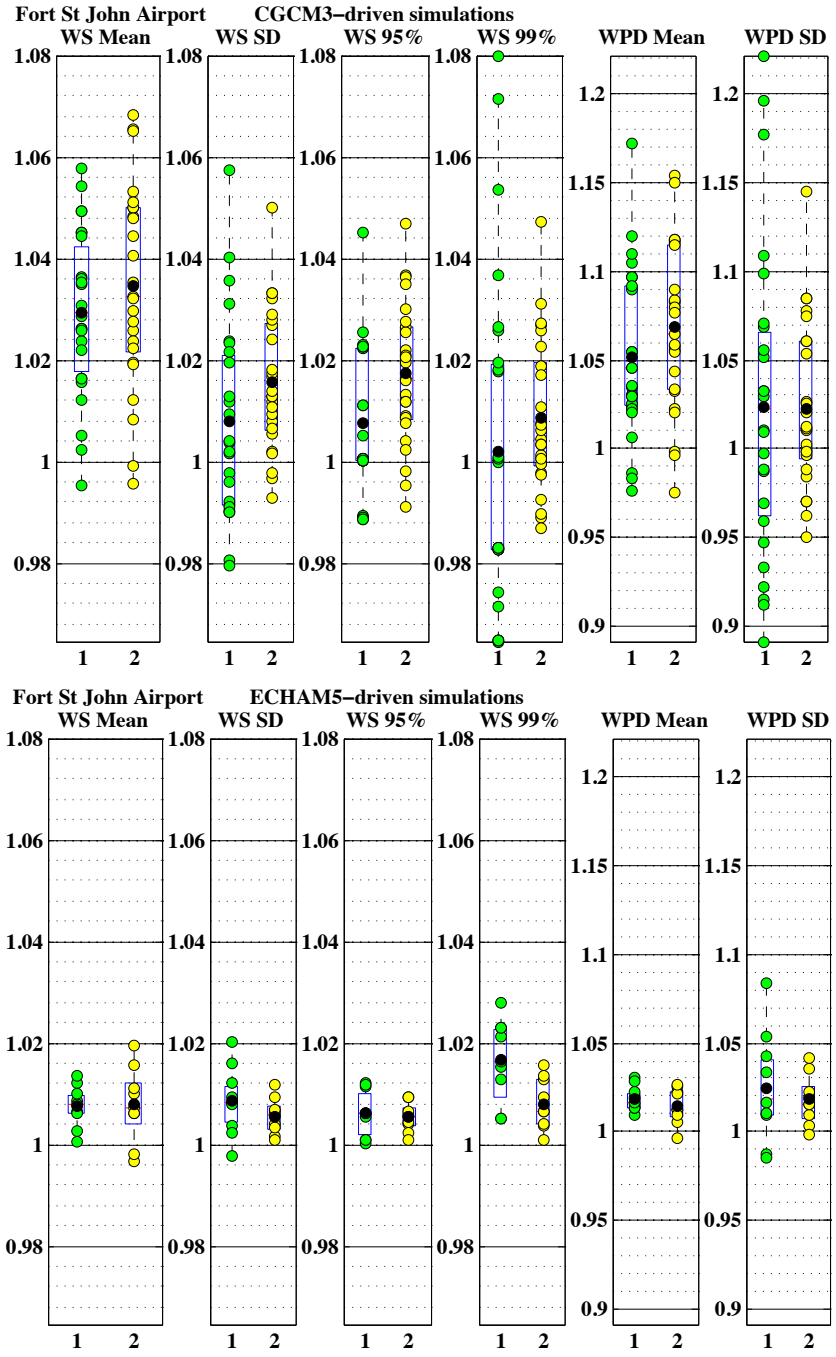

Figure 4.6: Box plots showing statistics of ensemble members for period 2031-2060 for the Fort St. John station normalized to the 1971-2000 values. The top set of plots represents CGCM3-driven simulations, while the bottom set represents ECHAM5-driven simulations. In the columns, wind speed is "WS", wind power density is "WPD", "SD" is standard deviation and "95%" and "99%" are 95th and 99th percentiles, respectively. The green dots represent ensemble members calibrated via the BC pathway, while the yellow dots are those calibrated via CF. In all cases, black dots are the ensemble means.

	Station Name	speed BC	speed CF	power BC	power CF	95th% BC	95th% CF	99th% BC	99th% CF
1	Abbotsford	0.7%	0.9%	-0.1%	0.1%	-0.3%	0.1%	0.5%	-0.1%
2	Castlegar	-1.2%	-0.7%	-1.9%	-1.7%	-0.5%	-0.4%	-0.2%	-0.2%
3	Comox	-0.7%	-1.0%	0.9%	-0.1%	1.1%	0.3%	0.4%	0.8%
4	Fort Nelson	2.1%	1.1%	2.4%	-2.6%	0.7%	0.2%	0.8%	0.8%
5	Fort St John	2.8%	3.1%	4.8%	5.3%	1.0%	1.2%	0.5%	0.5%
6	Kamloops	0.9%	0.5%	1.3%	0.0%	0.6%	0.1%	0.1%	0.4%
7	Kelowna	0.5%	0.2%	3.5%	1.0%	0.8%	0.3%	1.4%	0.6%
8	McInnes Isl.	1.6%	1.0%	6.5%	3.6%	3.1%	2.2%	2.0%	1.4%
9	Nanaimo	-1.4%	-1.1%	-0.6%	-3.6%	0.2%	-1.4%	0.1%	-0.5%
10	Penticton	-0.8%	-0.3%	0.6%	0.5%	0.6%	0.6%	0.8%	1.5%
11	Port Hardy	0.8%	0.5%	1.5%	-0.2%	1.1%	0.7%	0.1%	-0.3%
12	Prince George	1.4%	0.3%	2.9%	-4.8%	0.9%	0.1%	0.4%	-0.2%
13	Princeton	0.6%	-0.3%	1.6%	0.0%	0.3%	0.4%	0.0%	0.3%
14	Quesnel	2.2%	1.2%	6.0%	4.5%	1.8%	1.8%	1.3%	1.7%
15	Sandspit	1.0%	0.7%	2.6%	1.3%	1.5%	0.8%	0.6%	0.8%
16	Smithers	2.9%	1.7%	8.5%	6.0%	2.4%	1.7%	1.4%	1.4%
17	Terrace	4.0%	3.8%	7.4%	7.1%	2.3%	2.5%	2.9%	2.3%
18	Vancouver Int.	-0.6%	-1.1%	-0.1%	-2.5%	0.9%	-0.8%	0.9%	0.5%
19	Victoria Int.	-0.3%	-0.5%	-0.3%	-2.3%	0.0%	-1.6%	0.2%	-0.4%
20	Williams Lake	0.8%	0.6%	2.2%	0.8%	0.8%	0.8%	1.1%	0.0%
21	Calgary Int.	1.7%	1.4%	3.6%	1.5%	1.5%	1.3%	1.4%	0.6%
22	Cold Lake	1.8%	1.5%	4.5%	3.5%	1.4%	1.2%	1.1%	0.8%
23	Edmonton City	1.2%	1.6%	2.0%	2.6%	0.5%	0.5%	0.1%	0.3%
24	Edmonton Int.	1.2%	1.5%	1.8%	2.3%	0.3%	0.5%	0.1%	0.3%
25	Fort McMurray	1.8%	1.3%	4.2%	2.1%	1.1%	0.7%	1.1%	2.1%
26	Grande Prairie	2.8%	3.0%	3.3%	4.7%	0.8%	1.5%	0.4%	0.6%
27	Lethbridge	2.1%	1.9%	4.5%	3.9%	1.7%	1.1%	1.0%	0.8%
28	Medicine Hat	1.8%	1.7%	4.8%	4.8%	1.5%	2.2%	1.0%	1.3%
29	Peace River	2.7%	3.2%	5.0%	7.4%	1.1%	2.2%	0.4%	1.6%
30	Red Deer	0.1%	0.5%	-0.7%	-0.5%	-0.2%	-0.4%	0.2%	-0.4%

Table 4.1: Percentage changes in projected ensemble means of wind speed and wind power statistics for 2031-2060 from means of 1971-2000 observations, obtained by calibrating CGCM3-driven CRCM simulations using both the BC and CF pathways.

	Station Name	speed BC	speed CF	power BC	power CF	95th% BC	95th% CF	99th% BC	99th% CF
1	Abbotsford	-0.3%	0.3%	-5.8%	-3.2%	-1.8%	-0.8%	-3.0%	-1.7%
2	Castlegar	-1.5%	-1.1%	-2.9%	-2.5%	-1.1%	-1.0%	-0.1%	-0.4%
3	Comox	-0.6%	-0.7%	0.6%	0.0%	0.3%	-0.2%	1.7%	1.9%
4	Fort Nelson	-0.4%	-0.3%	-0.7%	-2.3%	0.0%	0.4%	0.5%	1.5%
5	Fort St John	0.7%	0.8%	1.8%	1.6%	0.8%	0.8%	1.4%	1.4%
6	Kamloops	-1.0%	-0.3%	-1.2%	0.6%	0.2%	0.9%	0.8%	1.7%
7	Kelowna	-0.6%	-0.4%	-0.8%	-1.3%	0.1%	-0.4%	0.1%	0.1%
8	McInnes Island	0.1%	0.0%	1.5%	0.3%	0.6%	0.8%	0.1%	0.1%
9	Nanaimo	-1.1%	-1.7%	-1.4%	-3.3%	-0.8%	-1.0%	0.4%	-1.0%
10	Penticton	-1.6%	-0.9%	-2.4%	-1.6%	-0.4%	-0.2%	-0.1%	0.5%
11	Port Hardy	0.4%	0.4%	1.5%	0.1%	0.6%	0.7%	-0.1%	0.0%
12	Prince George	-0.7%	-0.6%	-1.9%	-3.9%	-1.0%	0.8%	-0.4%	3.4%
13	Princeton	-1.4%	-1.0%	-1.0%	-2.6%	-0.8%	-0.7%	0.6%	-0.4%
14	Quesnel	-0.4%	-0.4%	0.9%	-0.2%	0.3%	0.0%	0.6%	0.2%
15	Sandspit	0.5%	-0.1%	2.9%	1.2%	1.4%	1.1%	0.9%	0.9%
16	Smithers	0.4%	0.1%	1.7%	1.2%	0.0%	-0.1%	-0.3%	-0.7%
17	Terrace	1.5%	1.9%	0.2%	1.7%	0.2%	1.0%	-0.9%	0.3%
18	Vancouver Int.	-0.4%	-0.7%	-1.1%	-2.4%	-0.1%	-1.0%	1.2%	0.0%
19	Victoria Int.	-1.1%	-1.3%	-2.8%	-4.7%	-1.2%	-2.6%	-0.1%	-0.9%
20	Williams Lake	-0.6%	-0.5%	-0.9%	-1.8%	-0.3%	0.5%	0.6%	0.5%
21	Calgary Int.	-0.2%	-0.2%	-0.4%	-1.1%	-0.3%	-0.3%	1.2%	1.4%
22	Cold Lake	-0.3%	-0.3%	-2.2%	-2.3%	-0.7%	-0.7%	-0.6%	-0.6%
23	Edmonton City	-0.5%	-0.4%	-2.3%	-1.9%	-0.7%	-0.4%	-1.6%	-0.7%
24	Edmonton Int.	-0.6%	-0.4%	-2.8%	-2.3%	-0.8%	-0.6%	-1.4%	-0.8%
25	Fort McMurray	-0.2%	-0.1%	-1.3%	-1.5%	-0.7%	-0.4%	-0.6%	0.9%
26	Grande Prairie	1.0%	1.1%	2.0%	1.3%	0.4%	0.3%	1.8%	0.3%
27	Lethbridge	0.6%	0.6%	1.7%	1.3%	0.7%	0.1%	1.2%	1.0%
28	Medicine Hat	0.2%	0.2%	0.8%	0.2%	0.4%	0.3%	0.5%	0.4%
29	Peace River	0.1%	-0.1%	0.4%	-0.4%	0.0%	0.0%	1.2%	0.6%
30	Red Deer	-1.2%	-1.0%	-4.2%	-4.2%	-1.2%	-1.5%	-1.7%	-1.6%

Table 4.2: As in Table 4.1 for the ECHAM5-driven simulations.

Tables 4.1 and 4.2 provide detailed quantitative statistics of the ensemble mean changes for the CGCM3-driven and ECHAM5-driven simulations, respectively. Some differences between the BC and CF calibration pathways are evident in Tables 4.1 and 4.2. While the Fort St. John (#5) station location has only a small difference between the changes in mean wind speeds resulting from the different calibration pathways, in other locations the differences are larger. These differences are especially large for mean power. For example, at the Prince George (#12) station the change in mean speed for the CGCM3 simulation from the historical period to the future period is 1.4% for the BC pathway vs. 0.3% for the CF pathway, while for mean power the difference is 2.9% vs. -4.8%. As discussed above, the two calibration pathways may give different means if either the simulated future distribution of wind speeds or the observed distribution of wind speeds has many speeds exceeding the simulated historical distribution of wind speeds. This appears to be a factor in the contradictory power projections at the Prince George station location because for that location the five CGCM3-driven CRCM historical simulations have maximum wind speeds that are exceeded by the observed wind speeds with percentages of occurrence of 1.4%, 1.6%, 0.7%, 0.4%, and 0.8%, respectively. Even though these frequencies of occurrence are relatively small, because they occur in the tail of the distributions the effect on the mean power can be significant due to the cubic relationship between wind speed and power. In the calibration process using the CF pathway each such wind speed calibration is set to the 100th percentile of the future simulation, causing the calibrated wind speeds to be underestimated. Hence the relative change in the wind power density for the CF pathway would be too low. This effect is reflected in decrease in the mean 99th percentile speed from the CF pathway, but not the BC pathway.

In addition to the Prince George station location, the Fort Nelson (#4), Kamloops (#6), Penticton (#10), Port Hardy (#11), Princeton (#13), Smithers (#16), Williams Lake (#20), Calgary (#21), Cold Lake (#22), and Fort McMurray (#25) station locations also have a relatively large number of observed wind speeds that exceed the maximum wind speeds in the simulated historical distribution, but few in the simulated future distribution of wind speeds, suggesting that the BC pathway is more reliable for those stations.

From Tables 4.1 and 4.2, it is clear that neither simulation projects large ensemble-mean increases in wind power at the station locations in the future. However, neither do these simulations project large decreases. It is noteworthy that the several of

the locations showing the largest increases are in regions near existing wind power facilities, such as the Fort St. John (#5) and Lethbridge (#27) stations. Tables 4.1 and 4.2 do not provide an indication of the range of the projected changes across the ensemble such as is presented in Figure 4.6, in which one can see from the distribution of ensemble means that a high percentage of the ensemble means show increases (many of which are considerably larger than the ensemble mean change). By and large, except over Alberta, the signs of projected changes from the two ensembles listed in Tables 4.1 and 4.2 agree, even if their magnitudes do not. This will become more evident when we look at the region-wide simulation results in Sec. 5.5.

Maps of ensemble mean change along with the robustness of this change are presented in Figures 4.7 through 4.10. In these Figures, the triangles indicate the mean wind speeds or wind power density, with a size and orientation determined respectively by the magnitude and sign of the ensemble-mean change (upward-oriented vertex indicating a positive mean change). The triangle colour characterizes the robustness of the projections, indicating the percentage of ensemble members that agree with the sign of the ensemble-mean change. For each quantity (mean wind speed and mean wind power density) separate maps are shown both for the entire study domain and for the southwestern portion of British Columbia where the density of stations is higher. Maps of 95th and 99th percentile mean wind speed are not particularly informative as 95th and 99th percentile mean wind speed does not increase by more than 2% for either calibration pathways at any station location (see Tables 4.1 and 4.2).

The results displayed in Figures 4.7 through 4.10 indicate that according to the CGCM3-driven CRCM, positive and robust relative changes in mean wind speed and wind power density are likely in southern Alberta, northeastern British Columbia and the nearby region of northwestern Alberta, and the coastal region around Terrace (#17) and Smithers (#16) near the coast. Southern British Columbia is likely to experience little change or small decreases. The ECHAM5 model projects smaller less robust relative changes or no change where the CGCM3 model projects positive and robust relative changes and in some cases decreases. There are robust increases at Fort St. John and Grande Prairie for both models, but the increase is less for ECHAM5.

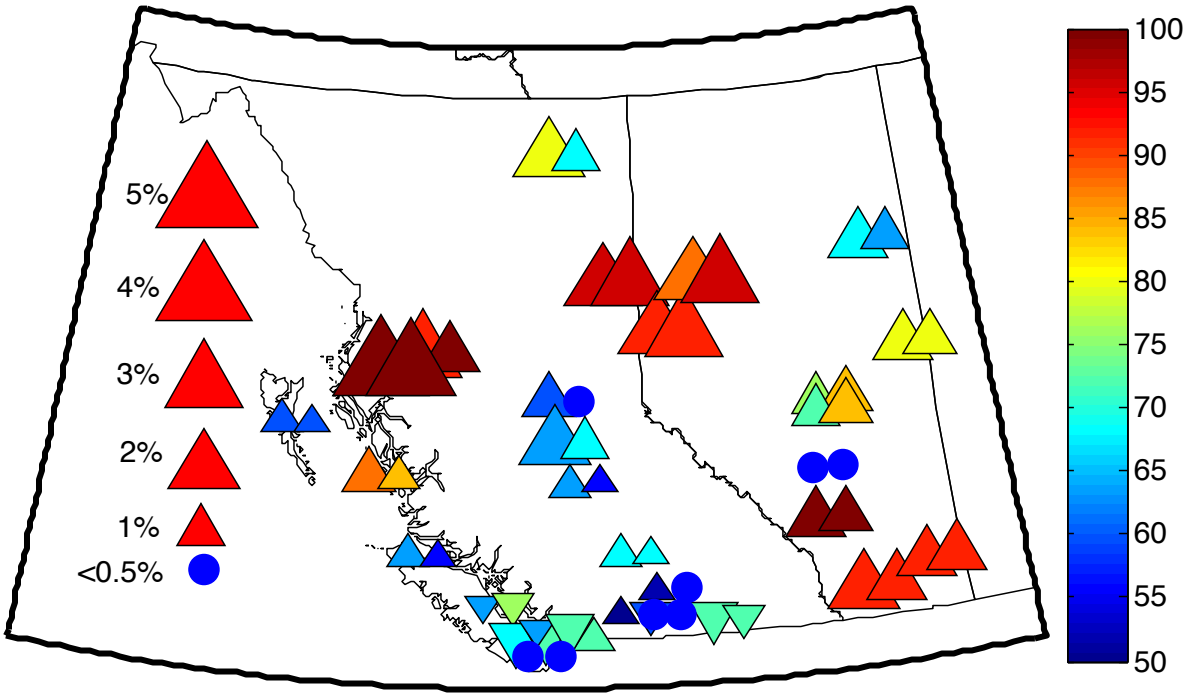

Figure 4.7: Map showing the percentage change in the ensemble mean of mean wind speeds for the calibrated 2031-2060 CGCM3-driven simulations with respect to the CGCM3-driven 1971-2000 simulations at the stations under consideration. The left triangle symbol of each pair of symbols represents the BC pathway at a station and the right symbol the CF pathway. The sizes of the triangles represent the magnitude of the change and the vertical vertex of triangles points in direction of change (positive upward). Colour represents the percentage of ensemble members agreeing in direction of change with the direction of the triangle (robustness). Blue filled circles represent absolute ensemble mean percentage change of less than 0.5% with no indication of robustness.

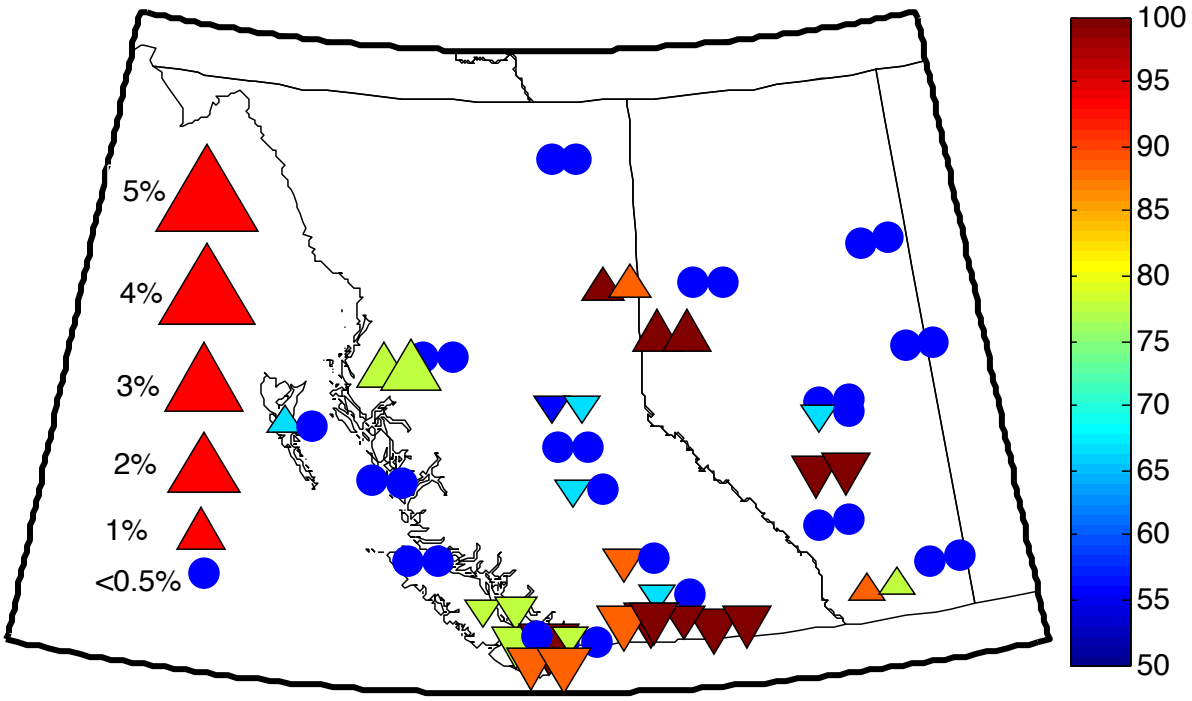

Figure 4.8: As in Figure 4.7 for ECHAM5-driven simulations.

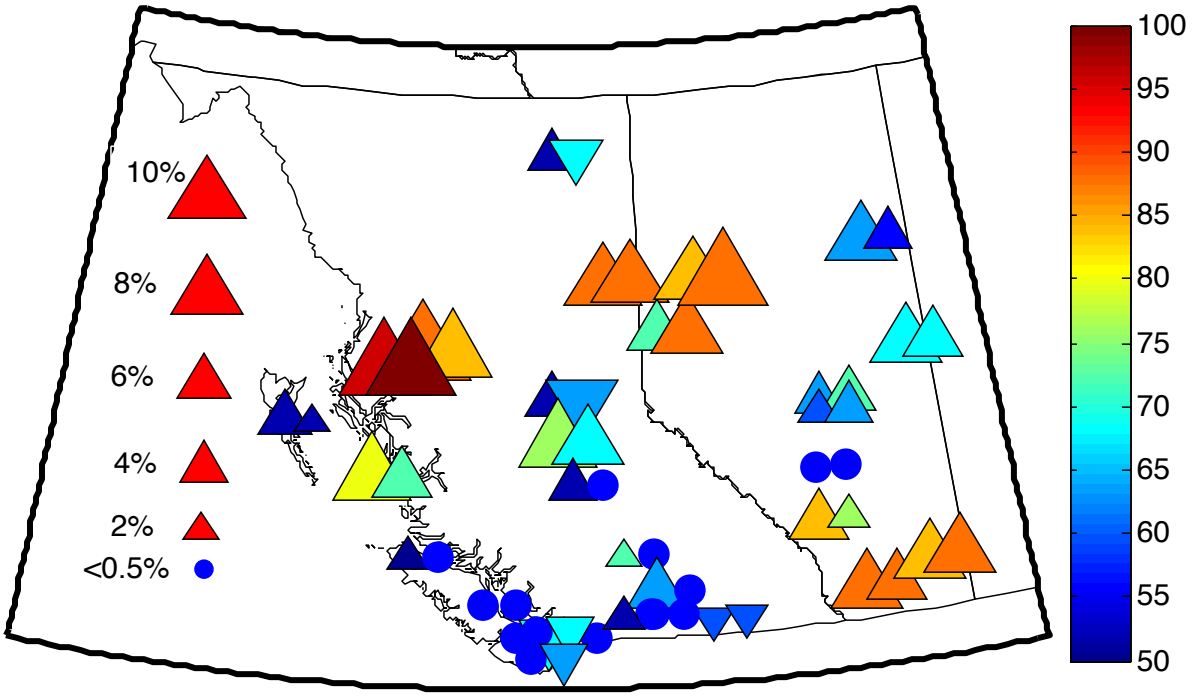

Figure 4.9: Map showing the percentage change in the ensemble mean of mean wind power density for the calibrated 2031-2060 CGCM3-driven simulations with respect to the CGCM3-driven 1971-2000 simulations at the stations under consideration. The left triangle of each pair of triangles represents the BC pathway at a station and the right triangle the CF pathway. The sizes of the triangles represent the magnitude of the change and the vertical vertex of triangles points in direction of change (positive upward). Colour represents the percentage of ensemble members agreeing in direction of change with the direction of the triangle (robustness). Blue filled circles represent absolute ensemble mean percentage change of less than 0.5% with no indication of robustness.

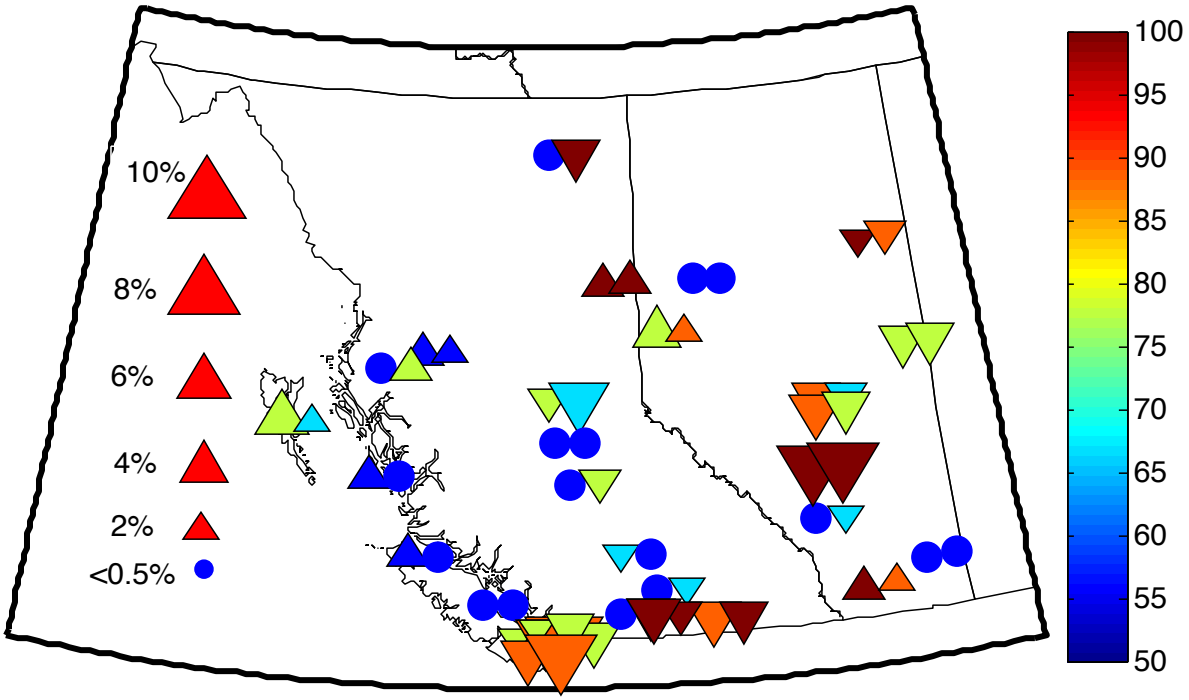

Figure 4.10: As in Figure 4.9 for ECHAM5-driven simulations.

4.8 Test of Calibration for Period 2001-2014

The calibration transfer functions were based on observations and model output from 1971-2000. Observations for the period 2001-2014 (present) can be used to test the accuracy of the calibration process using an equal length 14-year period 1971-1984 (past) for observed wind speeds in the calibrations. The Edmonton International Airport station (#24) is used for this test because at this station there was no difference between the homogenized monthly means and the raw monthly means for 1971-1984, so correction to the raw observed wind speeds discussed in Chapter 2 does not complicate the interpretation. The results are shown in Figure 4.11. The red dots indicating the observed means for 2001-2014 fall within the range of calibrated means and percentiles, as expected, but they fall outside the range of the calibrated standard deviations.

There are several possible explanations for this result. First, the change in instrumentation could have changed the observed distribution. Second, the model could underestimate natural variability. Third, the ensemble may be too small to capture the extent of natural variability. Fourth, by chance the realization of the real climate system may fall outside of the range of the ensemble. The histogram shown in Figure A.2 suggests that the first explanation is the most plausible. We see an increase in the probability of observed wind speeds falling in the range of 2 to 6 m/s and a decrease in the ranges wind speeds from zero to 2 m/s and greater than 6 m/s. This narrowing of the probability distribution explains the observed changes shown as red dots in the box plots of Figure 4.11: an increase in the mean wind speed, accompanied by decreases in the higher percentiles and standard deviation. However, it is difficult to distinguish between changes in the distribution due to natural internal variability and those due to changes in instrumentation.

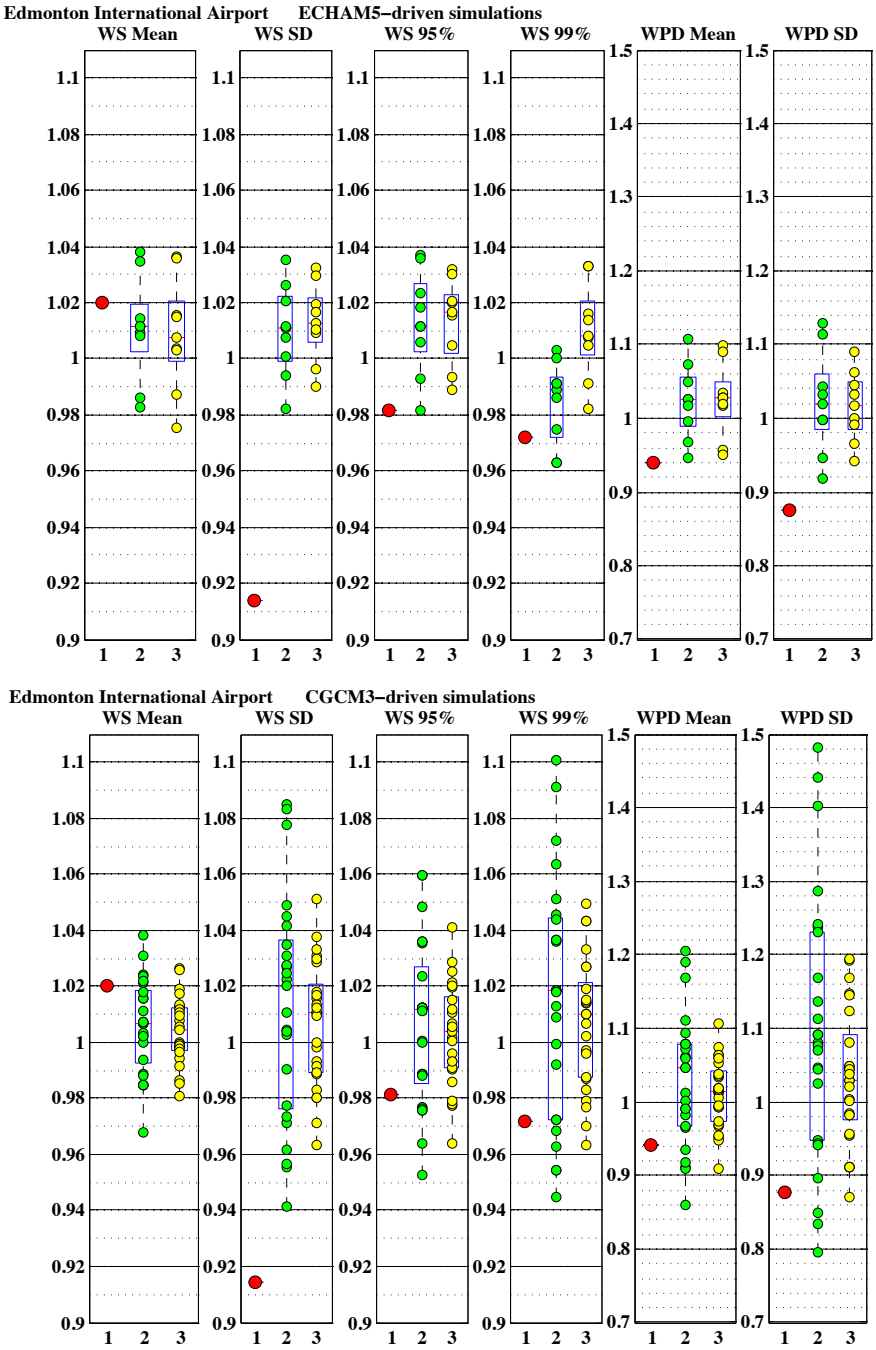

Figure 4.11: Box plots showing statistics of the simulation ensemble members for period 2001-2014 for the Edmonton International Airport station normalized to the 1971-1984 values. In the columns, wind speed is "WS", wind power density is "WPD", "SD"is standard deviation and "95%" and "99%" are 95th and 99th percentiles, respectively. The green dots represent ensemble members calibrated via the BC pathway, while the yellow dots are those calibrated via CF. In all cases, black dots are the ensemble means. The red dots are 2001-2014 observed values. 1971-1984 observations were used for the calibrations.

Chapter 5

Discussion of Uncertainties and Sensitivities

In the preceding chapters, observations and simulations of near-surface wind speed at thirty stations in the region were considered and calibrated future wind climate variables for those stations were presented. A number of uncertainties in these projected future wind speeds were mentioned briefly. In this Chapter, the sensitivity of the results to these uncertainties are considered in more detail. After showing that the relative future changes in wind climate in this region are quite insensitive to calibration, an estimate of the relative change in future wind climate is presented for the entire CRCM grid.

5.1 Overview of Uncertainties and Sensitivities in Calibrated Winds

To obtain Tables 4.1 and 4.2 and Figures 4.7 - 4.10, raw hourly wind speeds for 1971-2000 and ensembles of simulated wind speeds for both 1971-2000 and 2031-2060 interpolated to the station locations were used. The raw wind speeds were shown to contain a large number of zeros, some of which are undoubtedly low non-zero wind speeds, and, in the case of some stations, large numbers of missing values. Zero wind speeds were not removed or corrected for in this study for the reasons discussed in Chapter 2. In addition, the raw wind speeds were corrected using homogenized monthly mean wind speeds obtained from EC in an attempt to remove the effects of changes in the measuring equipment and the surrounding environment. The simulated

wind speeds have the uncertainties inherent in the driving GCM as well as internal variability across the ensemble members from the RCM and uncertainty associated with the accuracy and resolution of the RCM itself. Further, to use the simulated wind speeds to project future wind speeds calibration is required and, as we have shown, there are two calibration pathways that can yield different results. The calibrations also rely on the observations, which are uncertain. Hence in all there are five sources of uncertainties that will be discussed here:

- observational station data (problems in the raw data and correction process);
- driving GCMs (ECHAM5 vs. CGCM3);
- internal variability in CRCM, as represented by the ensemble;
- uncertainty associated with the accuracy and choice and resolution of the RCM; and
- calibration method.

As to the sensitivity of our results to the choice of RCM, only one model (the CRCM) was considered, so this uncertainty cannot be addressed in this study by comparison of simulations with the same driving conditions applied to more than one RCM. As to the uncertainty due to resolution of the RCM, in sections 3.3 through 3.5 it was shown that the higher spatial resolution model provided a somewhat less biased mean wind speeds and higher temporal correlation with respect to the observations than the lower resolution model at most stations.

As to uncertainty due to using two calibration pathways, for the distributions we have studied, this uncertainty was minor compared to the other uncertainties. This is shown in Figure 4.6, where the ensemble means and the range of the means is similar for both calibrations pathways. Use of Q-Q matching as opposed to the parametric Weibull distribution was evaluated as a significant source of uncertainty in view of the poor results obtained as discussed in Section 4.3.

5.2 Uncertainty due to Internal Variability and GCMs

Internal variability in the CRCM and the choice of driving GCM clearly have a substantial influence on the projected winds as is shown in Figure 4.6 for the Fort St.

John station, but further consideration of the uncertainty they introduce is outside the scope of this study. For the Fort St. John station, the calibrated ensemble mean future wind speed is projected to increase by about 1% for ECHAM5-driven simulations and 3% for CGCM3-driven simulations, but individual simulations range anywhere from a slight decrease in mean wind speed to a 6 to 7% increase for CGCM3-driven simulations and and from a slight decrease to a 2% increase for ECHAM5-driven simulations. The ECHAM5-driven simulations display much less internal variability than the CGCM3-driven simulations, which could be because the ensemble size is smaller, with smaller changes in mean wind speed and wind power density.

In Figure 4.6 the ensemble spreads are much larger than the differences in ensemble means of the two driving GCMs meaning that internal variability in the CRCM is a larger contributor to uncertainty than differences in the driving GCM. This relationship is characteristic of most of the stations as shown in the box plots in Appendices B and C. The ensemble mean for each GCM generally falls within the range of the means of the other GCM.

5.3 Sensitivity of Calibrated Simulated Winds to Correction of Raw Observed Wind Speeds

As mentioned above, the results presented in Tables 4.1 and 4.2 and Figures 4.7 - 4.10 have been calibrated using the 1971-2000 corrected observed wind speeds. It is conceivable that the results might differ if the raw observed wind speeds were used instead.

To test the sensitivity of the calibrated simulations to this correction of the raw observed wind speeds, the Grand Prairie station (#26) is used as an example because it has a correction that changed over the 1971-2000 period, as was shown in Figure 2.3. The corrected mean wind speed was 2% lower than the raw mean wind speed over that period (see Table 2.3). If using raw rather than corrected observed speeds in the calibration pathway causes changes to the calibrated normalized wind climate beyond that expected from a change in the mean wind speed due to the correction, then this station is one at which the difference should show up, rather than at stations for which the correction was constant for the entire 1971-2000 period. Figure 5.1 illustrates the effect on mean wind speed and mean wind power density of using raw as opposed to corrected wind speeds in the calibration pathways. In this case, there is a slight

downward shift in the means from using the corrected rather than the raw observed wind speeds. The shift is approximately 2%, as expected from the magnitude of the correction.

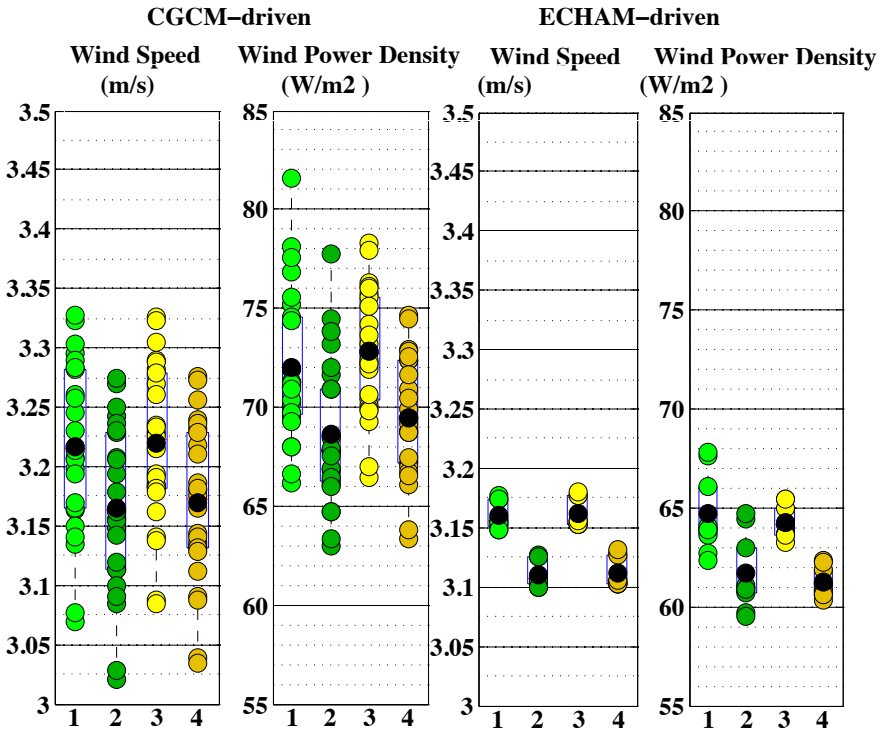

Figure 5.1: Box plots showing statistics of ensemble members for period 2031-2060 for the Grande Prairie station. The two left-hand plots represent CGCM3-driven simulations, while the two right-hand plots represent ECHAM5-driven simulations. The light green dots represent ensemble members calibrated via the BC pathway using raw observations, while the dark green dots represent ensemble members calibrated via the BC pathway using corrected observations. The yellow dots are calibrated via CF using raw observations, while the gold dots are calibrated via CF using corrected observations. In each case, black dots are the ensemble means. Observed wind speeds for 1971-2000 used for calibrations.

Figure 5.2 shows that normalizing the mean wind speed and mean wind power density to the 1971-2000 observed means largely erases the difference between the projections calibrated using the two different observational datasets shown in Figure 5.1. There are minor differences in the distribution of the simulation means, but it appears that the calibrated projected winds at this station are largely insensitive to the data differences if relative rather than absolute quantities are considered.

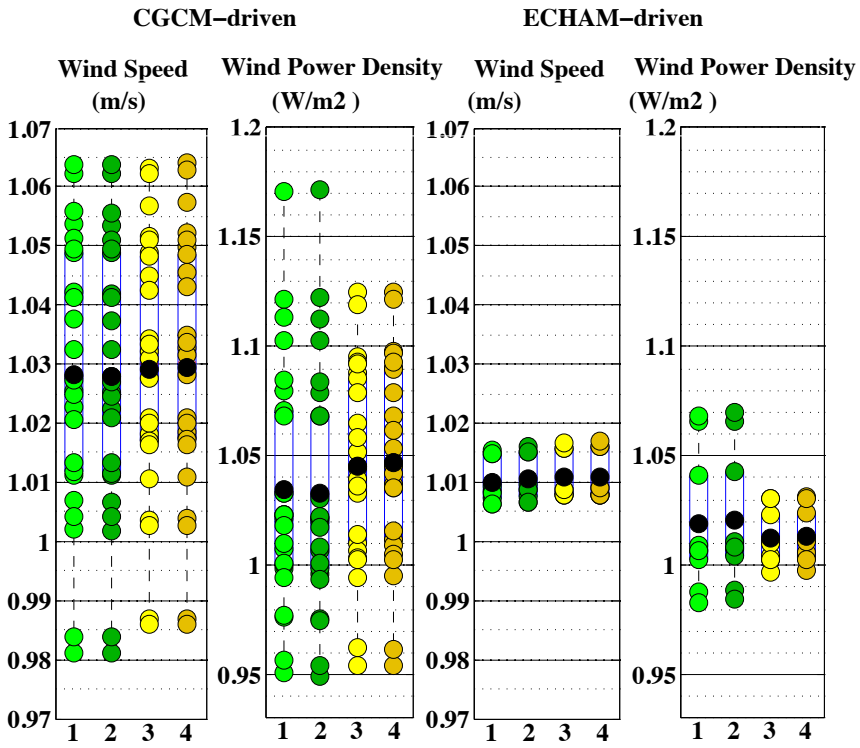

Figure 5.2: As in Figure 5.1, but with all quantities normalized to 1971-2000 observations.

5.4 Is Calibration of Model Simulations Necessary for Determining Relative Change?

In view of the results presented in Figures 5.1 and 5.2, the calibrated projections of *relative* change are essentially insensitive to the dataset used for calibration. This result implies that calibration against observations may not be necessary if the goal is to estimate relative future change in the wind climate. To test this idea, for each station, an ensemble of un-calibrated percentage changes in wind speed was obtained using each pair of 1971-2000 and 2031-2060 time-mean wind speeds from the simulation ensembles for both the ECHAM5-driven and the CGCM3-driven simulations. That is, un-calibrated relative changes were determined from the model simulations alone without any use of observational data. A similar ensemble of relative changes in time-mean wind power density was computed. In Figure 5.3, a scatterplot of the ensemble means of the relative change of time-mean wind speed for the 30 stations are plotted against the corresponding percentage changes in BC and CF calibrated mean wind speeds and wind power density for the CGCM3-driven and ECHAM5-

driven simulations for each station. The BC and CF calibrated mean wind speeds are calculated as previously described in Chapter 4.

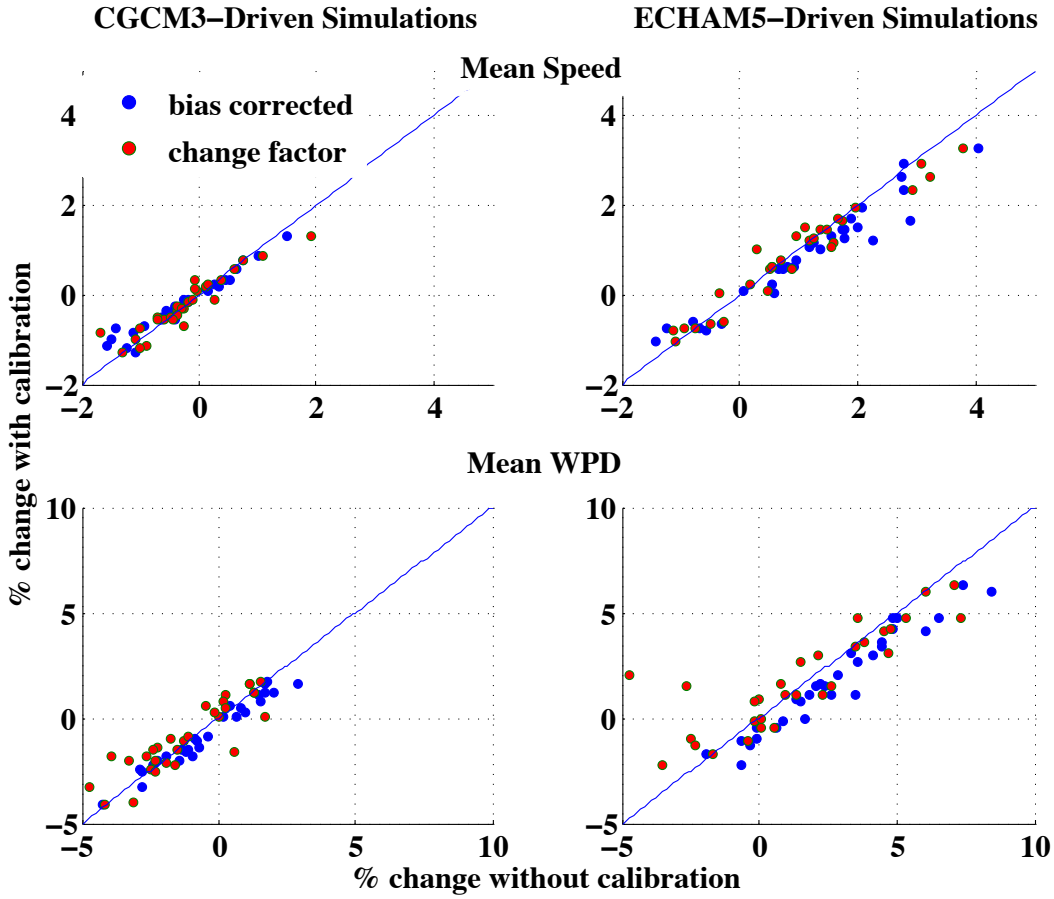

Figure 5.3: Scatterplots at the 30 station locations of percentage changes in simulated time-mean wind speeds (upper plots) and wind power density (lower plots) at each station calibrated using BC and CF pathways from 1971-2000 to 2031-2060 plotted against ensemble mean un-calibrated percentage change for all pairings of 1971-2000 and 2031-2060 time-mean wind speeds at the station. A line with a slope of one is shown for reference.

The scatter of the calibrated and un-calibrated relative changes is distributed about the 1:1 line in Figure 5.3. The un-calibrated relative changes appear to be a reasonable approximation to the calibrated relative changes at the station locations, although for wind power density the change-factor calibrated wind-power density appears to consistently show slightly larger changes than the bias-correction calibrated wind-power density relative to the un-calibrated percentage changes. Further, there appears to be a tendency for the un-calibrated percentage changes to be larger

at larger percentage changes, particularly for the CRCM-driven simulations. However, these differences between the calibrated and un-calibrated projections of relative change are generally small.

5.5 Projected Wind Climate at all CRCM Grid Points Without Calibration

If calibration is not necessary for estimating the relative future change in mean wind speed and power density at the station locations, this suggests that relative future changes can be estimated, not just at the stations, but throughout the entire CRCM domain. It is possible that an as yet unidentified selection bias is present in the agreement between the calibrated and un-calibrated projections of relative change, as almost all stations are at airports. We cannot assess the quality of this approximation at grid points away from station locations. Further, large-magnitude changes are more uncertain, as noted above. With these caveats in mind, Figure 5.4 presents maps of ensemble-mean relative change in wind speed and power density for both simulations. As was the case for the calibrated changes at station locations discussed in Chapter 4, over most of the region the un-calibrated ensemble-mean relative change in mean wind speed and power density in the ECHAM5-driven simulations is less than that in the CGCM3-driven simulations. However, the sign of change is generally consistent between the ECHAM5-driven and the CGCM3-driven simulations. For example, the region around Fort St. John in British Columbia and Grande Prairie and Peace River in northern Alberta shows a small increase in the ensemble means of the ECHAM5-driven simulations and a stronger increase in the ensemble means of the CGCM3-driven simulations for both wind speed and wind power density. The situation is similar for the region in southern Alberta around Medicine Hat and Lethbridge. These results indicate that the best-guess model projection is that the wind resource may slightly increase in regions where the wind climate is suitable for wind power generation (particularly in the north of British Columbia and Alberta). In Appendix C maps corresponding to Figure 5.4 show the results for December through February (DJF) and June through August (JJA).

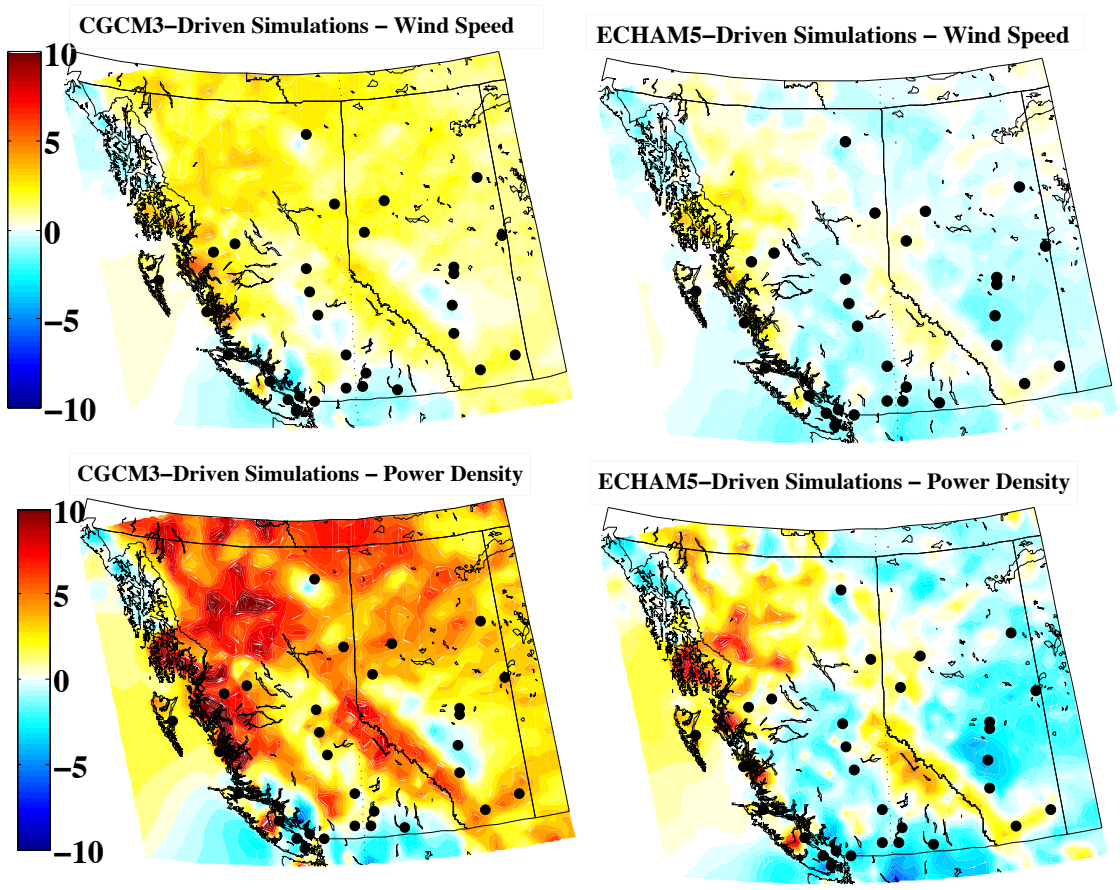

Figure 5.4: Percentage relative changes in annual mean wind speed (top two panels) and wind power density (bottom two panels) from 1971-2000 simulations to 2031-2060 simulations using CGCM3 (left panels) and ECHAM5 (right panels) driven CRCM smoothed from the original 45 km grid resolution without calibration from observations.

5.6 Robustness and Substantiality of Estimates of Relative Change in Wind Climate

Two further factors must be considered in the interpretation of the maps presented in Figure 5.4. The first factor is the degree to which the relative ensemble-mean changes shown are robust relative to the spread of the ensemble. The second is whether they are, in some sense, substantial compared to typical variations in the quantity of interest. One way to test the robustness of the changes is to divide the ensemble-mean change (as displayed in Figure 5.4) by the ensemble standard deviation at each grid point. The larger this value, the larger the mean change is

relative to the ensemble spread and the more robust the change is. In Figure 5.5, maps for this measure of robustness are shown for both ECHAM5-driven simulations and CGCM3-driven simulations in the top two panels of Figure 5.4, respectively. From the results shown in Figure 5.5, the GCMs both show robust relative increases in three areas of present wind farms (Fort St. John area, Lethbridge area and Cape Scott on Vancouver Island), but but are not in agreement for the area north of Medicine Hat and east of Calgary and Red Deer in Alberta. ECHAM5-driven simulations show robust decreases in most parts of Alberta as compared to robust increases in almost all of Alberta in the CGCM3-driven simulations.

While the relative changes in wind speed and wind power density are robust throughout most of the domain, they are still generally small: a change can be robust, but still insubstantial compared to typical variations in these quantities. The ensemble change divided by the temporal standard deviation of the annual-average means is a measure of the magnitude of the change relative to interannual variability. In Figure 5.6, contour maps for this measure are shown for both ECHAM5-driven simulations and CGCM3-driven simulations. It is instructive to compare these maps with the top two panels of Figure 5.4 and with 5.5. While there is some variation in this measure between the two maps, if we define (somewhat arbitrarily) a standard deviation greater than one as "substantial", then overall there are very few locations in the region where the changes are even close to being substantial. Similar maps for monthly and hourly-average means (which were not de-seasonalized) showed even lower relative magnitudes. It would be interesting to investigate how this quantity compares to the error in the observations, but that is beyond the scope of this study, since the latter is difficult to estimate. In the end, someone who has lived along the north coast of British Columbia long enough to notice when some years are windier than others might perceive an increase in the frequency of high wind years, but over most of the region the changes might not be noticed. In Appendix C maps corresponding to Figures 5.5 and 5.6 show the results for December through February (DJF) and June through August (JJA).

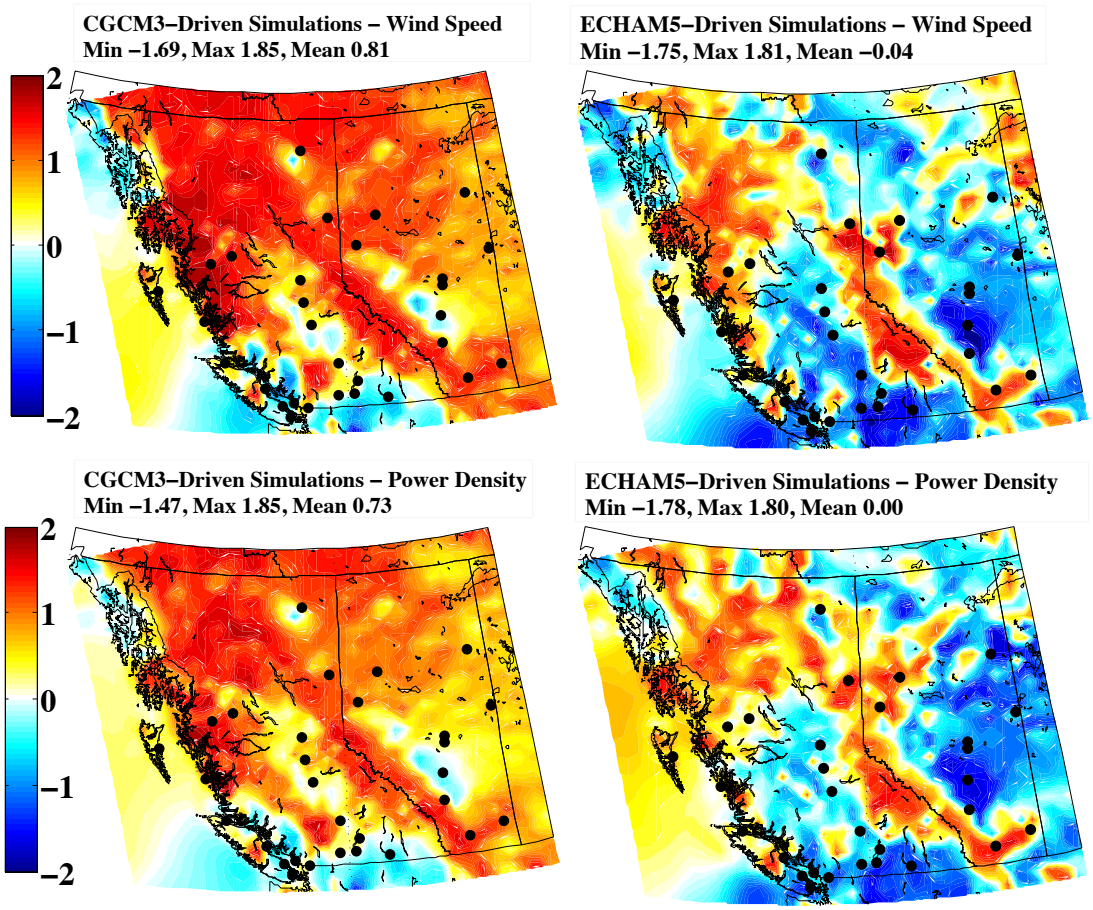

Figure 5.5: Robustness (ensemble relative change in annual mean wind speed divided by ensemble standard deviation) at each grid point with CGCM3-driven simulations in left panel and ECHAM5-driven simulations in the right panel.

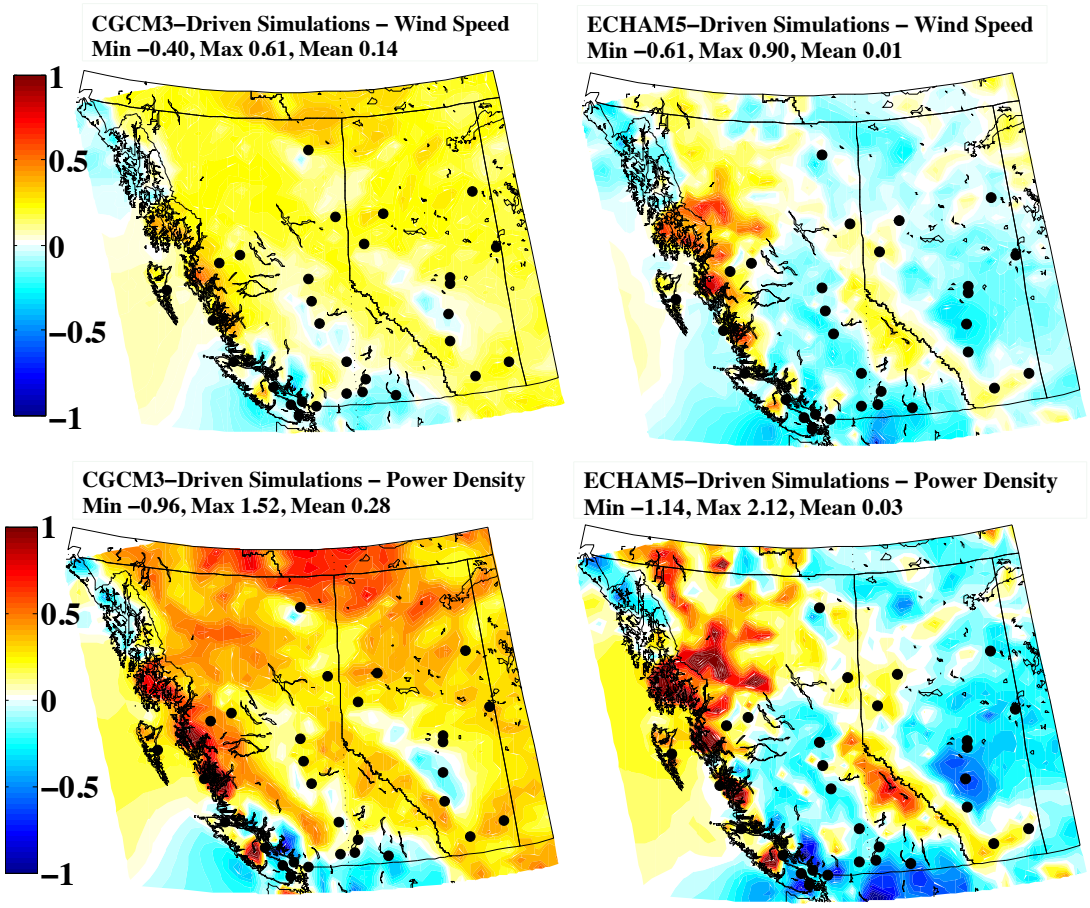

Figure 5.6: Substantiality (ensemble relative change in annual mean wind speed divided by the standard deviation of the annual-average means) at each grid point with CGCM3-driven simulations in left panel and ECHAM5-driven simulations in the right panel.

Chapter 6

Conclusions

This study uses wind speeds obtained from the dynamical downscaling of the global climate simulations to a regional scale to project the wind climate in the province of British Columbia and Alberta for the period 2031-2060 and compare it with the historical wind climate as estimated from long-term weather station observations. More specifically, one important product of this study is a collection of ensembles of wind speed distributions for the period 2031-2060 at 30 weather stations in the provinces of Alberta and British Columbia obtained using multiple CRCM simulations to downscale output from two GCMs, ECHAM5 and CGCM3. The GCMs were both forced by the SRES-A2 GHG emissions scenario. From the wind speed distributions, the mean wind speed, mean wind power density, 95th percentile wind speed, and 95th percentile wind speed and standard deviation of wind speed and wind power density were examined and ensemble means were found and calibrated using station observations. Due to the availability of multiple simulations, the ensemble of ECHAM5-driven projections of relative change of wind speeds for each station contained nine members and the CGCM3-driven contained 25 members.

Data quality represents a source of uncertainty in this study. The weather stations for which we have the long-term hourly data needed for calibration of future wind climate as well as estimation of the recent past wind climate were installed at airports to provide information for aviation and not primarily for the purpose of climate research. Wind speeds are sometimes missing or clearly inaccurate due to multiple rounding. In the last few years this situation seems to have improved with new anemometers installed at all of the stations that continue to operate in the region (NAV Canada, 2015). Unfortunately the wind climate varies greatly from year to year, so using just the last few years of wind speed data is not feasible for calibration

purposes or for estimating present day wind power resources.

At the locations of weather stations, no substantial changes in the wind climate are projected in the ensemble mean, although due to variability among the ensemble members relatively large changes cannot be ruled out at some stations. Stations near existing wind farms in southwestern Alberta and northeastern British Columbia show small (2% to 3%) and (4% to 5%) increases in the ensemble mean wind speed and mean power density, respectively, for the CGCM3-driven simulations. The increases were lower for the ECHAM5-driven simulations. The same or larger increases are projected at the near-coast stations of Terrace and Smithers, where there are presently no wind farms. At most other stations in the region the projected changes are smaller and in some cases of opposite sign between the CGCM3-driven and ECHAM5-driven simulations.

The quantitative assessment of uncertainties in projected change was a primary focus of this study. It was found that relative changes in the ensemble means were sensitive to the RCM/GCM combination used, but it was the internal variability of the members of each ensemble that resulted in the largest uncertainties, with the variability much higher for the CGCM3-CRCM than the ECHAM5-CRCM combination for the means of all of the climate variables examined. The results were only weakly sensitive to the calibration pathway used and the observations used in the calibration (when considering relative change).

In view of the weak sensitivity of the relative change in ensemble mean climate variables to the observational dataset and calibration pathway, an attempt was made to estimate relative changes in future wind climate at all CRCM grid points using only un-calibrated pairs of past and future period wind speed distributions. The results were compared at the station locations and it concluded that un-calibrated relative changes appear to be a reasonable approximation to the calibrated relative changes at the station locations. The relative changes appear to be robust, but not very substantial compared to the range of annual variability, in good general agreement with the projections at the stations.

The results of this study may be of interest to those planning to install or expand wind farms in the region as the over-all projection is that in most of the region large changes are not likely and in the areas that are presently being developed for wind farms small increases are possible. However, a number of uncertainties were identified that suggest caution, primarily uncertainties arising from the choice of driving GCM and internal variability in the ensembles of past and future simulations.

Appendix A

Zero Wind Speeds

The zero wind speeds in the observational data used in this study are more likely "calms", corresponding to wind speeds less than some minimum value, not bad data that should be removed. Confirmation of this can be found by examining the percentage of zero wind speeds reported at many of the stations in recent years (2010 - 2014). That percentage has decreased markedly in the last few years and the decrease coincides with increases in the percentages of one, two and three kilometre per hour wind speeds in the raw wind speeds. These changes may be due to the move by EC to replace mechanical (rotating cup) anemometers with sonic anemometers starting in late summer 2010 (NAV Canada, 2015). An apparent example of the effect of these changes is shown in Figure A.1, in which the monthly percentages of the raw wind speeds obtained from EC in km/hour are plotted for the Edmonton International Airport station.

Figure A.1 suggests that the wind speeds archived by EC as zero prior to 2012 for this station were actually wind speeds of zero to three km/hour. Something appears to have changed in early 2012 when wind speeds of five started to be archived (and the percentage of four and sixes dropped) and again in early 2013 when speeds of one, two and three started to be archived and the percentage of zeros dropped. It appears plausible that in 2012 the anemometer was replaced and possibly in 2013 the data archiving procedure was changed to allow recording of the higher resolution data provided by the new anemometer. In any case, the changes shown in Figure A.1 are common to all of the stations that are still operating and suggest that wind speed data from EC for the period 1971-2000, which is the period that will be used in the calibration of future simulated wind speeds in this study, is unreliable, particularly for low wind speeds. In this study, zeros were retained in the hourly wind speed

time series and were averaged over three- and six-hour periods to form time series for comparison with model wind speeds, which are means over three- and six-hour periods. It is arguable that the effect of these recent changes can be seen even in a comparison of the histograms of probability density function of observed raw wind speeds for 1971-1984 and 2001-2014 shown in Figure A.2, in which speed bins are now in m/s, even though the 2001-2014 histogram is only affected by two years of the raw data that includes higher resolution wind speeds. Alternatively, there could have been either a change in the wind climate from 1971-1984 to 2001-2014 or low-frequency variability, which is more likely given the results discussed below.

For the purposes of projecting wind energy into the future, the stations with higher fractions of zero wind speeds should be used with care in de-biasing models. As the primary goal is to characterize the wind energy resource in the future, it is unlikely that areas near these stations are useful sites for wind power generation due to their past observed low mean wind speeds. However, projection of wind speeds into the future at those stations with lower mean wind speeds may be useful for other purposes, such as characterizing pollution dispersal. For that reason, projections for all of the 30 stations are included in this study.

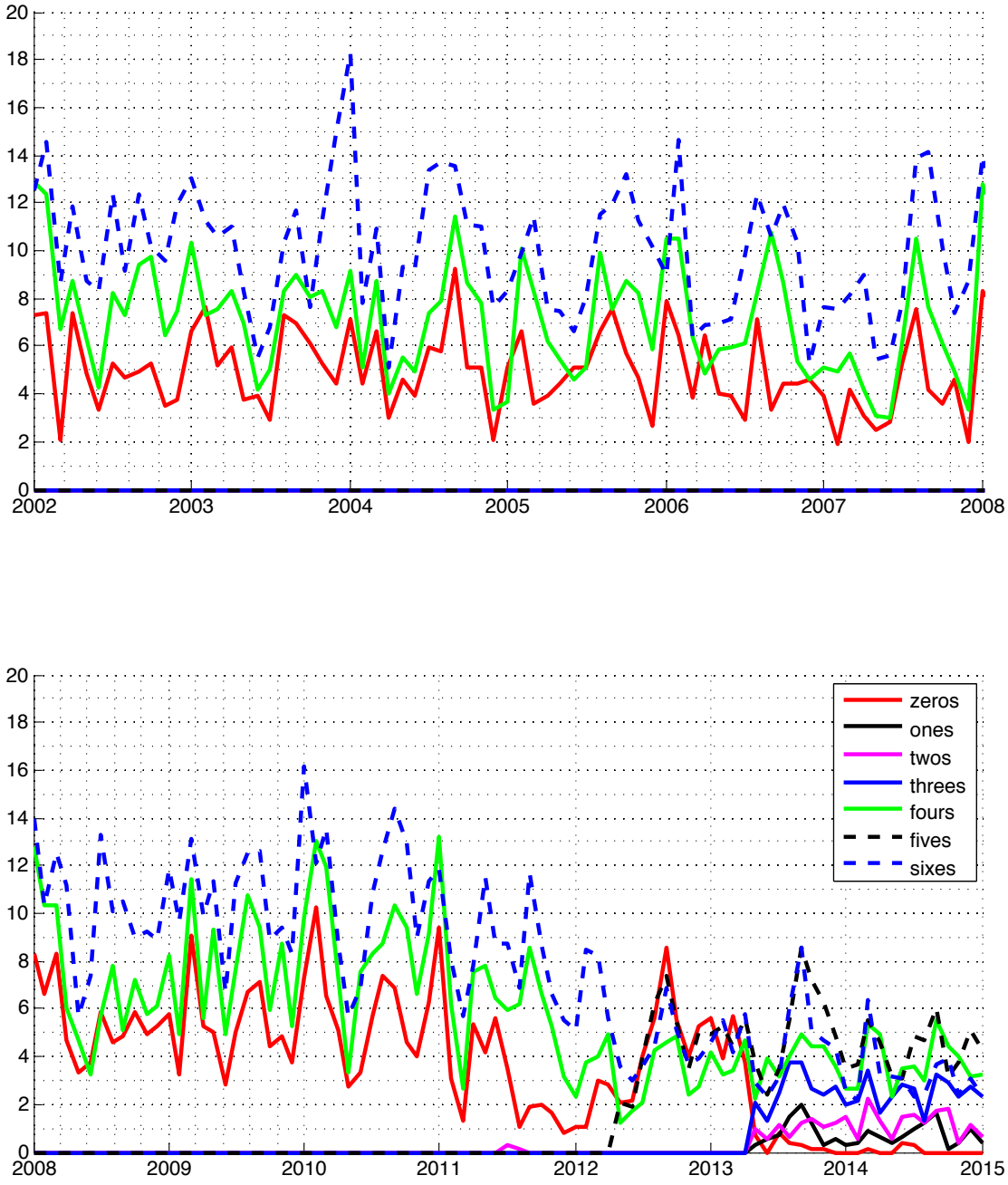

Figure A.1: Percentages of speeds of zero, one, two, three, and four km/hour in the raw hourly wind speeds by month for 2002-2014 provided by EC for the Edmonton International Airport station.

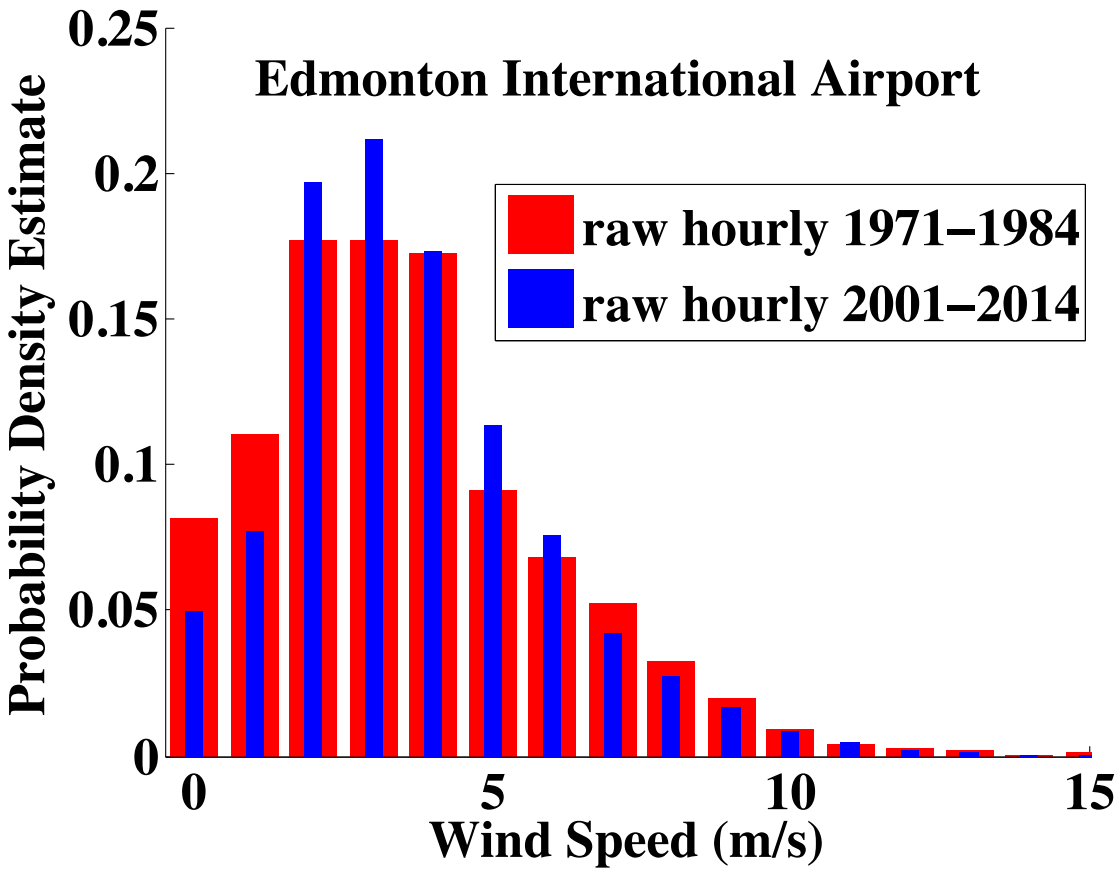

Figure A.2: Histogram estimates of the probability density function of the observed raw wind speeds at the Edmonton International Airport for 1971-1984 and 2001-2014.

Appendix B

Statistics of Ensemble Members for Period 2031-2060 normalized to the 1971-2000 values for all Stations

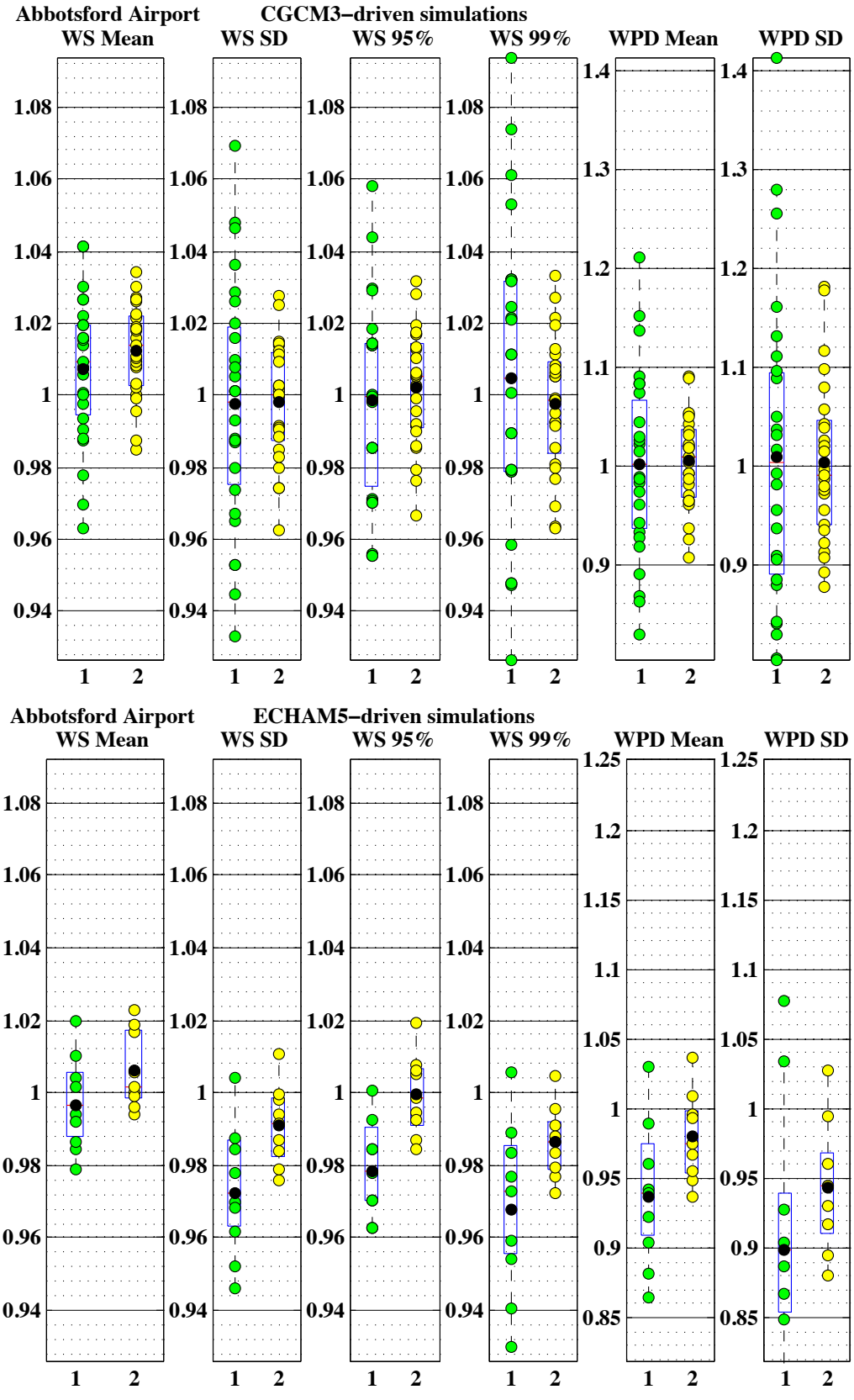

Figure B.1: As in Figure 4.6 for Abbotsford Airport station.

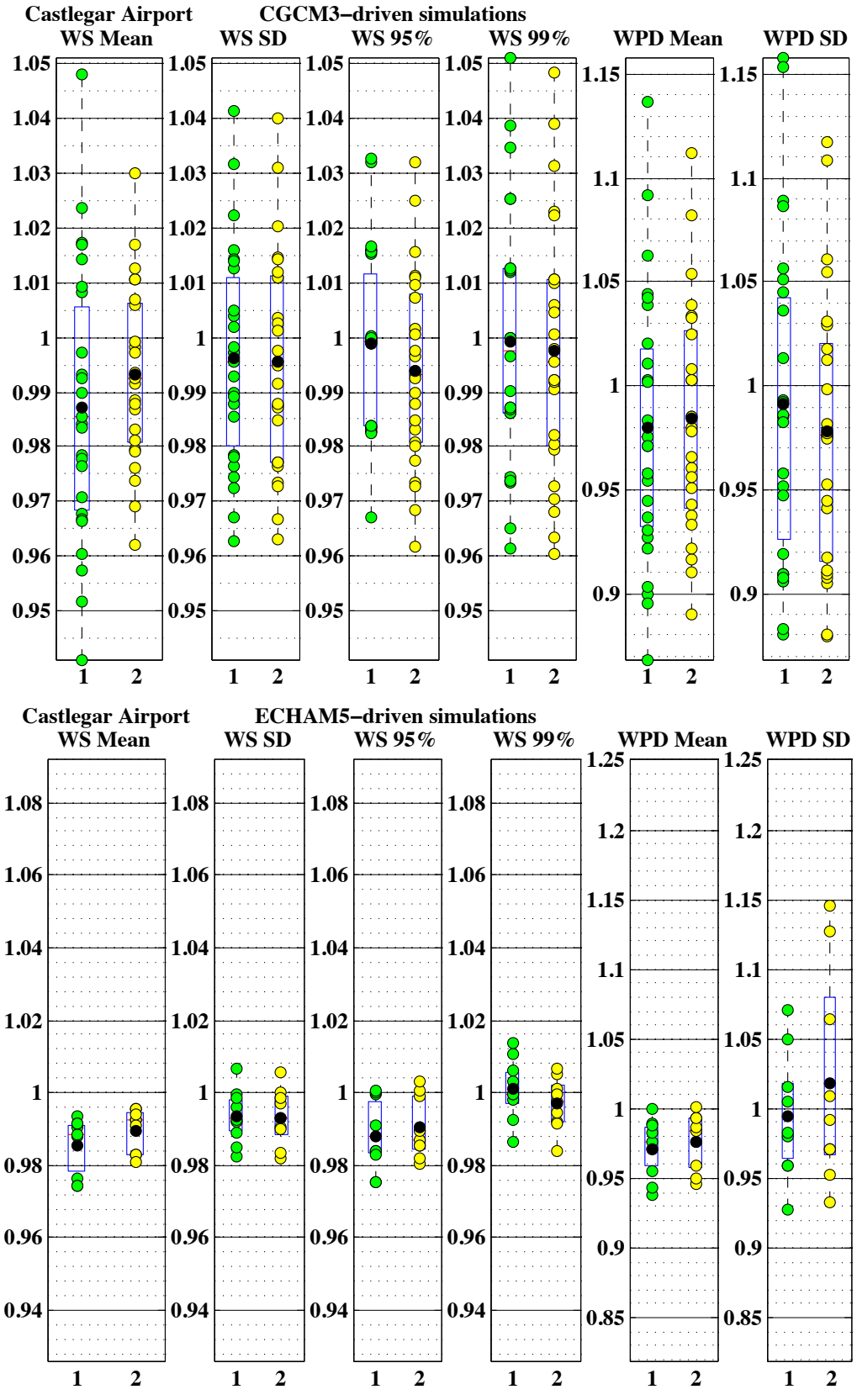

Figure B.2: As in Figure 4.6 for Castlegar Airport station.

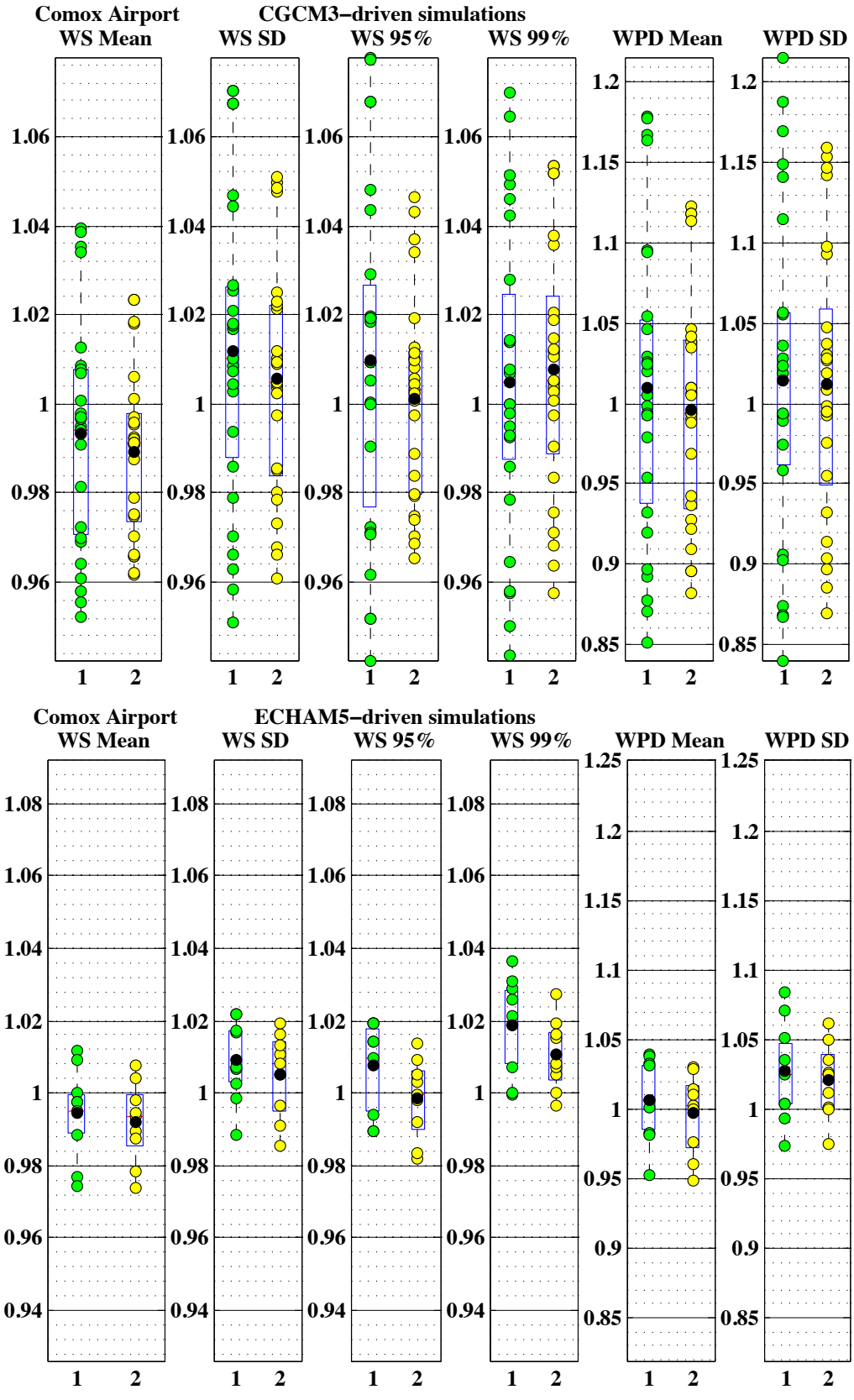

Figure B.3: As in Figure 4.6 for Comox Airport station.

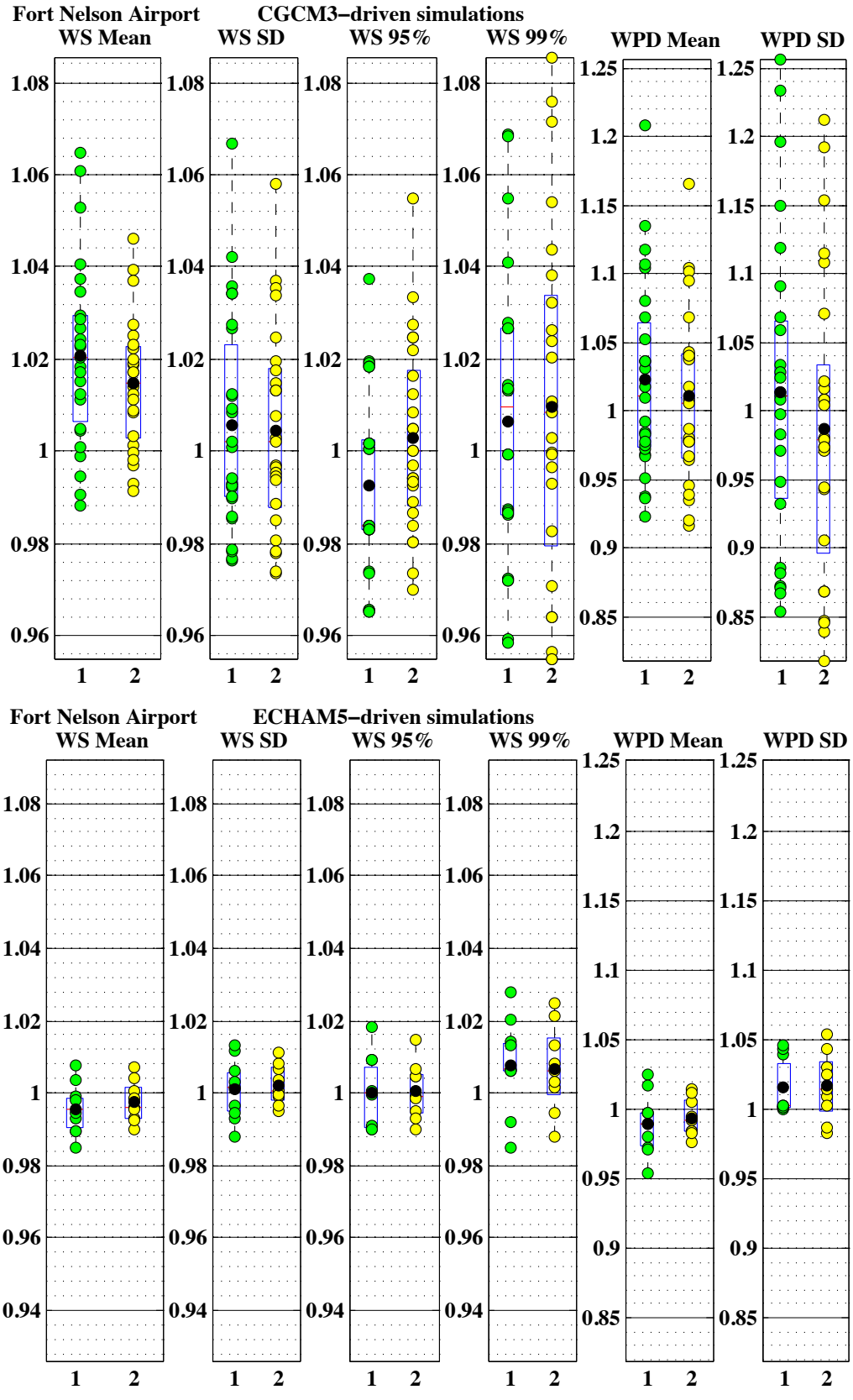

Figure B.4: As in Figure 4.6 for Fort Nelson Airport station.

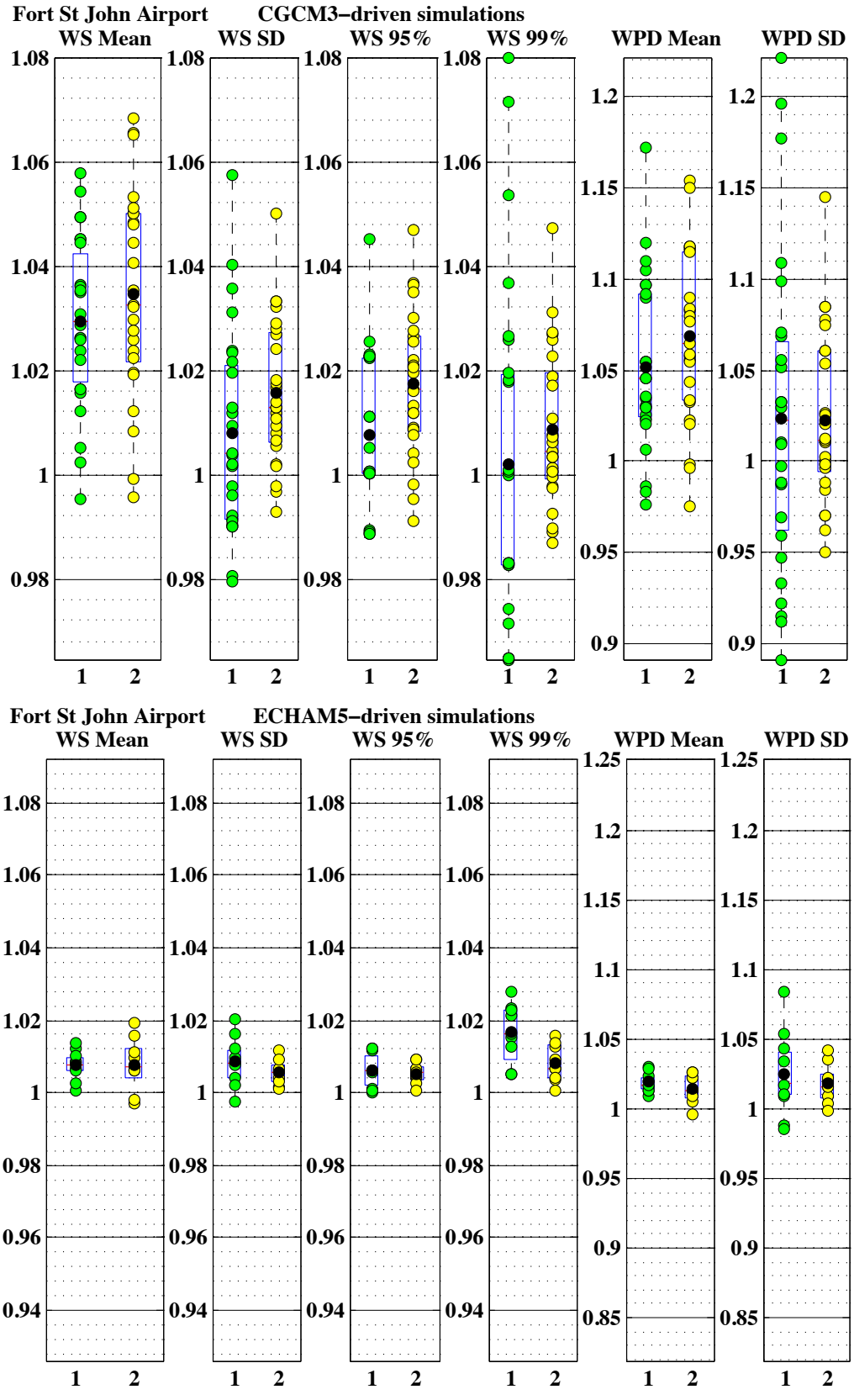

Figure B.5: As in Figure 4.6 for Fort St John Airport station.

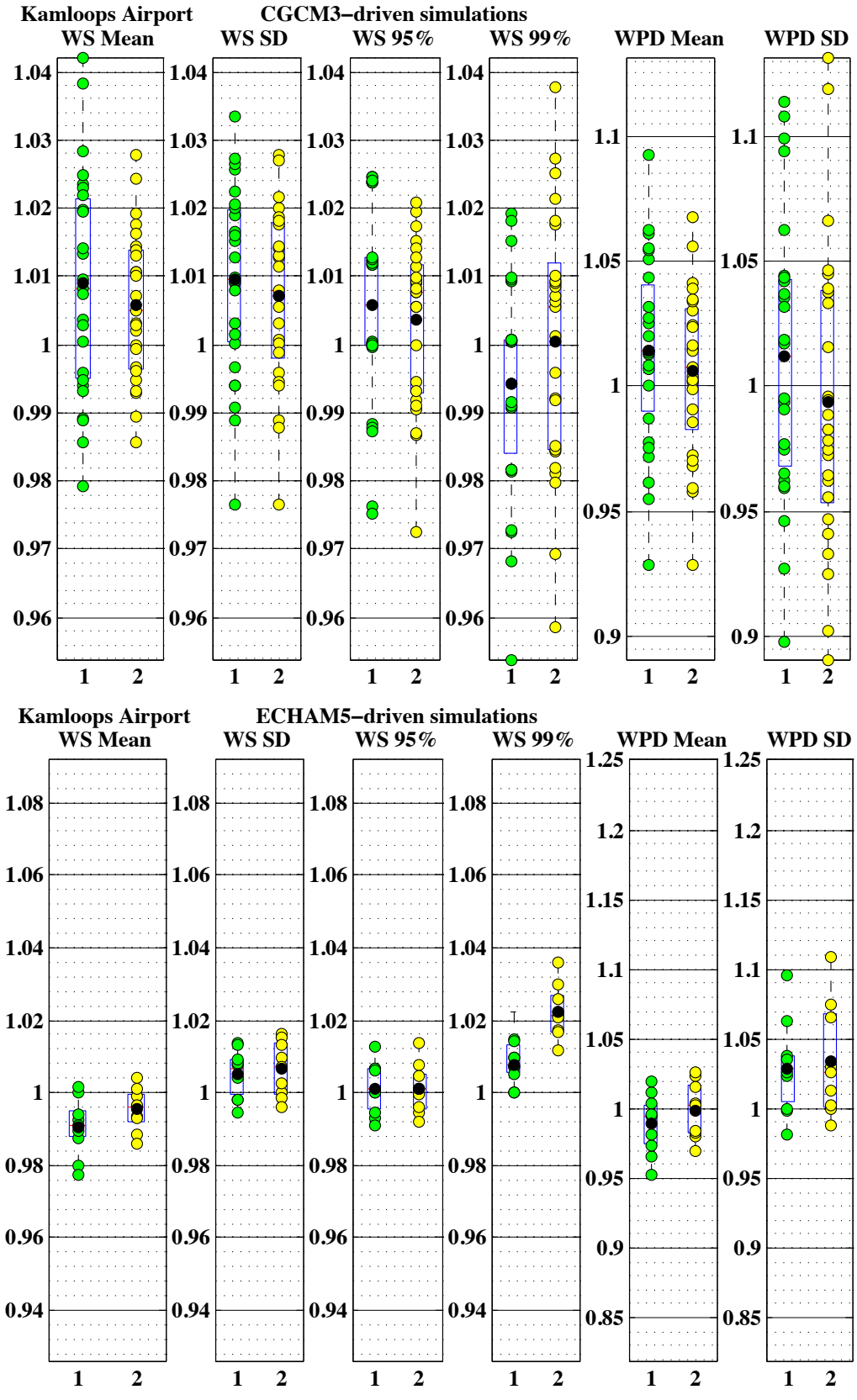

Figure B.6: As in Figure 4.6 for Kamloops Airport station.

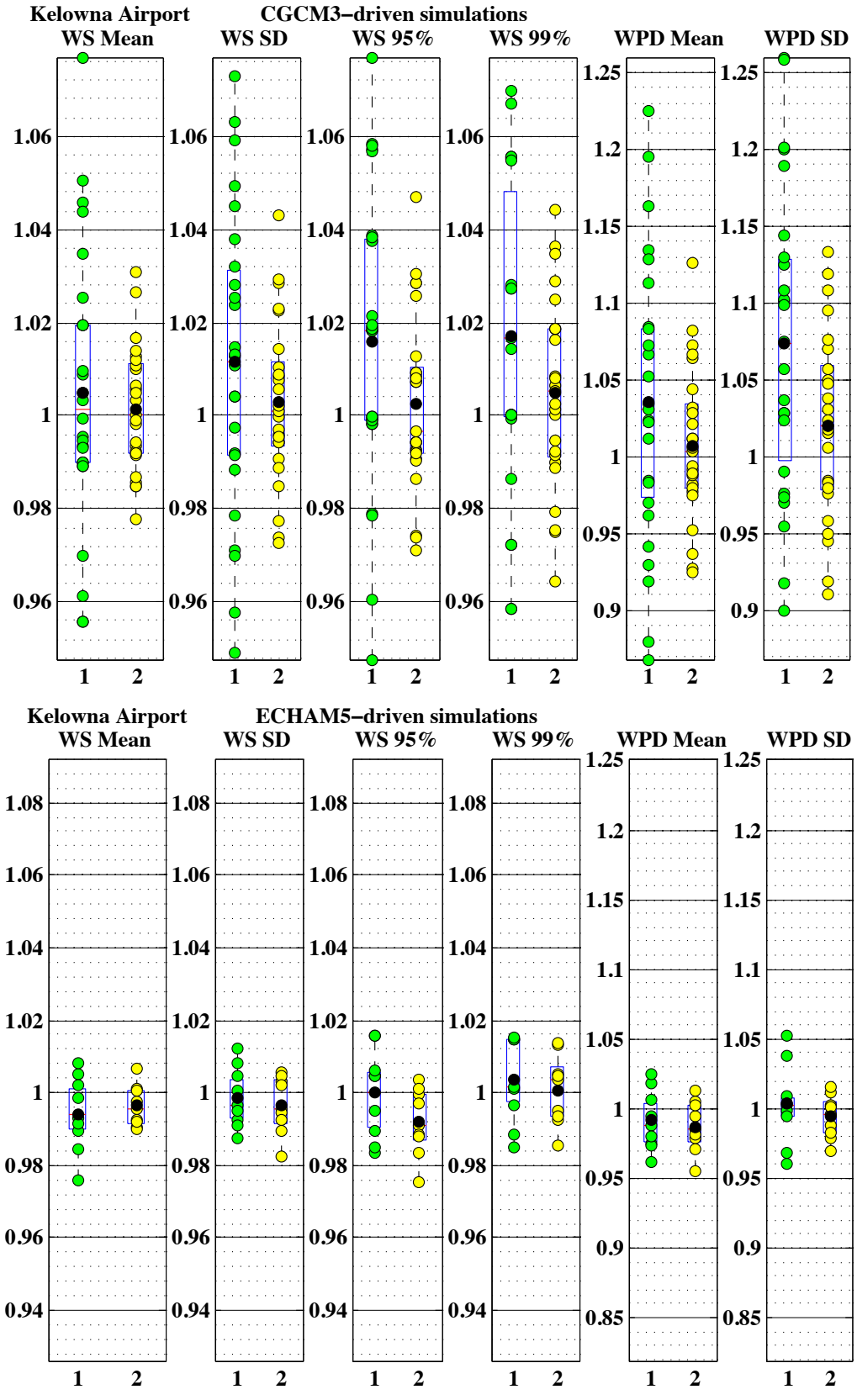

Figure B.7: As in Figure 4.6 for Kelowna Airport station.

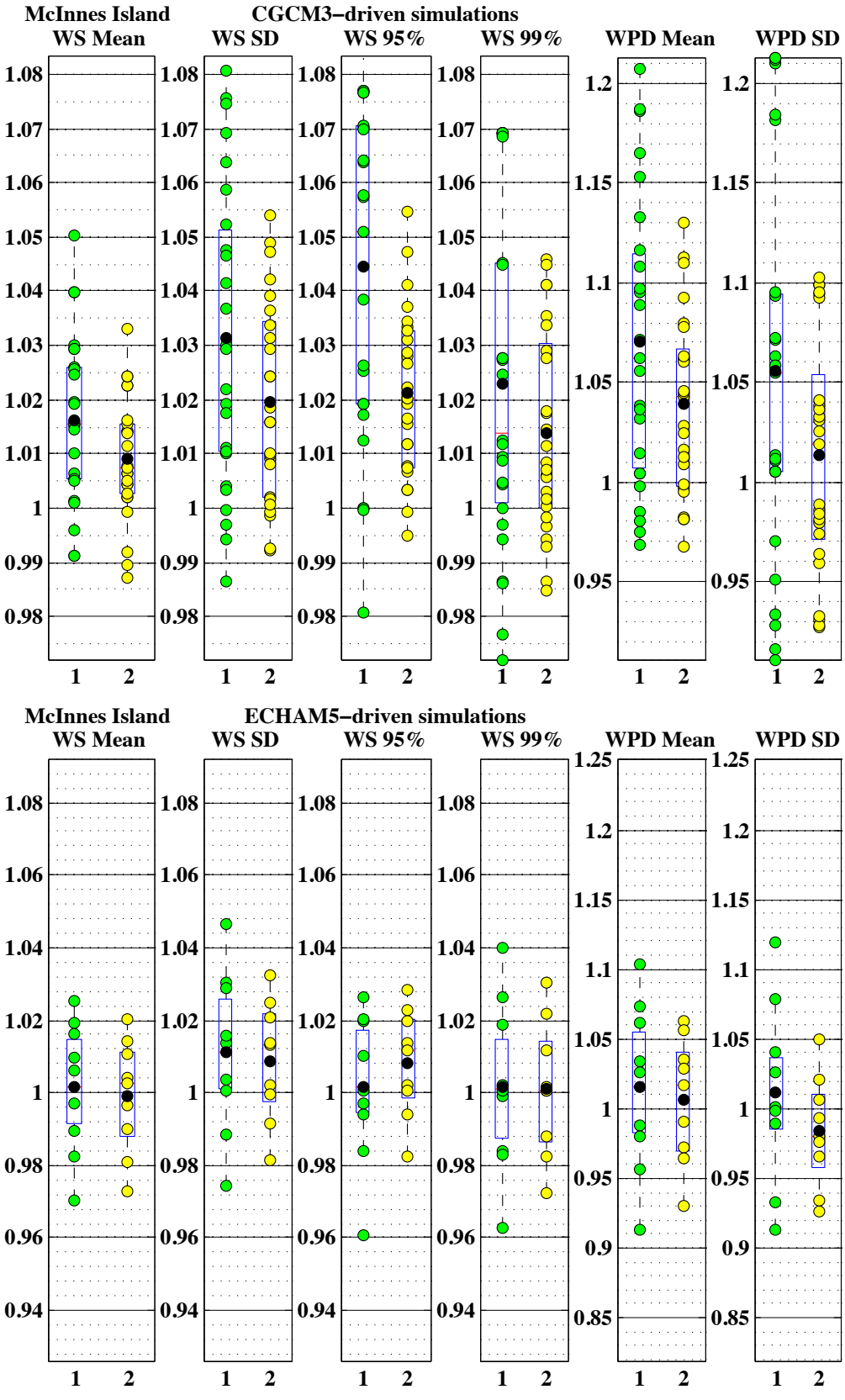

Figure B.8: As in Figure 4.6 for McInnes Island station.

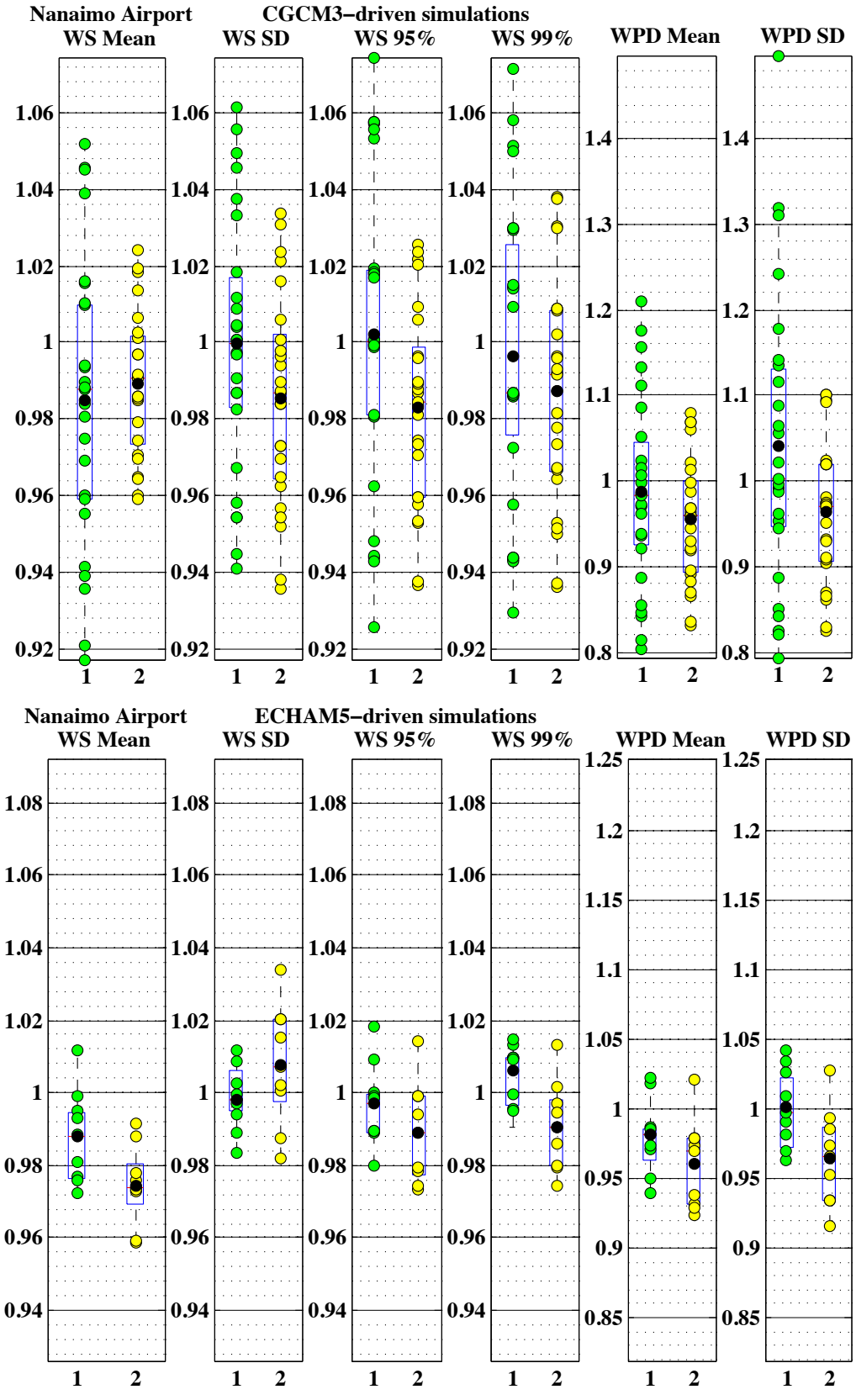

Figure B.9: As in Figure 4.6 for Nanaimo Airport station.

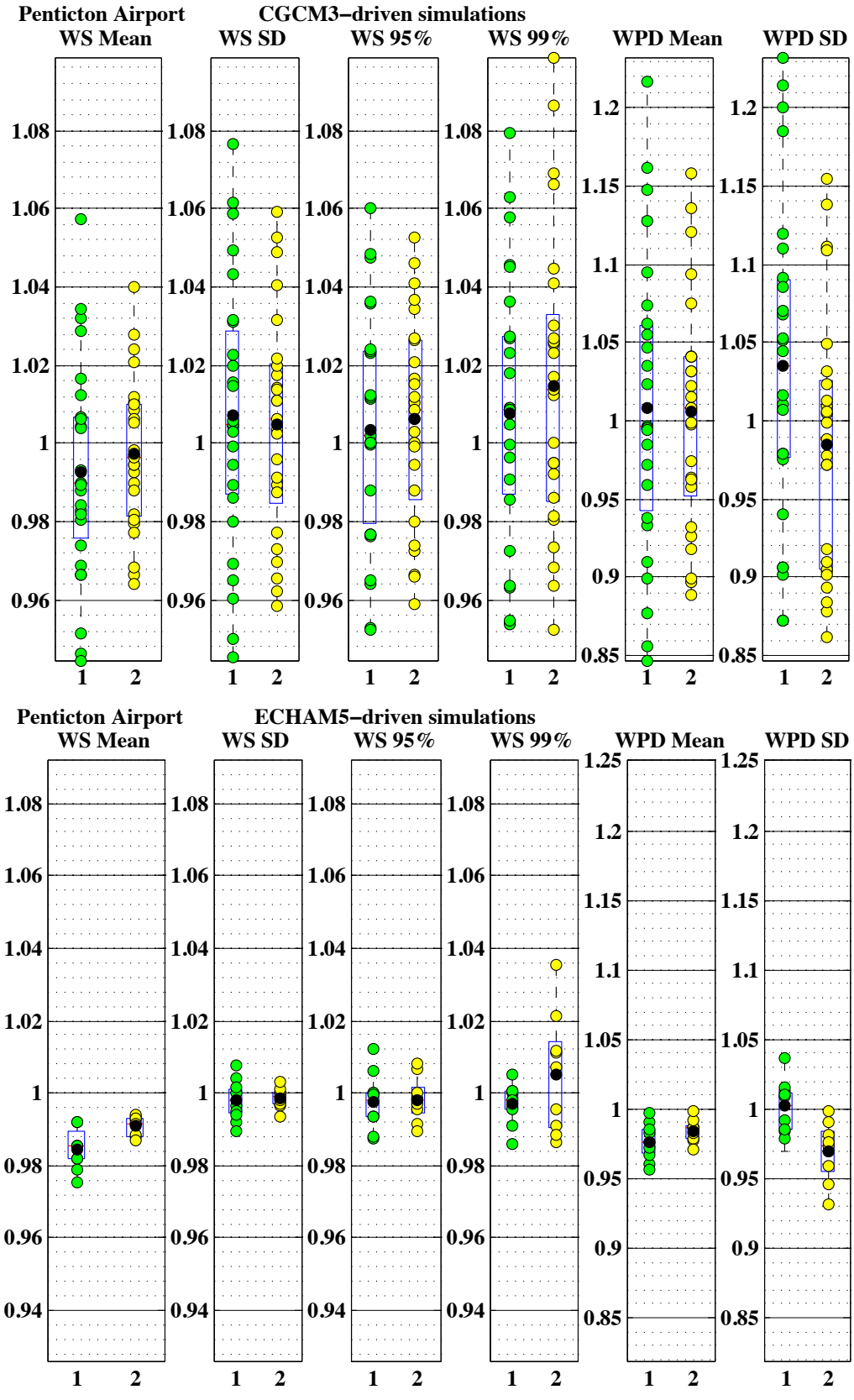

Figure B.10: As in Figure 4.6 for Penticton Airport station.

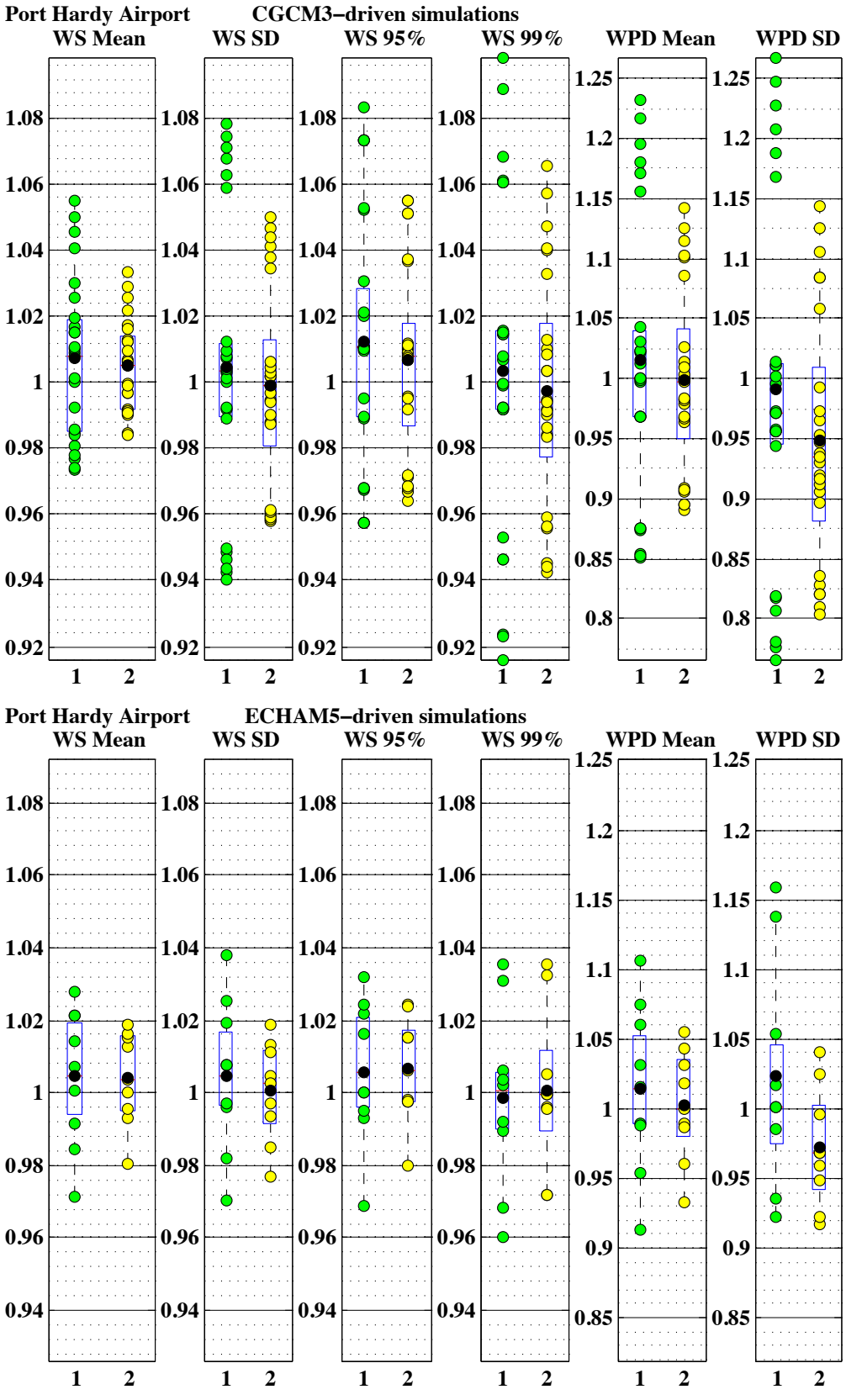

Figure B.11: As in Figure 4.6 for Port Hardy Airport station.

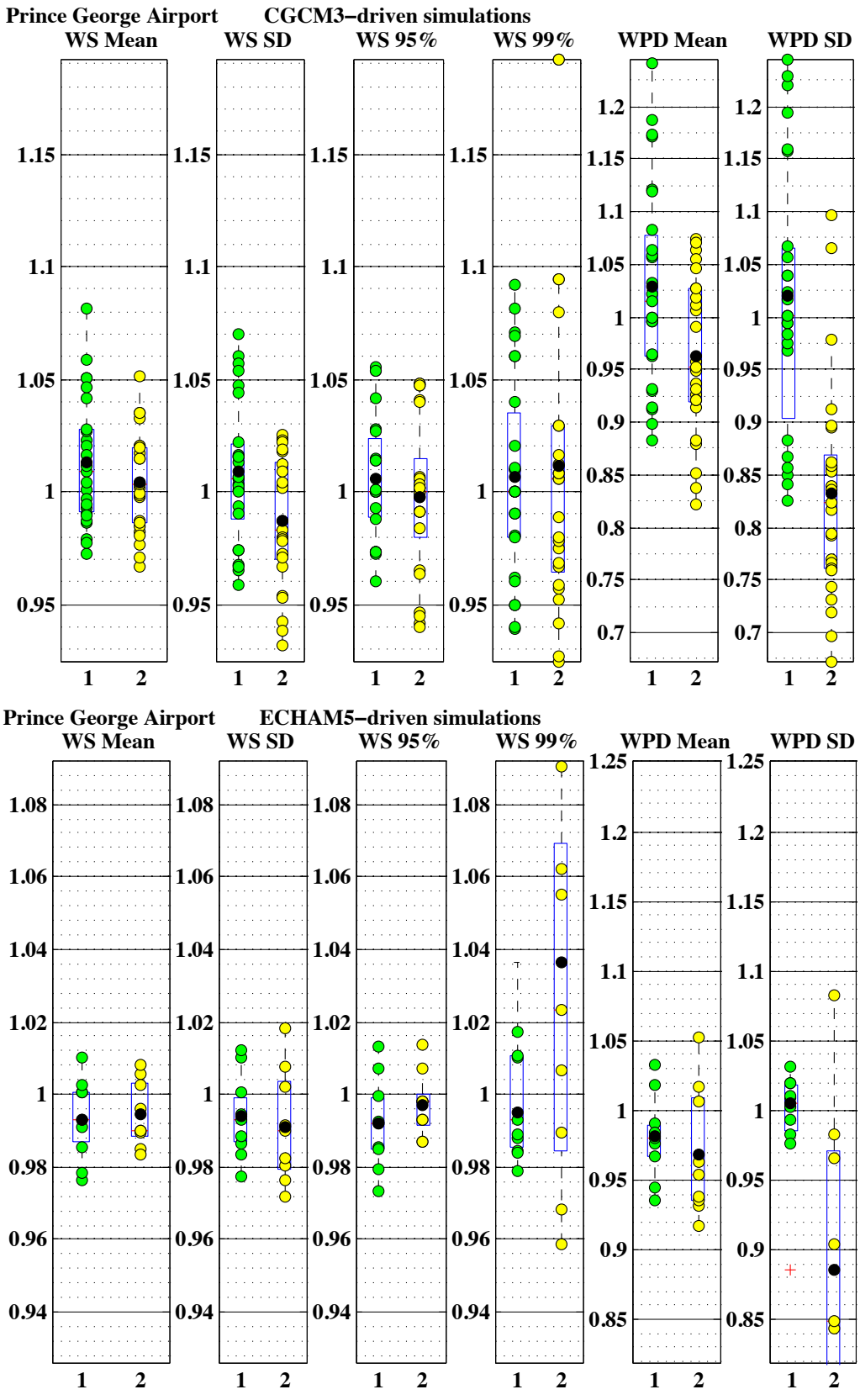

Figure B.12: As in Figure 4.6 for Prince George Airport station.

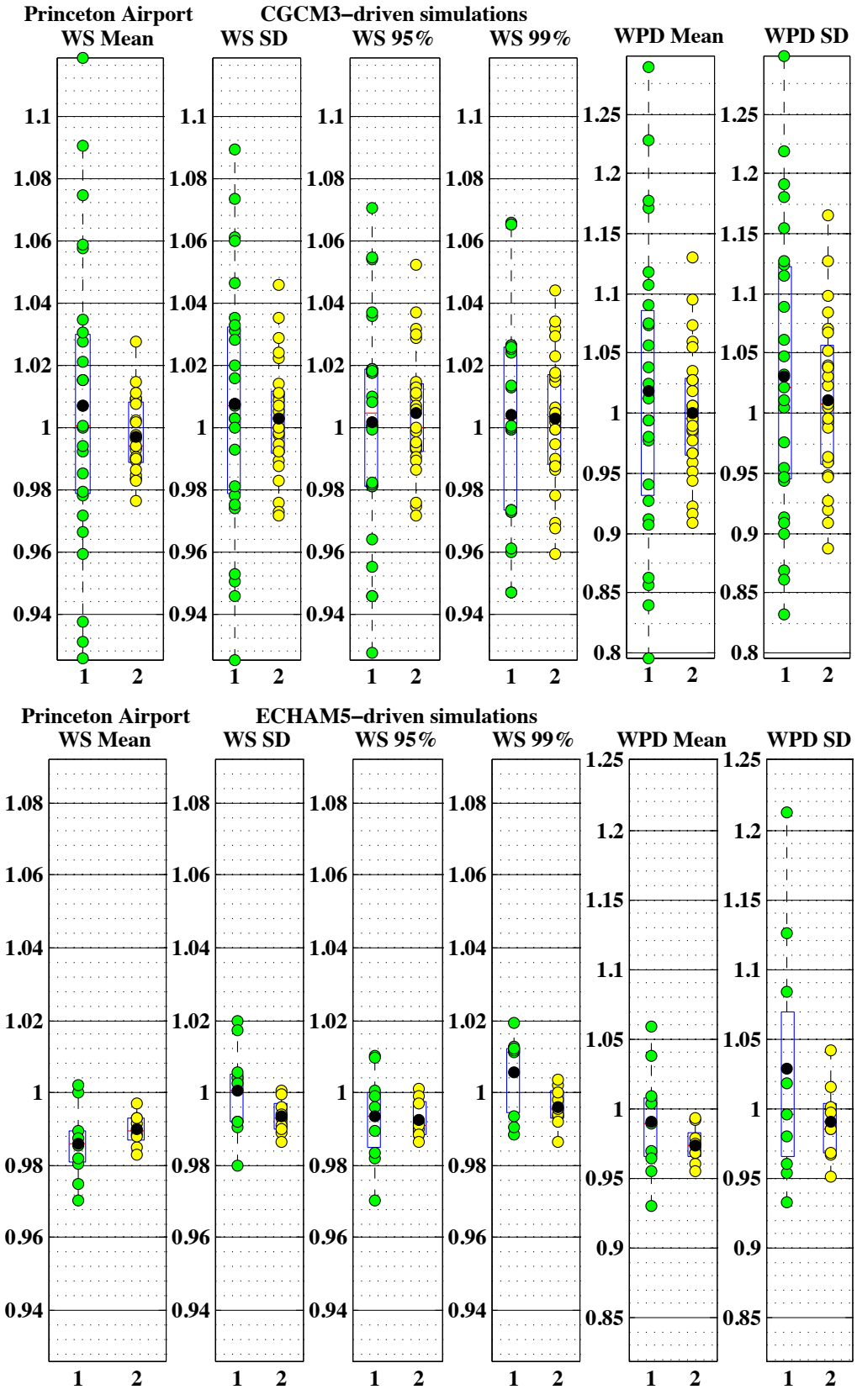

Figure B.13: As in Figure 4.6 for Princeton Airport station.

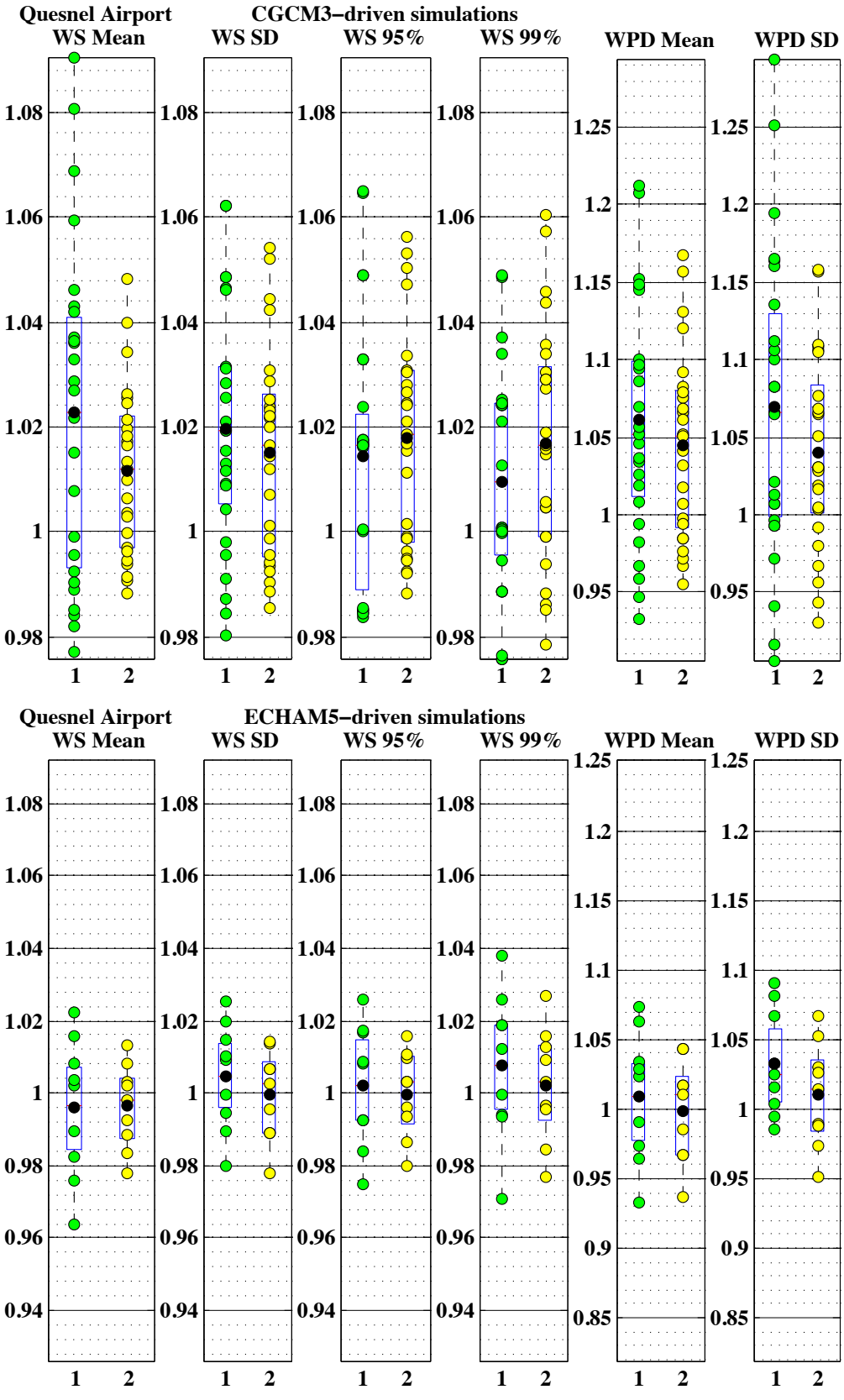

Figure B.14: As in Figure 4.6 for Quesnel Airport station.

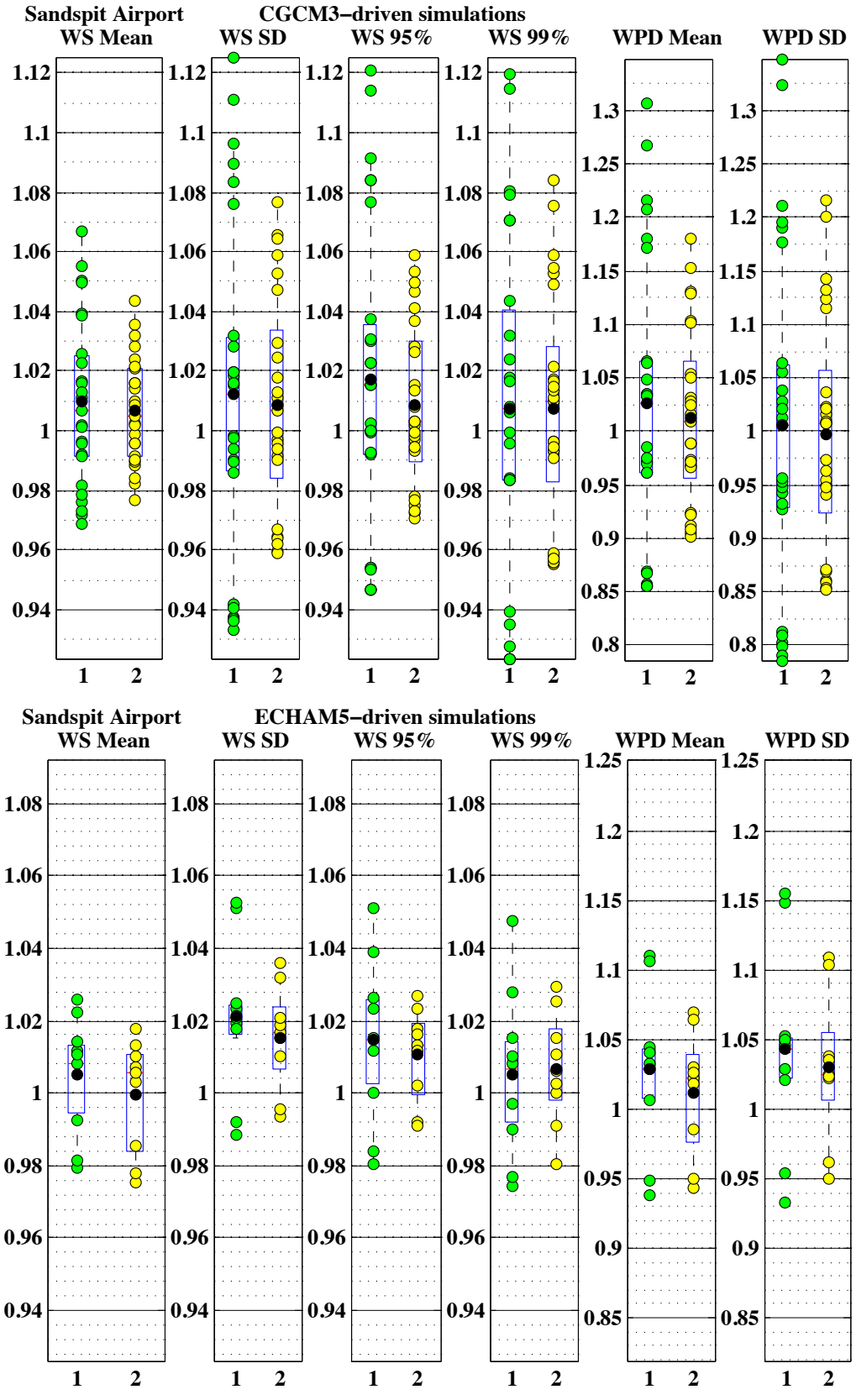

Figure B.15: As in Figure 4.6 for Sandspit Airport station.

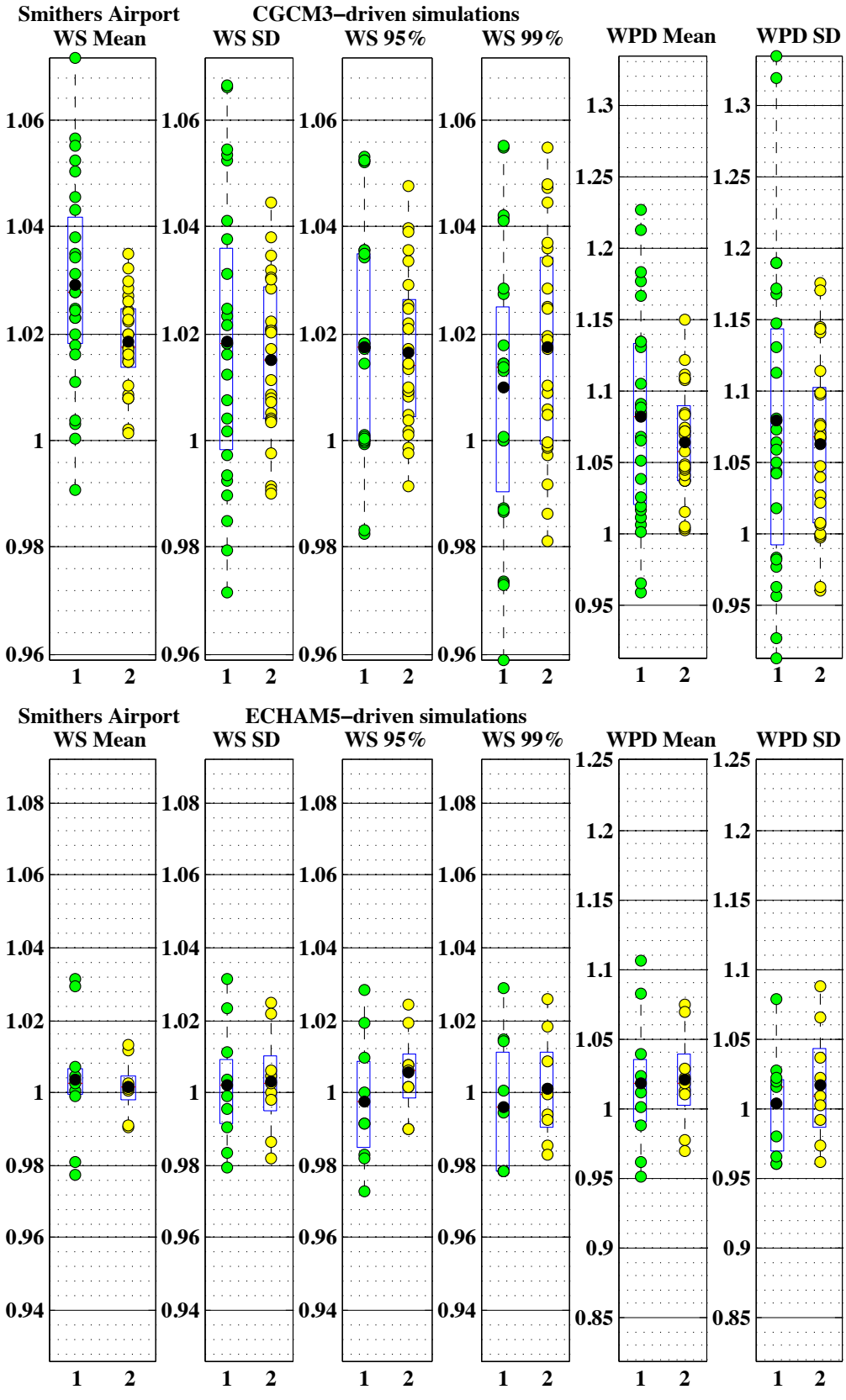

Figure B.16: As in Figure 4.6 for Smithers Airport station.

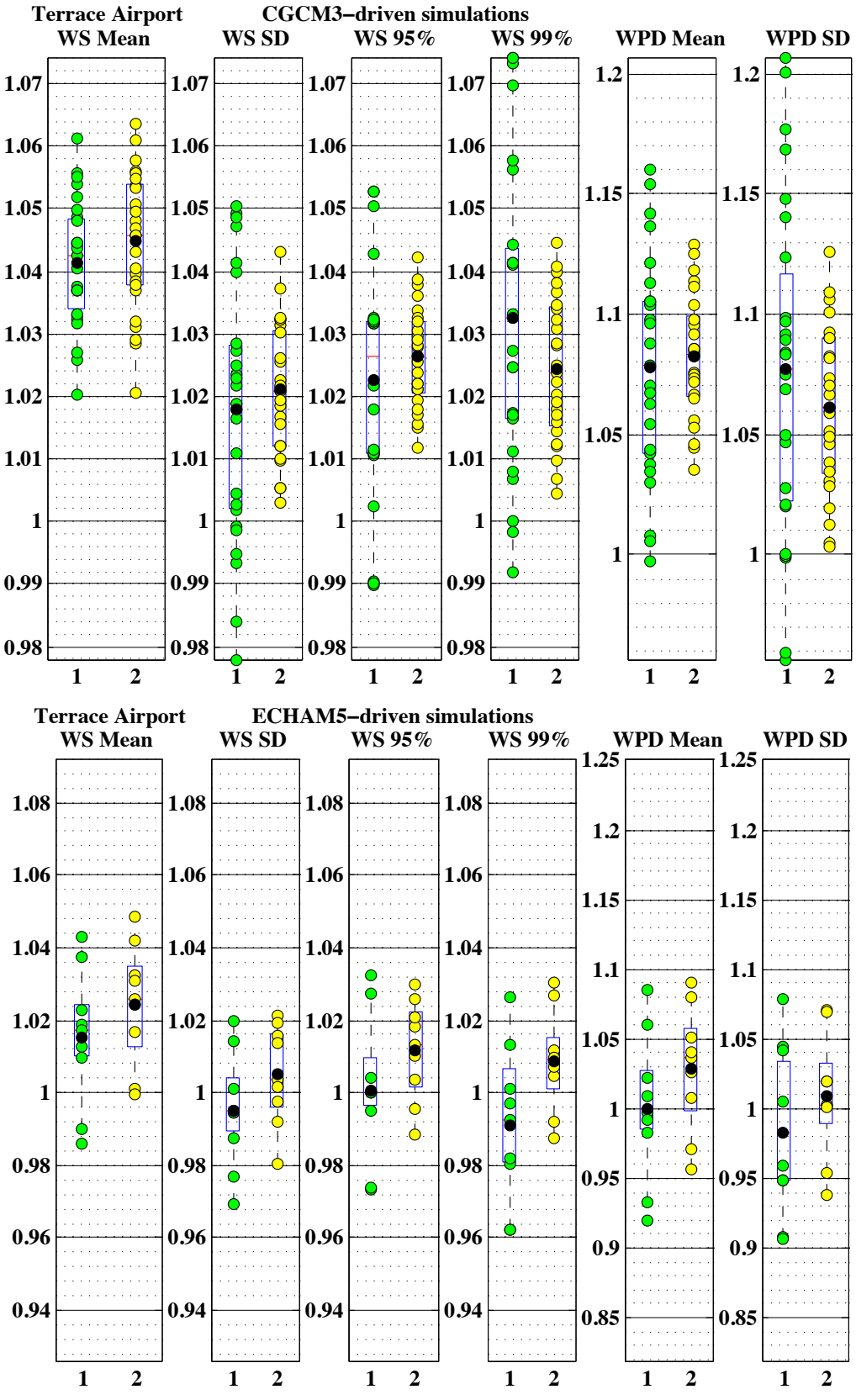

Figure B.17: As in Figure 4.6 for Terrace Airport station.

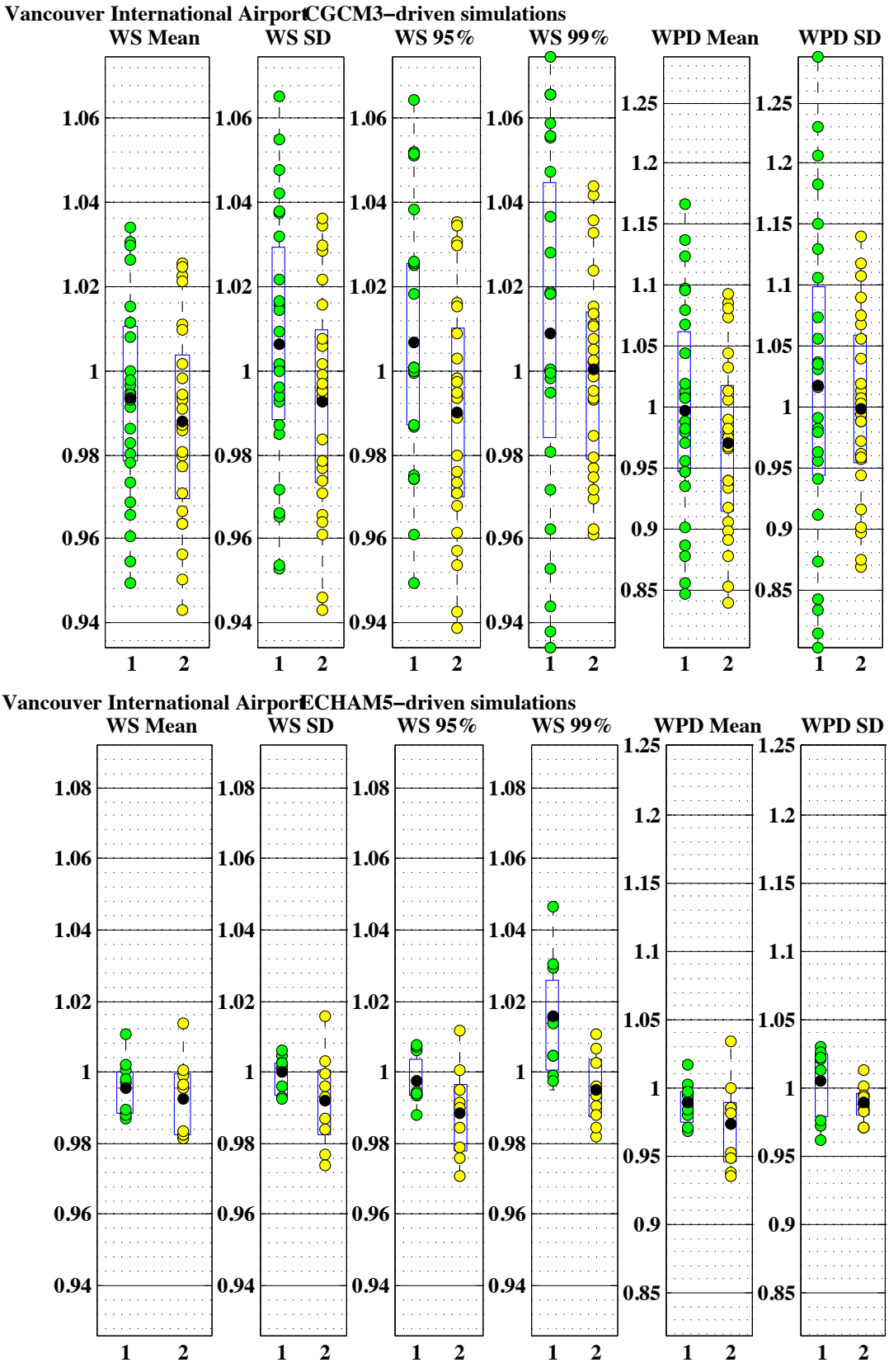

Figure B.18: As in Figure 4.6 for Vancouver International Airport station.

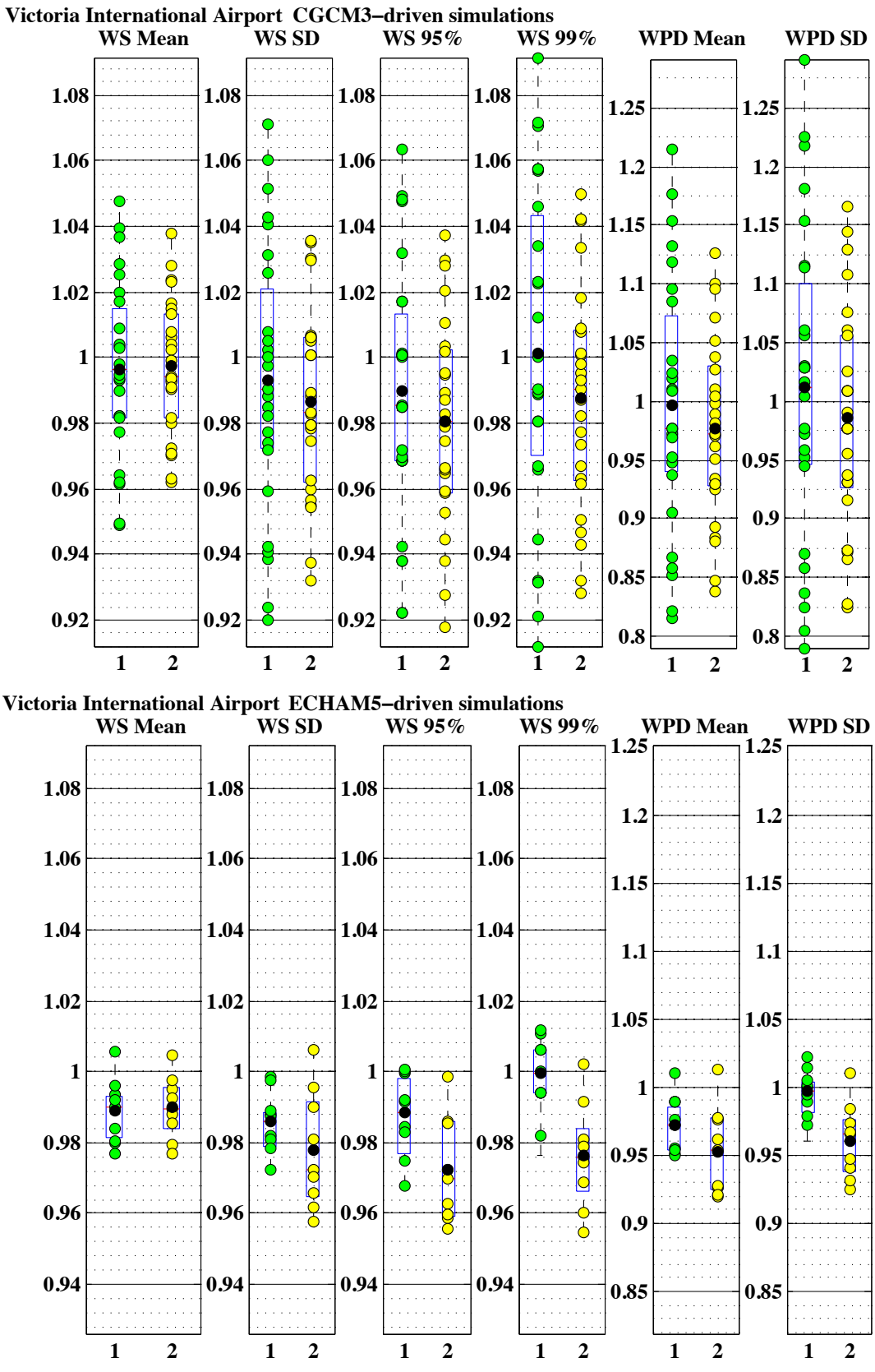

Figure B.19: As in Figure 4.6 for Victoria International Airport station.

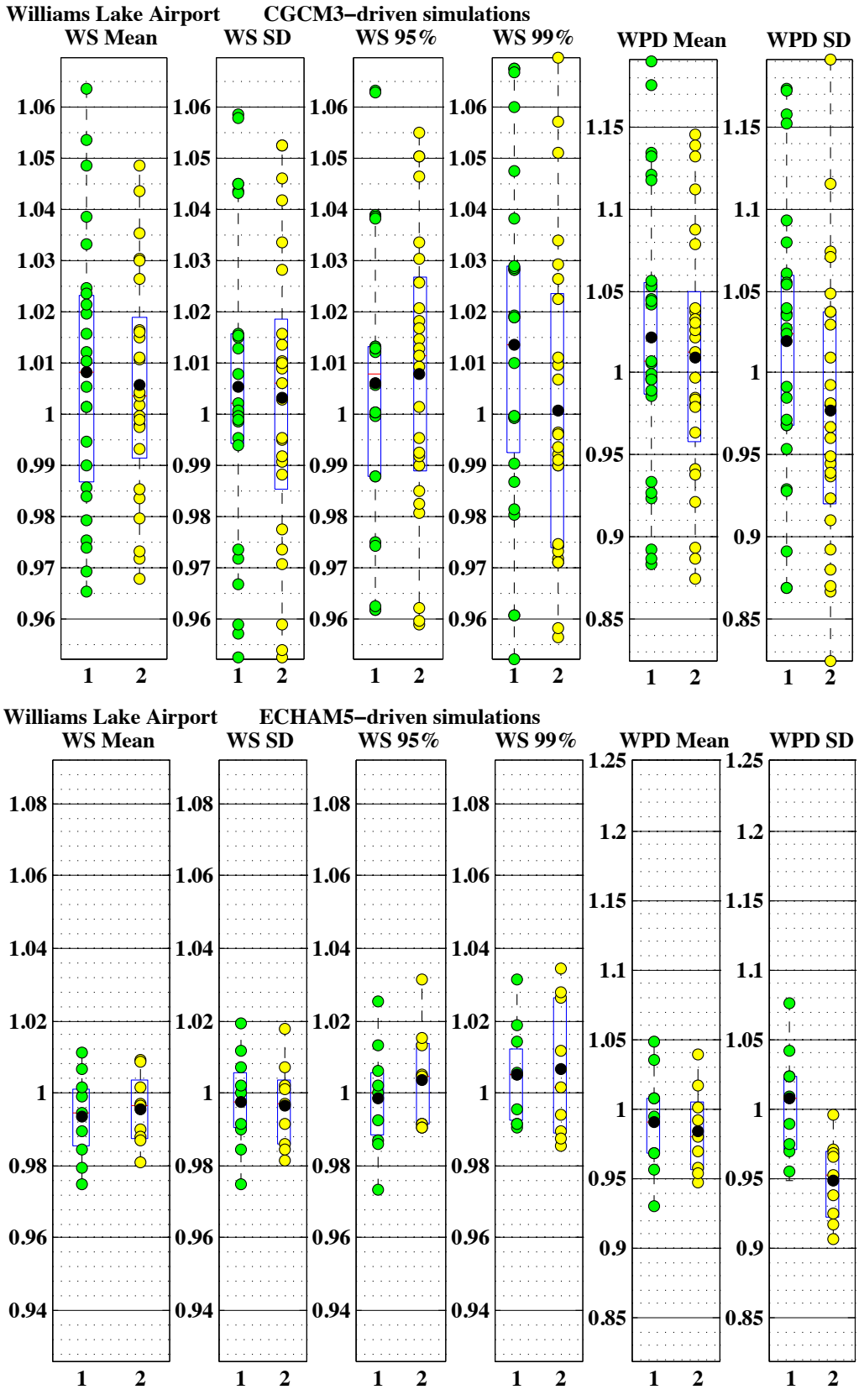

Figure B.20: As in Figure 4.6 for Williams Lake Airport station.

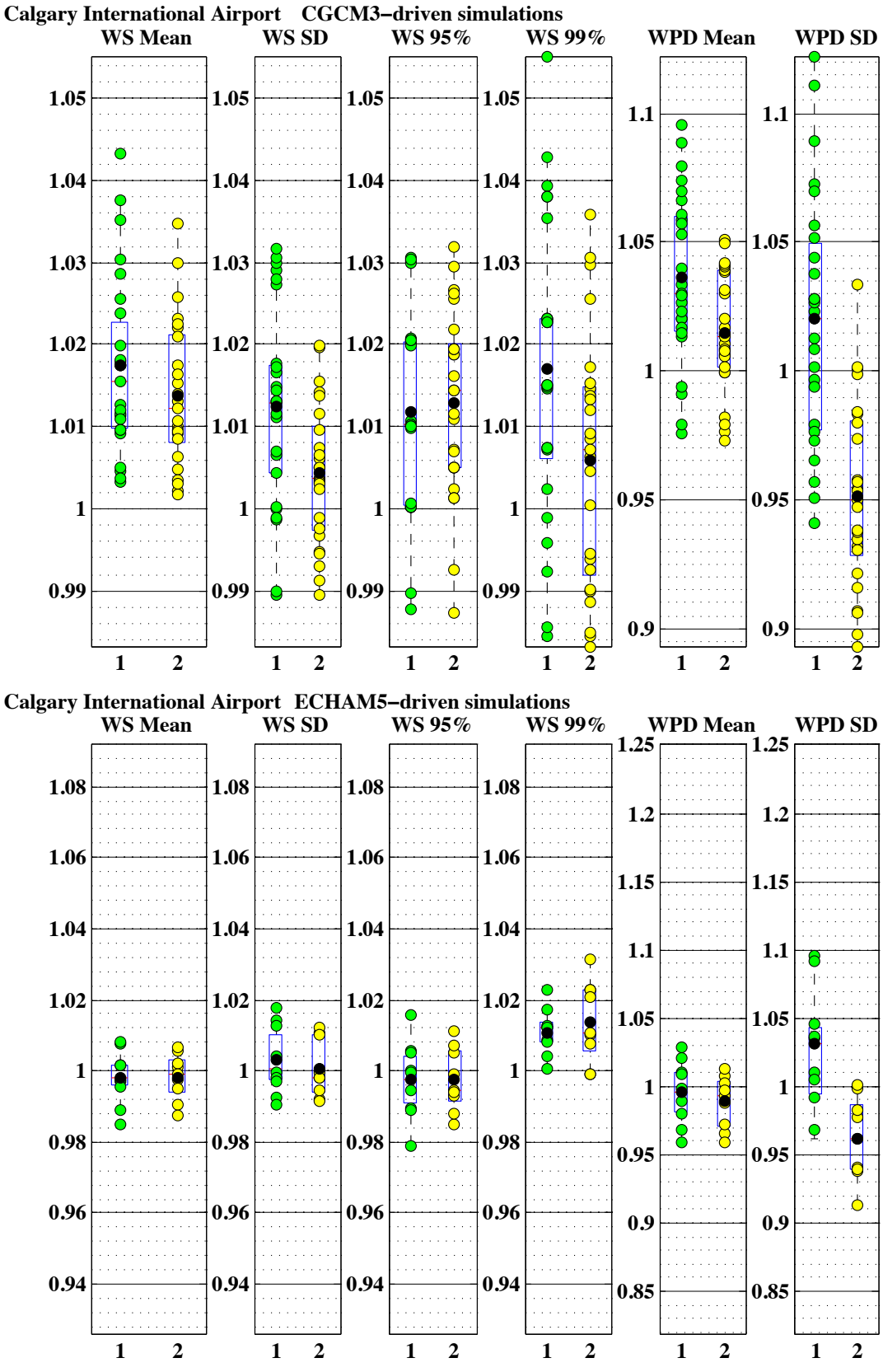

Figure B.21: As in Figure 4.6 for Calgary International Airport station.

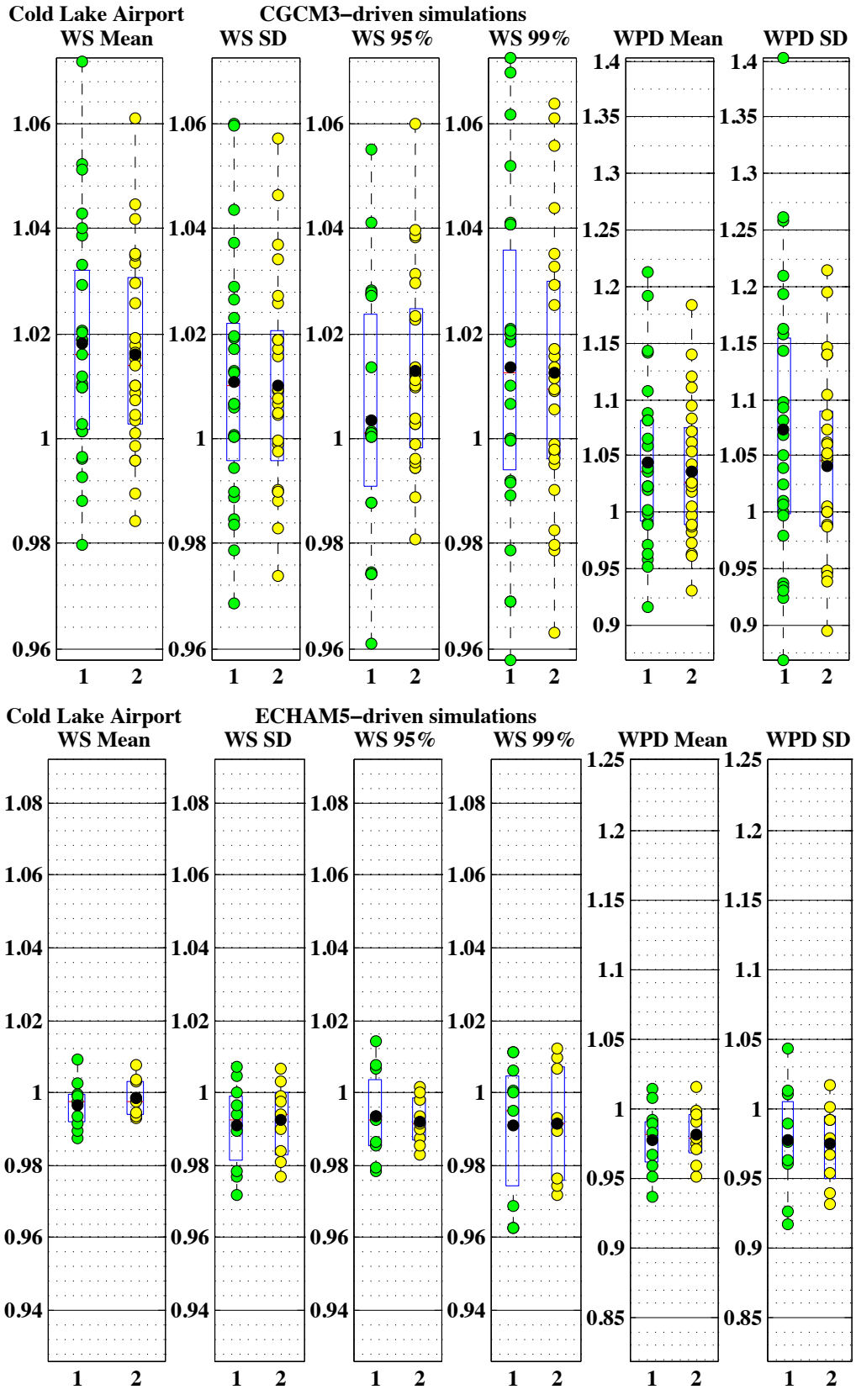

Figure B.22: As in Figure 4.6 for Cold Lake Airport station.

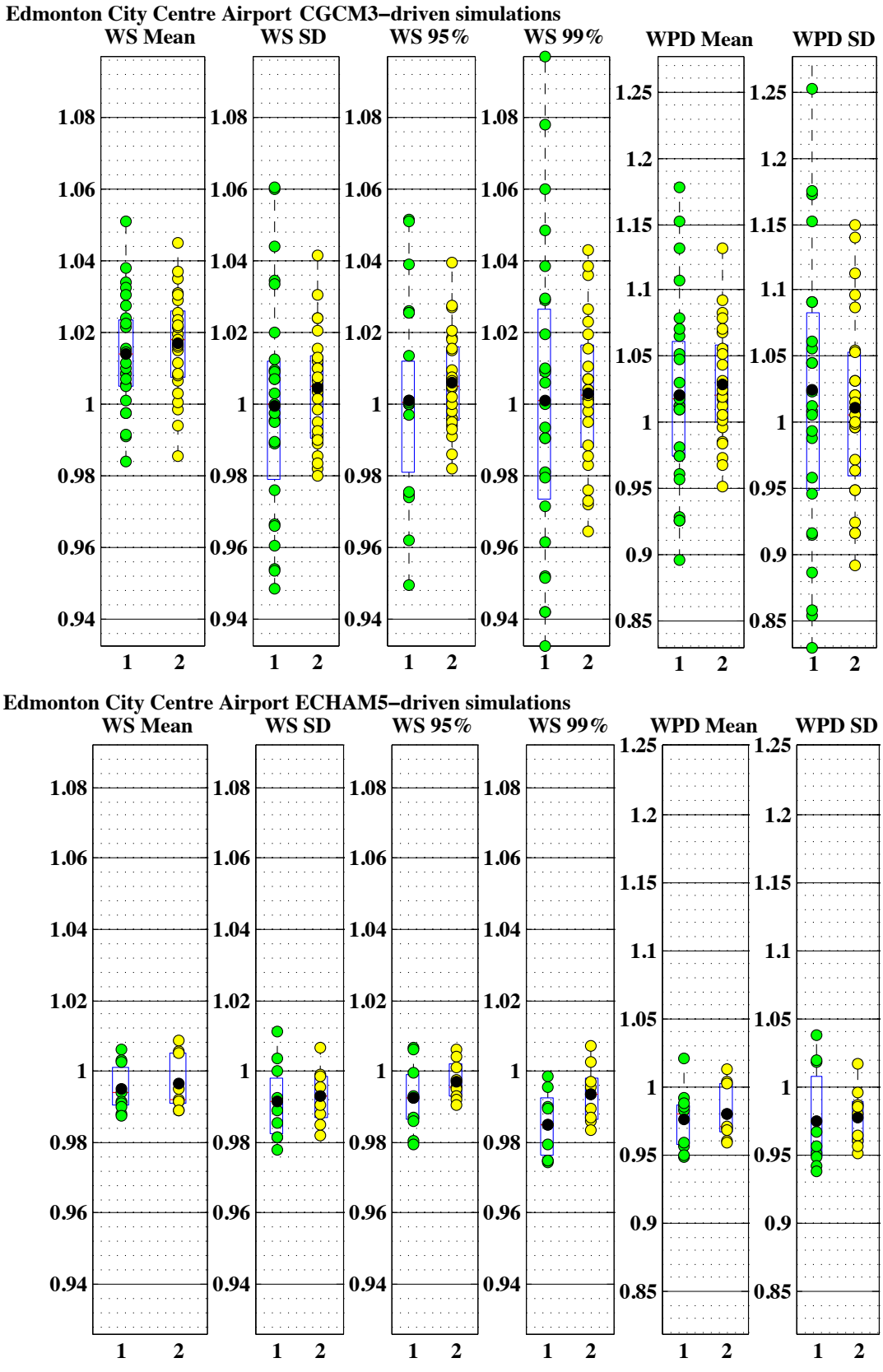

Figure B.23: As in Figure 4.6 for Edmonton City Centre Airport station.

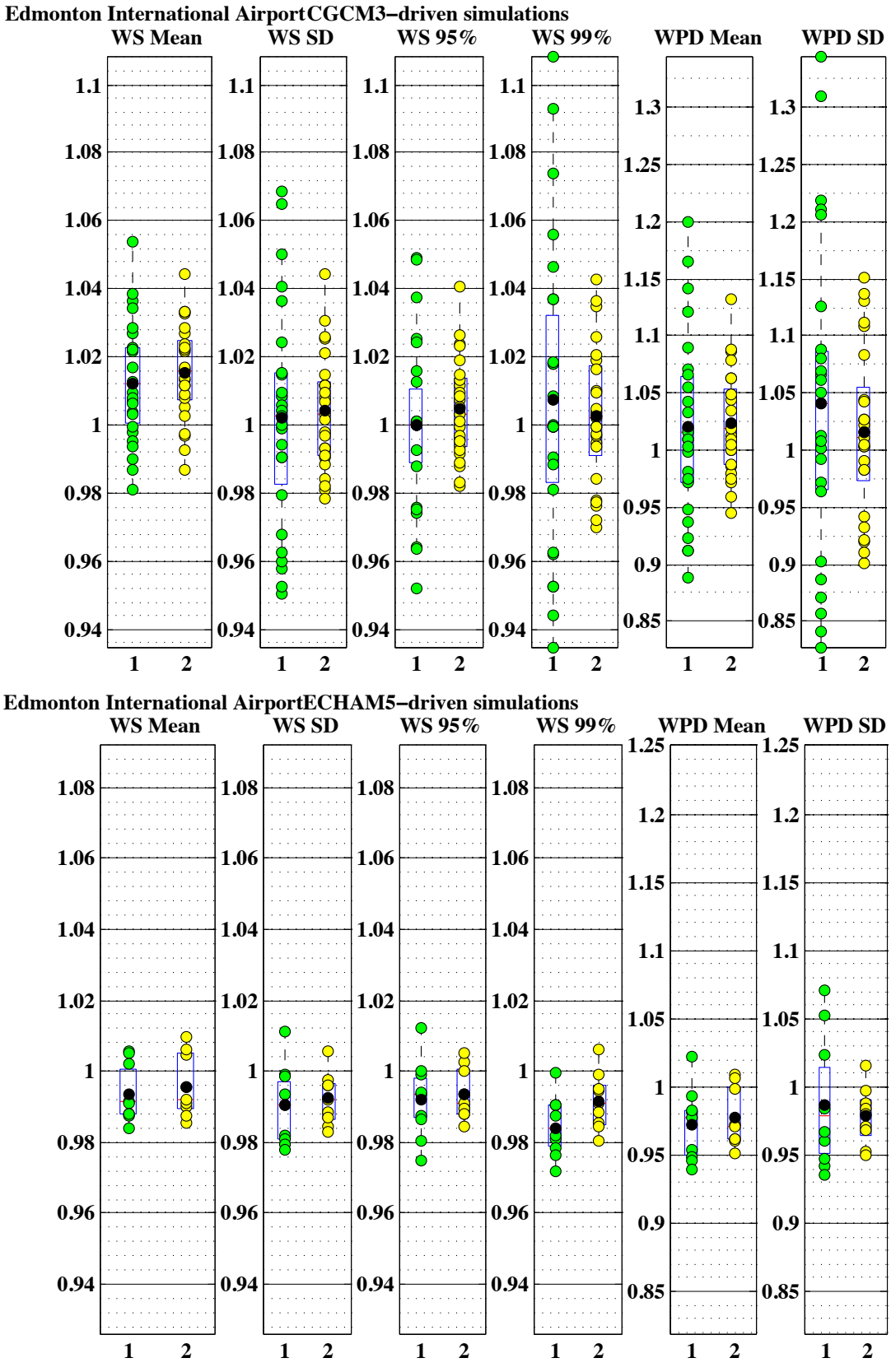

Figure B.24: As in Figure 4.6 for Edmonton International Airport station.

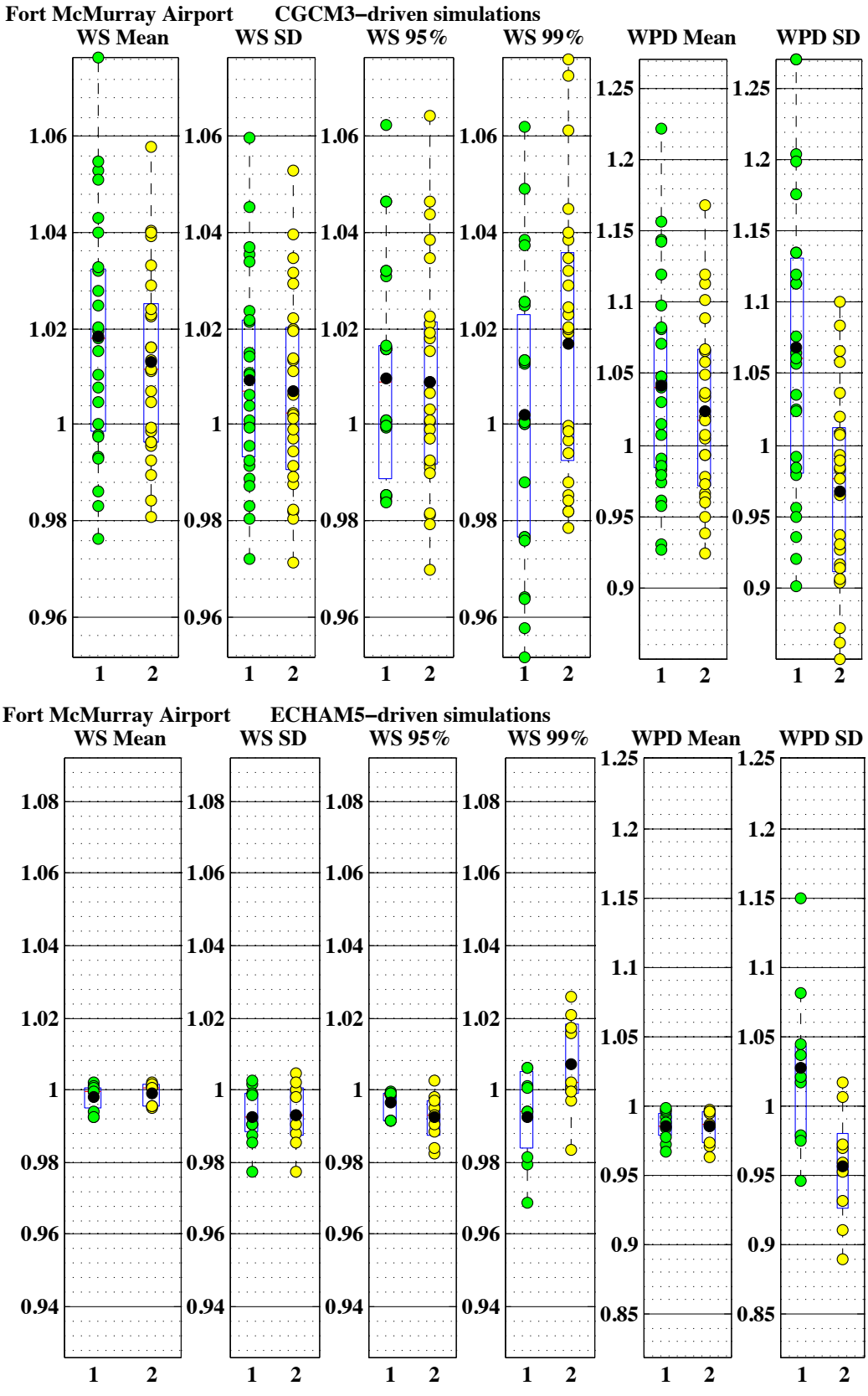

Figure B.25: As in Figure 4.6 for Fort McMurray Airport station.

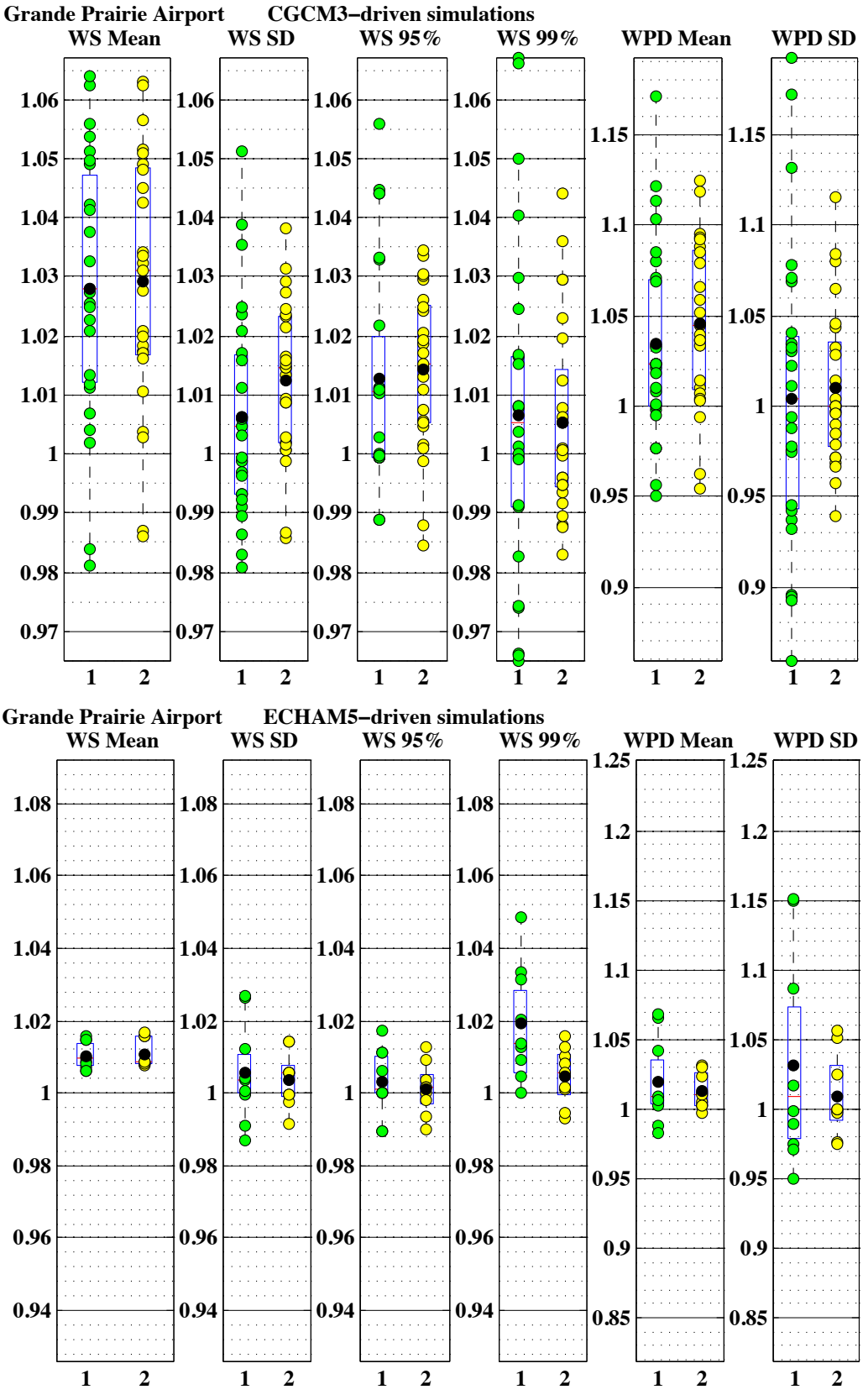

Figure B.26: As in Figure 4.6 for Grande Prairie Airport station.

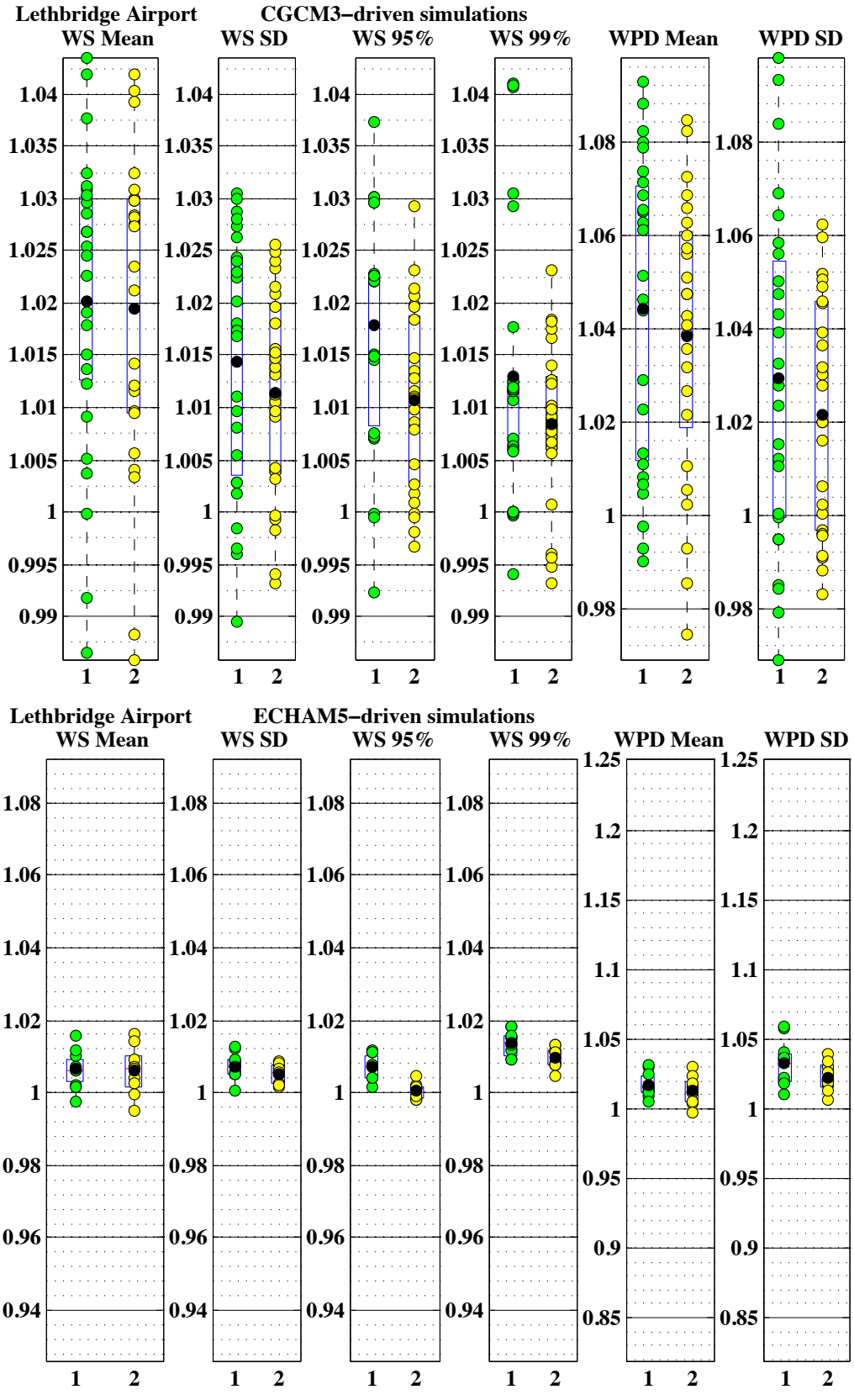

Figure B.27: As in Figure 4.6 for Lethbridge Airport station.

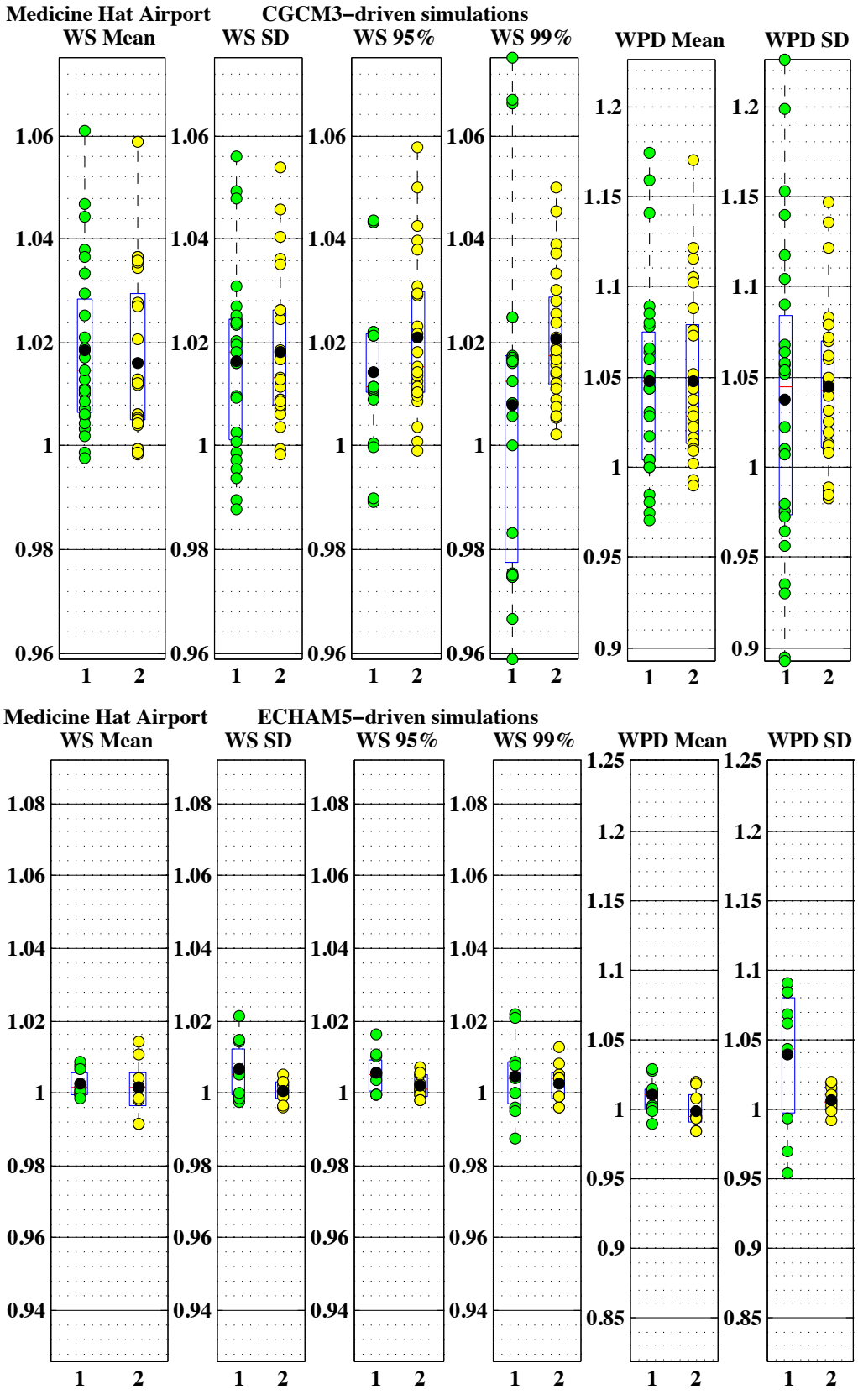

Figure B.28: As in Figure 4.6 for Medicine Hat Airport station.

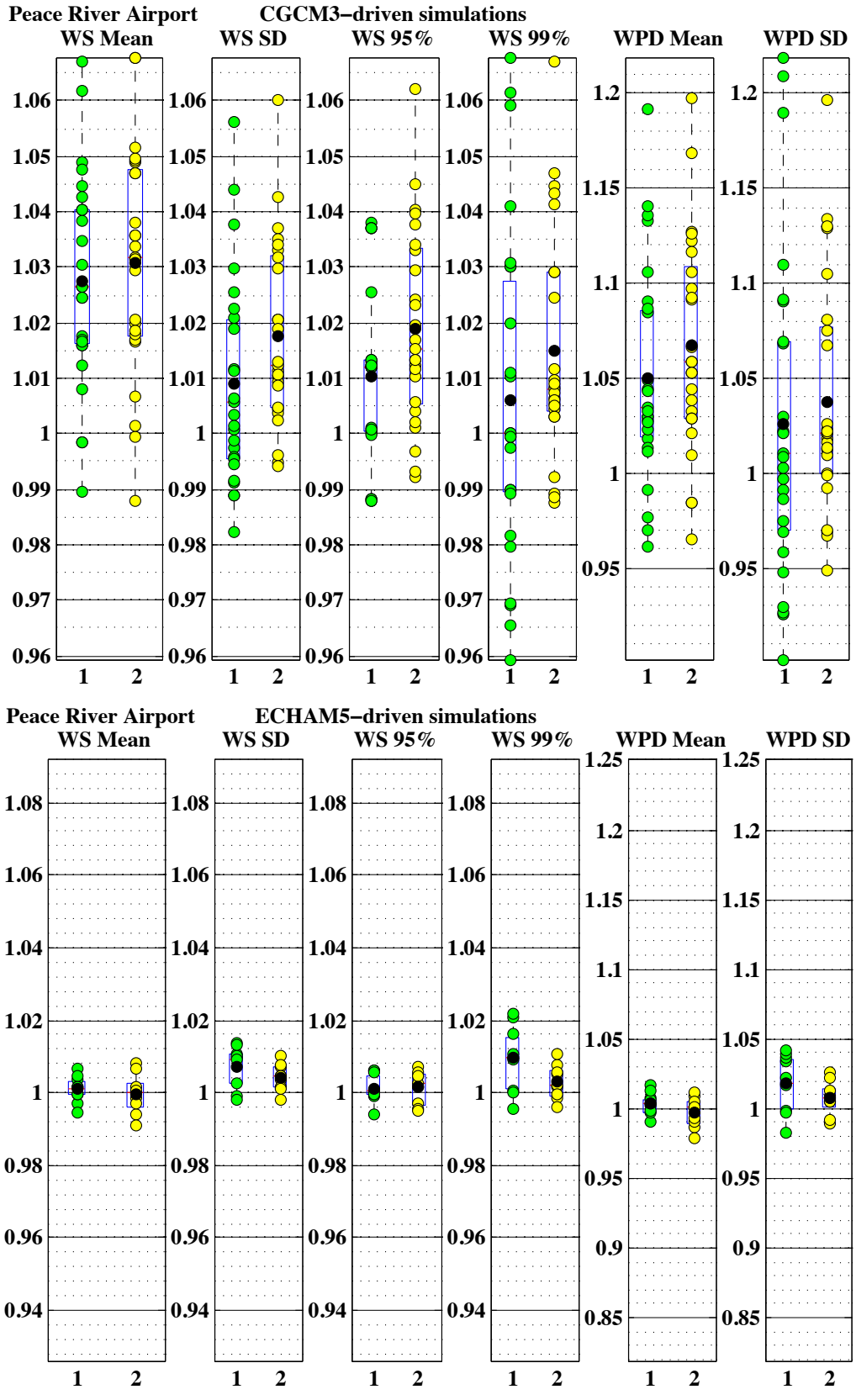

Figure B.29: As in Figure 4.6 for Peace River Airport station.

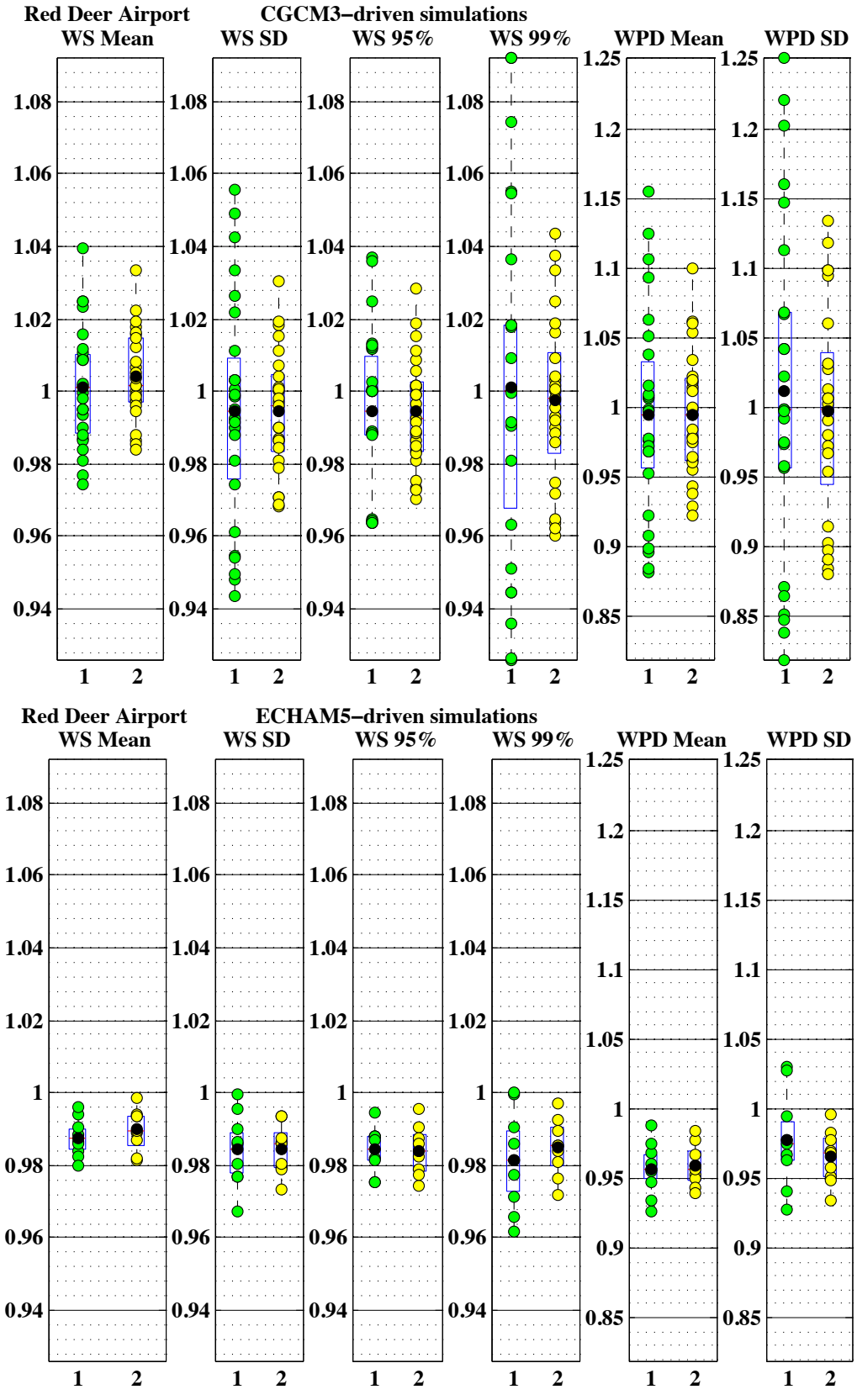

Figure B.30: As in Figure 4.6 for Red Deer Airport station.

Appendix C

Seasonal (DJF and JJA) changes in wind speed and power density

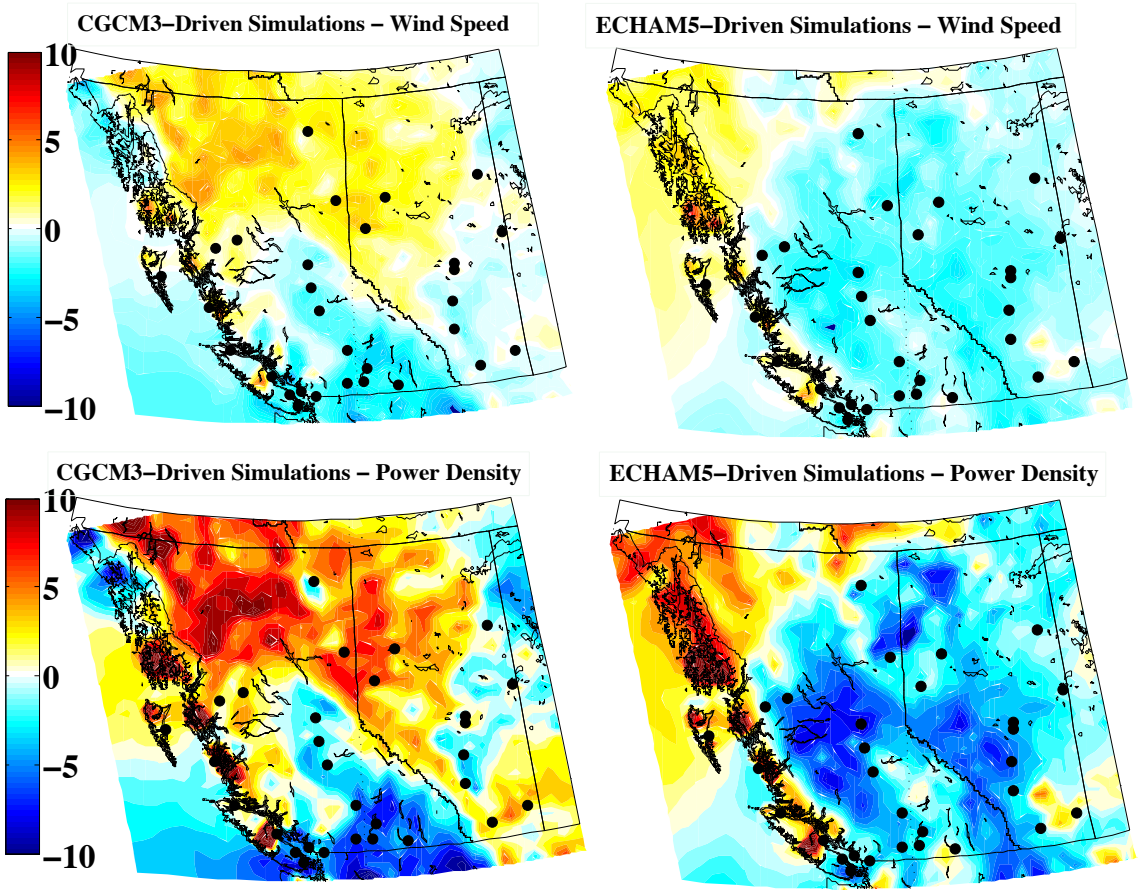

Figure C.1: As in Figure 5.4 for December through February (DJF). Colours depict percentage change (2031-60 minus 1971-2000).

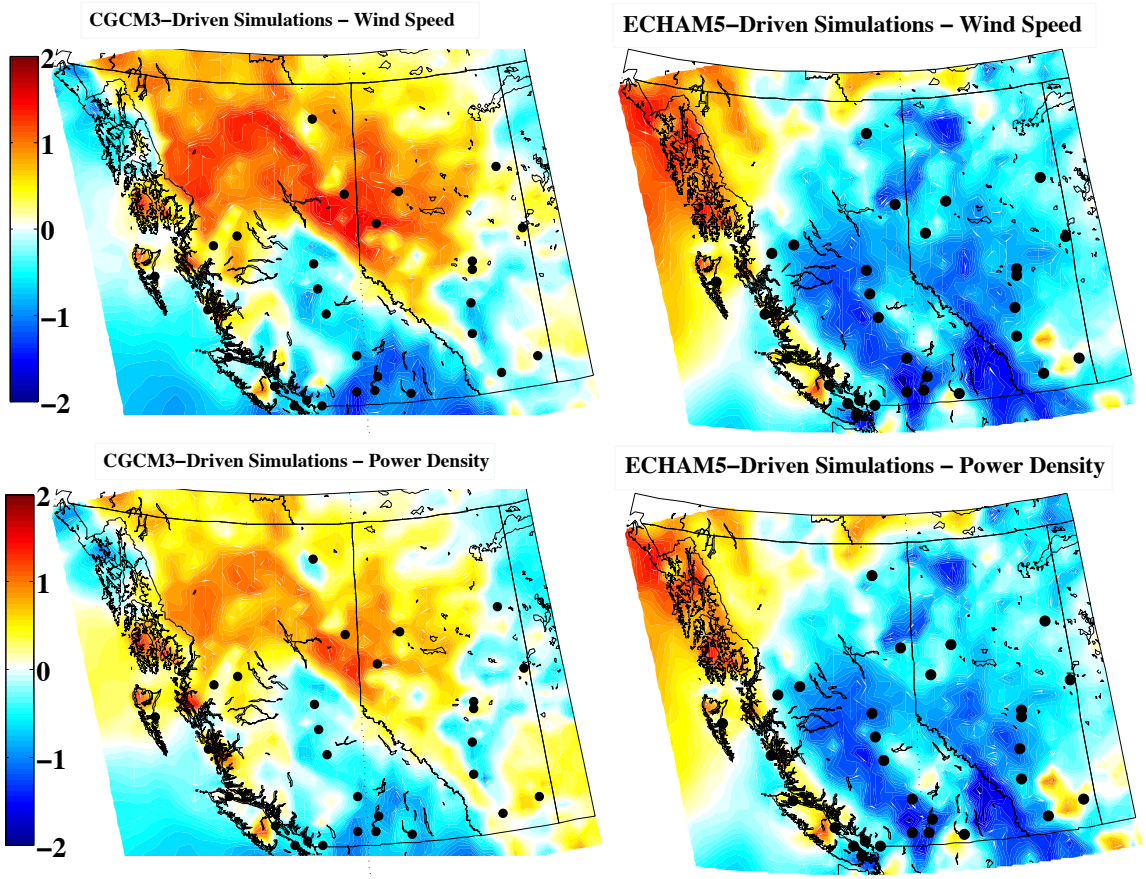

Figure C.2: As in Figure 5.5 for December through February (DJF). Colours depict mean change (2031-60 minus 1971-2000) in units of the inter-ensemble standard deviation.

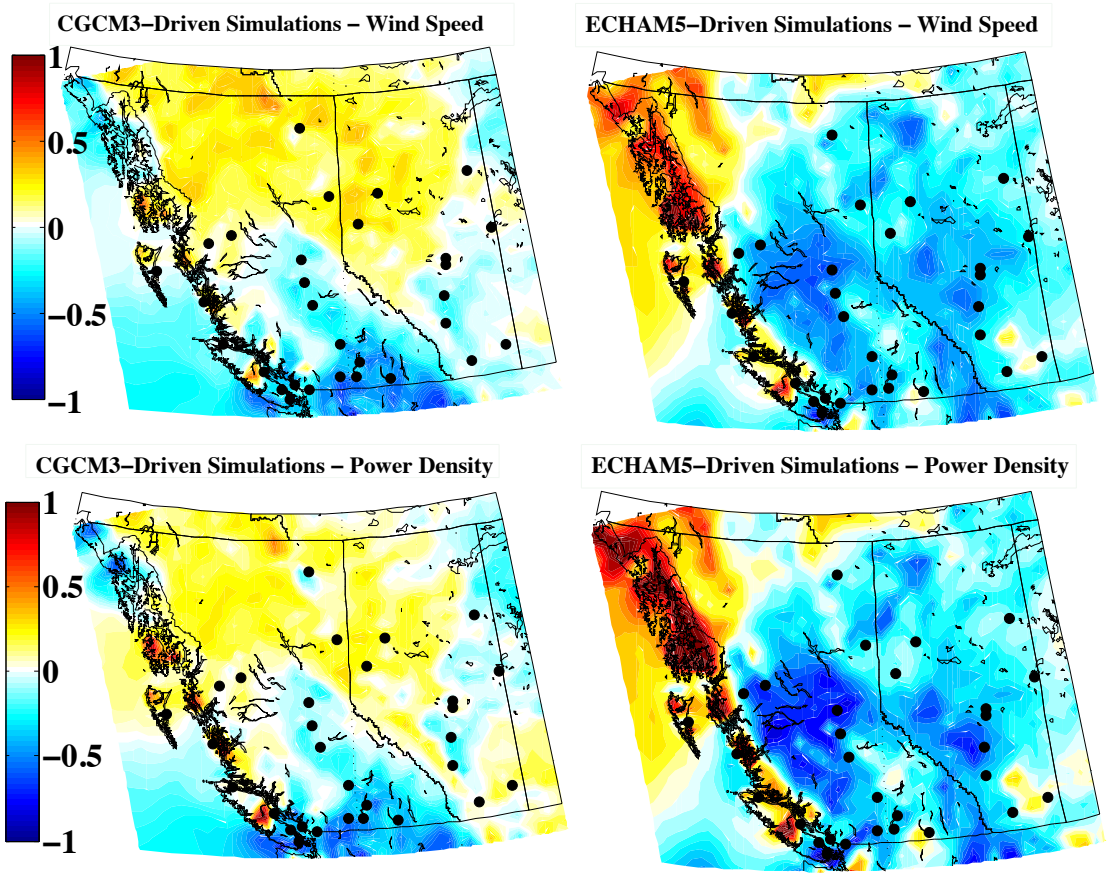

Figure C.3: As in Figure 5.6 for December through February (DJF). Colours depict mean change (2031-60 minus 1971-2000) in units of the inter-annual standard deviation.

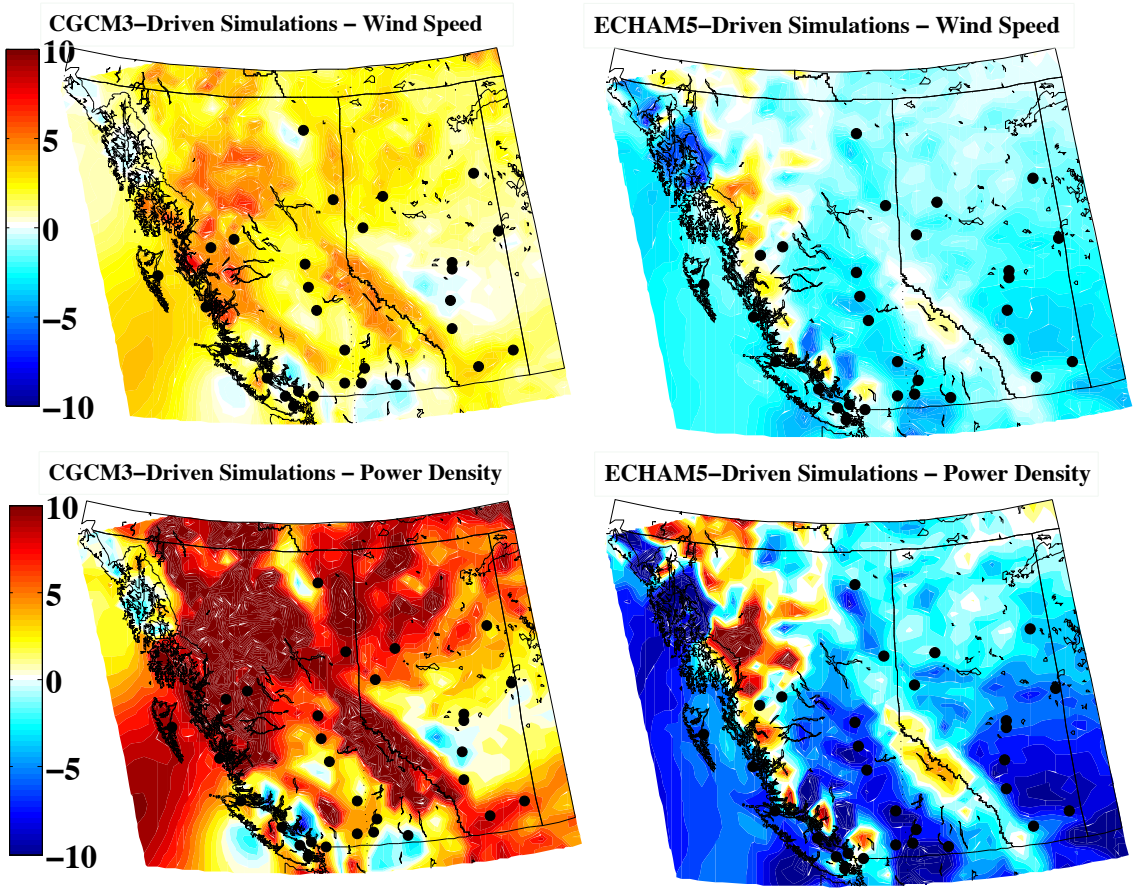

Figure C.4: As in Figure 5.4 for June through August (JJA). Colours depict percentage change (2031-60 minus 1971-2000).

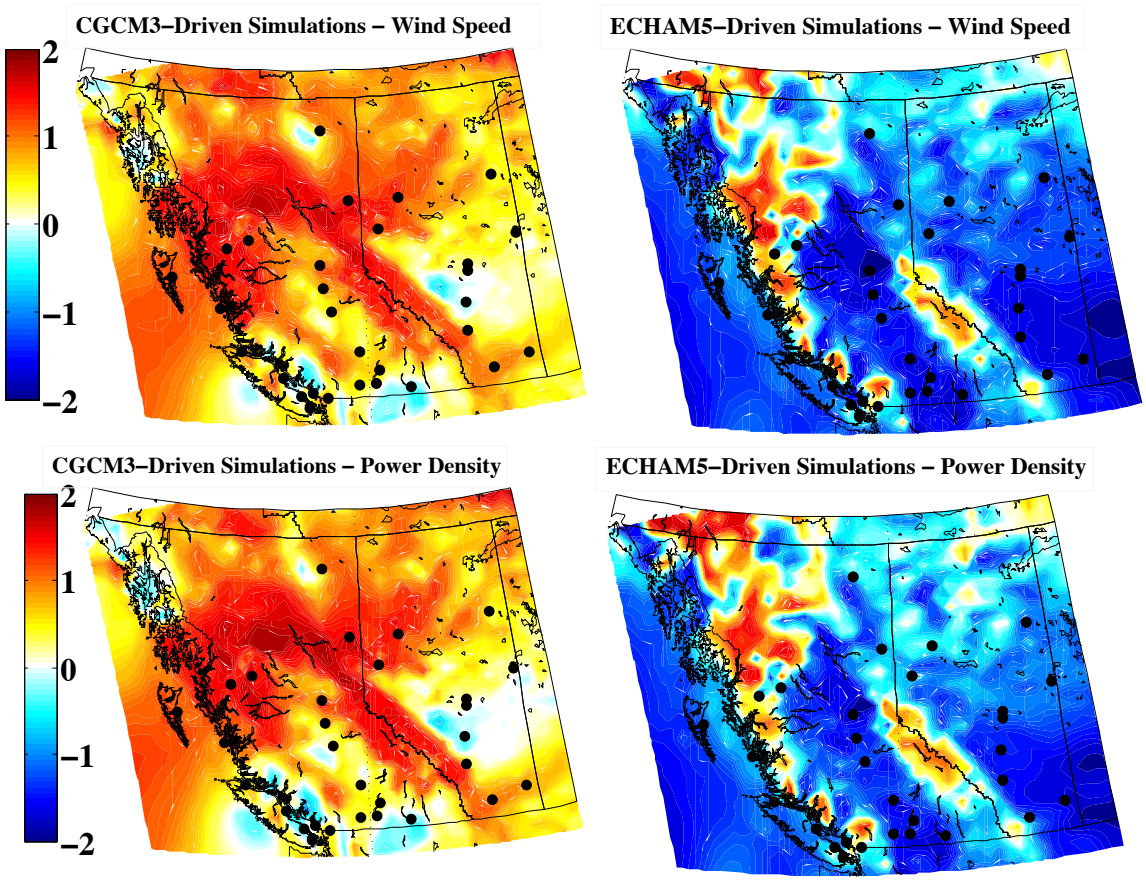

Figure C.5: As in Figure 5.5 for June through August (JJA). Colours depict mean change (2031-60 minus 1971-2000) in units of the inter-ensemble standard deviation.

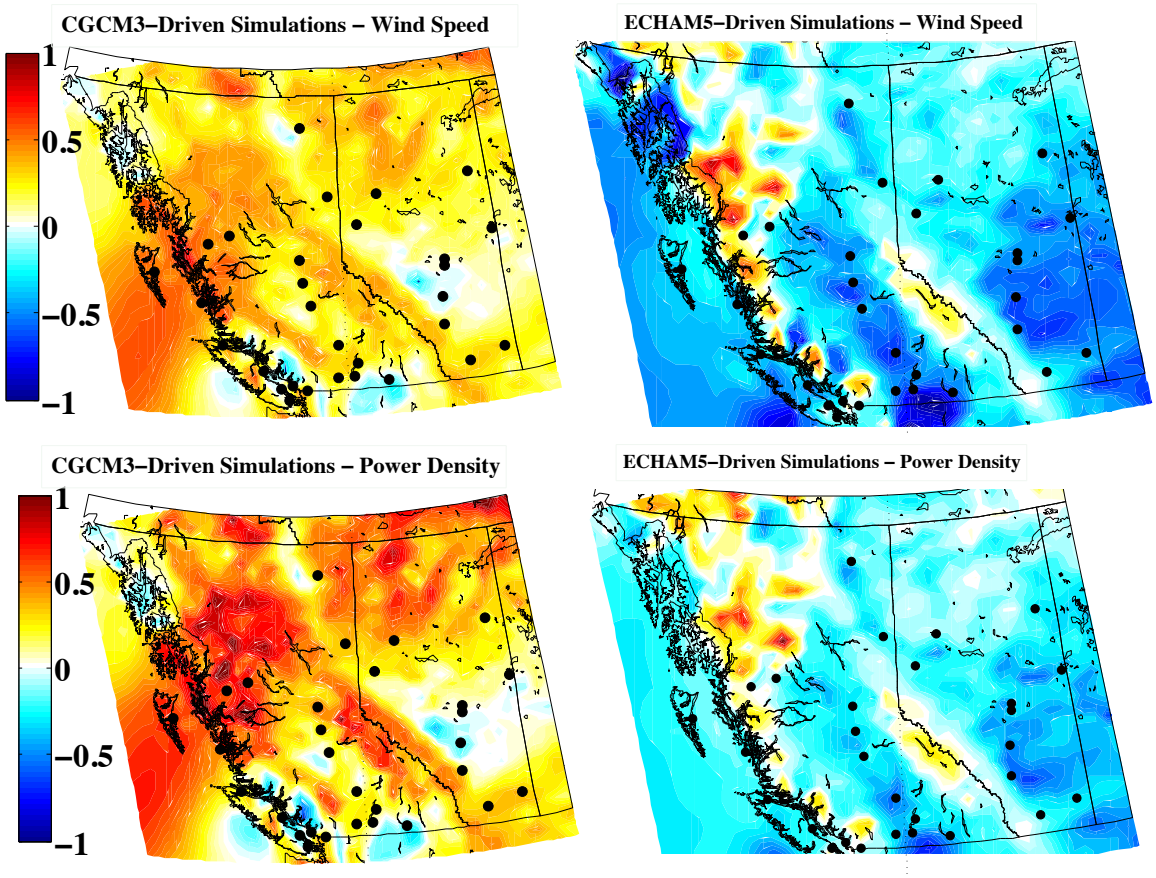

Figure C.6: As in Figure 5.6 for June through August (JJA). Colours depict mean change (2031-60 minus 1971-2000) in units of the inter-annual standard deviation.

Bibliography

Alberta Energy, 2015: Electricity Statistics. Alberta Energy, [Retrieved July 8, 2015], http://www.energy.alberta.ca/Electricity/682.asp.

Amante, C., and B. Eakins, 2009: ETOPO1 1 Arc-Minute Global Relief Model: Procedures, Data Sources and Analysis. NOAA Technical Memorandum NESDIS NGDC-24. National Geophysical Data Center, NOAA. [Accessed March 5, 2015].

B.C. Ministry of Energy and Mines, 2015: Electric generation and supply. BC Ministry of Energy and Mines, [Retrieved July 8, 2015], http://www.empr.gov.bc.ca/EPD/Electricity/supply/Pages/default.aspx.

Breslow, P. B., and D. J. Sailor, 2002: Vulnerability of wind power resources to climate change in the continental United States. *Renew. Energy*, **27**, 585–598.

Canadian Wind Energy Association, 2015: Installed Capacity. [Retrieved July 8, 2015], http://canwea.ca/wind-energy/installed-capacity/.

Caya, D., and R. Laprise, 1999: A Semi-Implicit Semi-Lagrangian Regional Climate Model: The Canadian RCM. *Mon. Weather Rev.*, **127**, 341–362.

Curry, C. L., B. Tencer, K. Whan, A. J. Weaver, M. Gigure, and E. Wiebe, 2015: Searching for added value in simulating climate extremes with a high-resolution regional climate model: A multi-scale study over Western Canada. Submitted to Atmosphere-Ocean, May 6, 2015.

Curry, C. L., D. van der Kamp, and A. H. Monahan, 2012: Statistical downscaling of historical monthly mean winds over a coastal region of complex terrain. I. Predicting wind speed. *Climate Dynamics*, **38 (7-8)**, 1281–1299.

Diaz-Nieto, J., and R. L. Wilby, 2005: A comparison of statistical downscaling and climate change factor methods: impacts on low flows in the river thames, united kingdom. *Climatic Change*, **69 (2-3)**, 245–268.

Eagland, N., 2015: B.C.'s wind-power projects stuck in doldrums, industry players say, as province pushes Site C dam. *The Province*, http://www.theprovince.com/technology/wind+power+projects+stuck+doldrums+industry+players+province+pushes+Site/10966335/story.html.

Haerter, J. O., S. Hagemann, C. Moseley, and C. Piani, 2011: Climate model bias correction and the role of timescales. *Hydrology and Earth System Sciences*, **15 (3)**, 1065–1079.

He, Y., A. H. Monahan, C. G. Jones, A. Dai, S. Biner, D. Caya, and K. Winger, 2010: Probability distributions of land surface wind speeds over North America. *J. Geophys. Res.*, **115**, D04 103.

Ho, C. K., D. B. Stephenson, M. Collins, C. A. T. Ferro, and S. J. Brown, 2012: Calibration strategies: A source of additional uncertainty in climate change projections. *Bull. Amer. Meteor. Soc.*, **93**, 21–26.

Holt, E., and J. Wang, 2012: Trends in Wind Speed at Wind Turbine Height of 80 m over the Contiguous United States Using the North American Regional Reanalysis (NARR). *J. Appl. Meteor. Climatol.*, **51**, 2188–2202.

Kalnay, E., and Coauthors, 1996: The NCEP/NCAR 40-Year Reanalysis Project. *Bull. Amer. Meteor. Soc.*, **77**, 437–471.

Kiani, B., A. Rowe, P. Wild, L. Pitt, A. Sopinka, and T. F. Pedersen, 2013: Optimal electricity system planning in a large hydro jurisdiction: Will British Columbia soon become a major importer of electricity? *Energy Policy*, **54**, 311–319.

Mansbach, D. K., and D. R. Cayan, 2010: Statistical downscaling of wind for California wind farms with an application to 21st century climate change scenarios. *1st Conference on Weather, Climate, and the New Energy Economy (Atlanta, GA, January 2010)*.

Manwell, J. F., J. G. McGowan, and A. L. Rogers, 2012: *Wind Energy Explained: Theory, Design and Application*. John Wiley & Sons Ltd., Chichester, West Sussex, UK, pp.92-96.

Mesinger, F., and Coauthors, 2006: North American Regional Reanalysis. *Bulletin of the American Meteorological Society*, **87**, 343–360.

Monahan, A. H., 2014: Wind speed probability distribution. *Encyclopedia of Natural Resources*.

Monahan, A. H., T. Rees, Y. He, and N. McFarlane, 2015: Multiple Regimes of Wind, Stratification, and Turbulence in the Stable Boundary Layer. *Journal of the Atmospheric Sciences*, **72**, 3178–3198.

Nakicenovic, N., and Coauthors, 2000: *Emissions Scenarios. A Special Report of Working Group III of the Intergovernmental Panel on Climate Change*. Cambridge: Cambridge University Press.

National Renewable Energy Laboratory, 2014: Wind Data Details, Dynamic Maps, GIS Data, and Analysis Tools (updated February 6, 2014). [Accessed March 5, 2015], http://www.nrel.gov/gis/wind_detail.html.

NAV Canada, 2015: Techwatch, Winter 2015 Edition. [Accessed June 28, 2015], http://www.navcanada.ca/EN/media/Publications/TECHWATCH%20-%20Winter%202015.pdf.

Penner, D., 2014: Cape Scott Wind Farm gives Island power a boost. *Times Colonist, August 10, 2014*, downloaded on July 28, 2015 from: http://www.timescolonist.com/business/cape-scott-wind-farm-gives-island-power-a-boost-1.1305531.

Piani, C., G. P. Weedon, M. Best, S. Gomes, P. Viterbo, S. Hagemann, and J. O. Haerter, 2010: Statistical bias correction of global simulated daily precipitation and temperature for the application of hydrological models. *Journal of Hydrology*, **395 (34)**, 199–215.

Plummer, D. A., and Coauthors, 2010: Climate and Climate Change over North America as Simulated by the Canadian RCM. *Journal of Climate*, **19 (13)**, 3112–3132.

Pryor, S. C., R. J. Barthelmie, and J. T. Schoof, 2012: Past and future wind climates over the contiguous USA based on the North American Regional Climate Change Assessment Program model suite. *J. Geophys. Res.*, **117**, D19 119.

Rasmussen, D. J., T. Holloway, and G. F. Nemet, 2011: Opportunities and challenges in assessing climate change impacts on wind energy? a critical comparison of wind speed projections in California. *Environ. Res. Lett.*, **6**, 024 008.

Sailor, D. J., M. Smith, and M. Hart, 2008: Climate change implications for wind power resources in the northwest United States. *Renew Energy*, **33**, 2393–2406.

Salathe, E. P., R. Steed, C. F. Mass, and P. H. Zahn, 2008: A high-resolution climate model for the US Pacific Northwest: mesoscale feedbacks and local responses to climate change. *J. Clim.*, **21**, 5708–5726.

Tye, M. R., D. B. Stephenson, G. J. Holland, and R. W. Katz, 2014: A Weibull Approach for Improving Climate Model Projections of Tropical Cyclone Wind-Speed Distributions. *J. Climate*, **27**, 6119–6133.

Wan, H., X. L. Wang, and V. R. Swail, 2010: Homogenization and Trend Analysis of Canadian Near-Surface Wind Speeds. *Journal of Climate*, **23**, 1209–1225.